Ove Bjørn Wilson

The influence of porous plates on effective drainage and imbibition rates

Doktoravhandlinger ved NTNU

2004:104

ACKNOWLEDEGEMENT

I which to thank my advisors, Professor Svein M. Skjæveland and Professor Ole Torsæter, for all their patient, excellent support, guidance and always having the door open for me when needed.

It has been challenging to combine this research study with other duties at Reslab. I would therefore like to thank Reslab for all support during this study. Furthermore, all engineers in Reslab who contributed in data logging and took good care of my experiments if I was out of the office.

I would also thank Norsk Hydro ASA for their support and participation in this research.

SUBJECT INDEX

Page

LIST OF TABLES

LIST OF FIGURES

1. SUMMARY

The goal in petrophyscial studies is very often to obtain representative capillary pressure curves in conjunction with Sw-RI relationships for log interpretation. The most frequently used techniques today are centrifugation, the porous plate and the mercury injection techniques.

Unlike the other methods, the strength of the porous plate technique is the possibility to establish both primary drainage, spontaneous imbibition, forced imbibition and secondary drainage without changing set up, conditions or method. In addition, the technique can be combined with resistivity measurements. The weakness is that the method requires a long experimental turnaround time.

Even though techniques like the membrane technique[6], the continuous injection technique[7], and the semi dynamic method[8] have been introduced to the industry with a significant reduced turnaround time, the porous plate method is still believed to be the most representative method. Its popularity in special core analysis has not dropped even after these new techniques were introduced to the industry.

The aim of this study is to experimentally test layered porous plate prototypes in capillary experiments for different capillary sequences, using all types of fluid pairs at different conditions, varying from ambient to extreme reservoir condition. The layered porous plate method is identical to the porous plate method, except for ceramic construction. In addition to this, the aim is to investigate if there is possible hysteresis between the two porous plate techniques, and investigates if this is related to reduced turnaround time. In other words, investigate how and when diaphragms influence drainage and imbibition rates in capillary experiments.

Another aim is to investigate if the layered porous plate technique can improve the continuous injection technique.

In this study a method of quantifying the influence of porous plates on effective rates at any stage and capillary sequence has been developed. The method is based on analysing transient capillary behaviour.

This PhD thesis is based on the following publications:

1. O.B. Wilson, B.G. Tjetland and A. Skauge.:"Porous plate influence on effective drainage rates in capillary pressure experiments" SCA 2001, Edinburgh.

2. O.B.Wilson and S.M. Skjæveland.: "Porous plate influence on effective imbibition rates in capillary pressure experiments" SCA 2002, Monterey California.

3. O.B. Wilson.: " What is the fastest turnaround time to establish a reliable and reproducible Sw-RI relationship from porous plate and continuous injection experiments" NFES, Distinguish Lecture on cost efficient technology seminar, December 2002, Stavanger Oil Museum.

4. O.B. Wilson.:" Obtaining representative hierarchies and mechanisms in experimental petrophyscial studies, using different experimental techniques" NFES, Distinguish Lecture of the month in September 2003, Stavanger.

2. INTRODUCTION

Log interpretation

Almost all oil and gas produced today comes from accumulations in the pore spaces of reservoir rocks like sandstones, limestones and dolomites. The amount of hydrocarbons contained in a unit volume of the reservoir is the product of its porosity by the hydrocarbon saturation.

In addition to porosity and hydrocarbon saturation, the volume of the formation containing hydrocarbons is needed in order to estimate total reserves and to determine if the accumulation is commercial. Knowledge of thickness and the area of the reservoir are needed for computation of its volume. To evaluate the producibility of a reservoir, it's is necessary to know how easily fluid can flow through the pore system.

The main petrophysical parameters needed to evaluate a reservoir, are porosity distribution, hydrocarbon distribution, thickness, area and permeability. Unfortunately few of these parameters can be measured directly. Instead, they must be derived or inferred from the measurement of other petrophysical parameters of the formations. A large number of parameters can be measured. They include, amongst others, resistivity, bulk density, interval transit time, spontaneous potential, natural radioactivity, and hydrogen content of the rock. Log interpretation is the process by which these measurable parameters are translated into the desired petrophysical parameters of porosity distribution, hydrocarbon distribution, permeability, producibility, lithology, etc.

The drilling process itself further complicates this translation. In drilling through a formation, the fluids in the pores of the rock surrounding the borehole may be displaced or contaminated by the invasion of the drilling fluid. Occasionally, the rock matrix may even be altered. Since the petrophysical parameters of virgin reservoirs are usually needed, the well logging tools must be able to see beyond the contaminated zone into the virgin formation. Alternatively, the interpretation technique must be able to compensate for the contamination.

Of all the rock parameters measured by today's logging tools, resistivity is of particular importance. This tool has a deep depth of investigation and is essential for saturation determinations in the virgin, non-invaded portion of the reservoir. Neither oil nor gas conducts electrical current. Therefore, in practice resistivity distribution is converted to saturation distribution by using the Archie's[17] derived conversion factor, called saturation exponent. According to Schlumberger[18], saturation exponent is close to 2 for most formations.

Capillarity of reservoirs

The equilibrium fluid saturation distribution in a petroleum reservoir, prior to production is governed by the pore space characteristics. This is a result of the non-wetting phase, normally hydrocarbons, entering pore space initially occupied by the wetting fluid, normally water, during migration of hydrocarbons from a source rock region into a reservoir trap. A pressure differential is required for the non-wetting phase to displace the wetting phase and this is equivalent to a minimum threshold capillary pressure and is dependent of pore size.

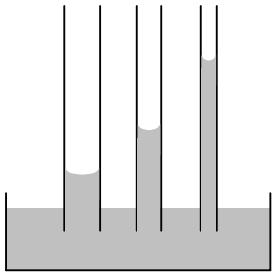

Figure 2.1 Capillary rise above free water level

The physical significance of a threshold pressure in an oil reservoir may be appreciated by the analogy of a capillary rise of water in different vertical glass tubes suspended in an open tray of water, as seen in figure 2.1.

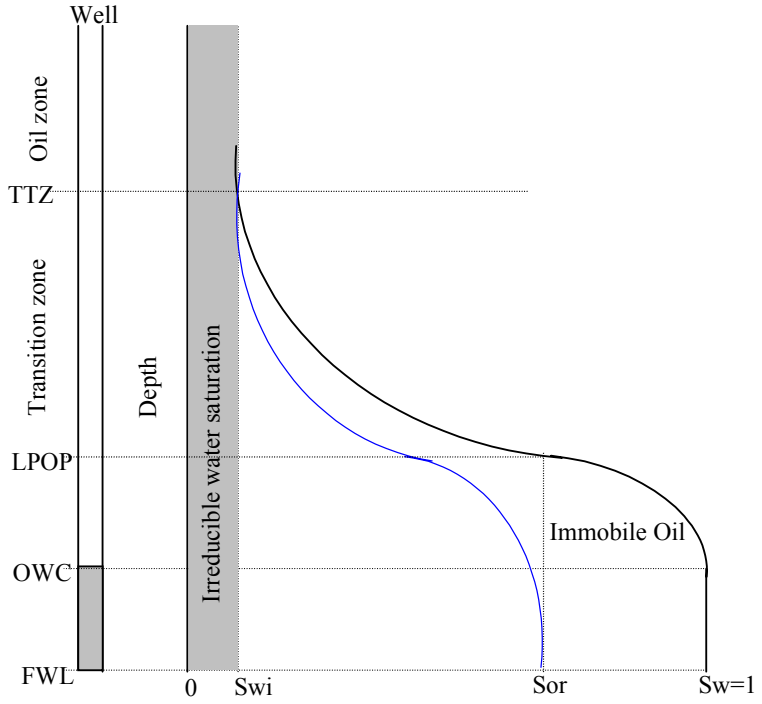

Figure 2.2 Static water saturation distribution, definition of contacts and transition zone in a homogeneous reservoir

Figure 2.2 illustrates saturation distribution in a homogeneous reservoir. Free water level, FWL, is an imaginary surface at which the pressure in the oil zone equals that in the water zone. In other words, free water level is the oil-water contact in the absence of the capillary forces associated with a porous medium, i.e. in a well. The threshold capillary pressure, found in the reservoir is proportional to height above the free water level, where 100% water saturation is found.

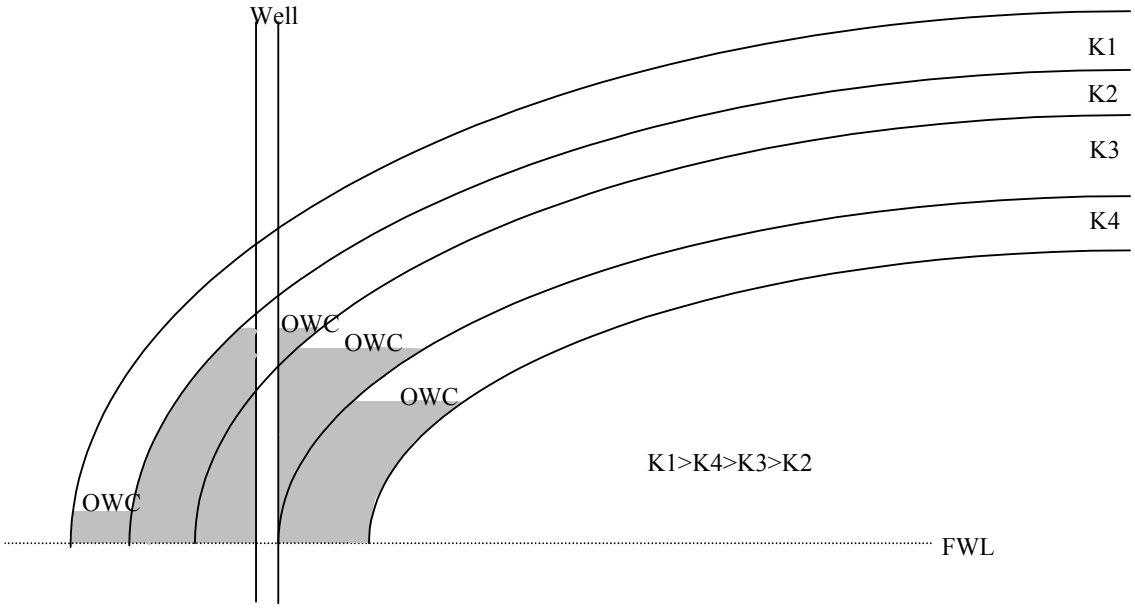

Figure 2.3 Observed water-oil contact and their relationship with free water level in a layered reservoir with common aquifer

The free water level is a property of the reservoir system, while an oil-water contact observed in a particular well will depend on the threshold pressure of the rock type present in the vicinity of the well. Figure 2.3 illustrates that the oil-water contact is related to lithology for a specific scenario. In the above example, oil water contacts above free water level are a function of pore characteristics of the layers.

The relationship between height above free water level and capillary pressure is derived from consideration of the gravity-capillary pressure force equilibrium. Using free water level as datum plane and defining its position in the reservoir as the place where the oil phase pressure, p_o equals the water phase p_w, one obtains

$$P_{c(FWL)} = P_o - P_w = 0 \qquad (1).$$

At some height h, above free water level, the pressure is,

$$P_o = P_{FWL} - \rho_o gh \text{ and } P_W = P_{FWL} - \rho_W gh \quad (2).$$

Therefore, the capillary pressure at a depth equivalent to h above free water level is,

$$P_c = P_o - P_w = (P_{FWL} - \rho_o gh) - (P_{FWL} - \rho_w gh) = gh(\rho_w - \rho_o) \quad (3).$$

Experimental capillary pressure curves are used in interpretation by converting experimental capillary pressure curves to a height h, above free water level described above. If a capillary pressure experiment at a laboratory is performed at other conditions than reservoir conditions, the used experimental data must be converted to more representative conditions before calculating height h above free water level. This is achieved by using the equation,

$$P_{C(res)} = P_{C(lab)} \cdot \frac{(\sigma \cos\theta)_{res}}{(\sigma \cos\theta)_{lab}} \quad (4).$$

Representative core material

The goal in experimental petrophysical studies is often to obtain representative capillary pressure curves in conjunction with Sw-RI relationships for log interpretation. Several processes might influence this, summarised as follows:

The whole core is usually drilled and collected in a core barrel on site. The undisturbed reservoir section is usually cored using water or oil based mud systems. During the coring process, overburden stress, pore pressure and temperature are released. Mud filtrate invasion is often not avoidable during this process. Filtrate invasion might therefore influence the wettability of the core. In addition, the pressure depletion itself might disturb pore integrity. This is especially important to consider when dealing with cores from unconsolidated gas reservoirs.

After the core has been brought to surface, it is usually cut into one-metre sections and transported to the laboratory. This process might alternate the pore integrity. Furthermore, mud filtrate might continue to invade during transport. After the core sections arrive to the laboratory, Seal Peals are usually cut, waxed and stored for special core analysis at a later stage. It is not unusual to initiate a special core analysis study, on preserved core material, several years after preservation. Bacteria growth during storage over time might also be a serous problem.

By taking all these elements into consideration, it is questionable if it is ever possible to analyse a core that is representative. However, petrophysicists and reservoir engineers still need experimental data in order to reduce the uncertainty in log evaluation and reservoir simulations. We will therefore restrict the discussion and stay focused on laboratory-induced artefacts.

First, in order to simulate first time invasion we need to render the wettability towards a strongly water wet preference without disturbing integrity. Fresh preserved core plugs are usually mounted into individual core holders, exposed to a reference confining pressure, and then cleaned by flooding alternating sequences of solvents. Mineralogy is therefore a key factor. Several clay minerals such as fibrous illite and smectite might be critical with respect to drying or cleaning. These are both rate and solvent sensitive and might result in fine migration towards the upstream end of the core plug during the cleaning process. Other minerals have strong affinity to hydrocarbons, which might be difficult to remove.

During recent years, it has therefore now almost become a standard to initiate pre-studies prior to sophisticated special core analysis programs. The reason for this is to determine an effective cleaning procedure, which is harmless to plug integrity but able to alternate wettability to a water wet preference. A study like this usually consists of XRD to determine mineralogy, testing of different cleaning procedures, SEM evaluation for investigating integrity and finally verifying the preference by performing clean state wettability tests.

Another aspect of obtaining representative capillary pressure curves is conditions. It is obvious that the geometry of pores and throats are different compared with atmospheric conditions. Throats will be smaller at net overburden compared with a respective unconfined scenario. Hence, the capillary pressure curve itself is a function of applied stress. The effect of overburden on porosity, permeability and formation resistivity factor is therefore usually investigated prior to initiating capillary drainage.

By assuming that both stress and preference are representative prior to invasion, it is reasonable to believe that the selection of experimental technique is independent on the result. This is often observed by, for instance, comparing a mercury injection curve, performed on the core plug under stress, with a corresponding porous plate experiment. In other words, independent of fluid pair by applying respective interfacial tensions transformations. However, this does not give any information about restored wettability.

Hysteresis between Sw-RI relationships during capillary drainage is very often observed for different fluid pairs in a given lithology. When oil invades a capillary, there might be a wettability alteration over time. Hysteresis in Sw-RI relationships, caused by different fluid

pairs, might be thought of as differences in restored wettability achieved during capillary drainage. Sw-RI relationships are not a quantitative measurement for wettability. However, describing first time invasion using representative fluid pairs will result in a more representative imbibition curve, which is strongly dependent on obtained wettability.

Scope of work

Even though techniques like the membrane technique[6], the continuous injection technique[7], and the semi dynamic method[8] have been introduced to the industry with a significant reduced turnaround time, the porous plate method is still believed to be the most representative method. Its popularity in special core analysis has not dropped even after these new techniques were introduced to the industry. One explanation for this is that the porous plate technique can be used for all types of conditions, fluid pairs, capillary sequence, in combination with other petrophysical parameters and has no end effects, while the other techniques have a lot of restrictions or are based on a model for calculating saturation.

The layered porous plate method is identical to the porous plate method, except for ceramic construction, which is highlighted in chapter 4. Taken into consideration the familiarity with the homogenous porous plate technique, the layered porous plate technique has a potential to become the new standard in porous plate technology. The motivation behind the research in this thesis could therefore be summarised as follows:

The aim of this study is to experimentally test the layered porous plate prototypes in capillary experiments for different capillary sequences, using all types of fluid pairs at different conditions, varying from ambient to extreme reservoir condition.

The industry is sceptical to new techniques. One of the targets is therefore to investigate if there is possible hysteresis between the two porous plate techniques and investigate if this is related to reduced turnaround time. In other words, investigate how and when diaphragms influence drainage and imbibition rates in capillary experiments.

Another aim is to investigate if the layered porous plate technique can improve the continuous injection technique, which is claimed to yield reliable and representative saturation exponents in approximately 14 days.

3. MICROSCOPIC PHYSICS

An experimental study, involving invading and defending phases in porous media, requires knowledge of important properties like wettability of the fluids and the interfacial tension between them. Such properties play an essential role in capillary flow through microscopic pores.

This chapter introduces some concepts used later in the thesis. Since some of them are used differently in the literature, definitions and examples are reported to clarify how the concepts are used in this work.

Interfacial tension

At the interface between two immiscible liquids there will be interactions between molecules of different types and the interfacial tension arises due to the attractive forces between the molecules in the different fluids. Generally, the interfacial tension of a given liquid surface is measured by finding the force across any line on the surface divided by the length of the line segment. Thus, the interfacial tension becomes a force per unit length, which is equal to the energy per surface area.

Consider a spherical water droplet in equilibrium with a surrounding vapour, where gravitational forces are neglected. The curved surface leads to a pressure difference between the water phase and the gas. The pressure inside the droplet on the concave side of the surface is expected to exceed the pressure on the convex side. Let γ denote the interfacial tension of the droplet surface. Then, the free energy of the surface is given by $4\pi R2\gamma$ where R is the radius of the droplet. Assume that the radius of the droplet is increased by dR because of molecules condensing on the surface. The corresponding surface free energy increases with $8\pi R\gamma dR$. This energy has to be balanced by the pressure forces between the droplet and the vapor. Let $\Delta p>0$ denote the pressure difference between the droplet and the vapor. Then, the work required to increase the size of the droplet by dR becomes

$$\Delta p \cdot 4\pi R^2 dR = 8\pi R\gamma dR \tag{5}.$$

Thus, the pressure between the surface of the droplet and the gas becomes

$$\Delta p = \frac{2\gamma}{R} \tag{6}.$$

This equation is called the Young-Laplace equation and has the general form

$$\Delta p = \gamma(\frac{1}{R_1} + \frac{1}{R_2}) \quad (7),$$

Where R_1 and R_2 are the principal radii of curvature of the interface. In the above example the droplet was assumed to be a perfect sphere with $R_1=R_2=R$.
For a curved water-oil interface, the fundamental Young-Laplace equation can be written as

$$P_c = P_o - P_w = \gamma(\frac{1}{R_1} + \frac{1}{R_2}) \quad (8),$$

where P_c is the capillary pressure. The radius of curvature directed into the oil phase is positive, and the radius directed into the water phase is negative. In general the capillary pressure is the pressure in the non-wetting phase minus the pressure in the wetting phase. Depending on the curvature of the surface, the capillary pressure can be positive or negative.

For two-phase flow in porous media, the interfacial tension of curved pore-interfaces gives rise to a capillary pressure P_c between the two immiscible liquids. At pore level, the curvature of the interface is assumed to be equal to the pore size, denoted r. Thus the capillary pressure between the fluids in a pore of size r is approximately given by $2\gamma/r$.

Wettability
The wettability of a liquid is defined as the contact angle between a droplet of the liquid in thermal equilibrium on a horizontal surface. Depending on the type of surface and liquid, the droplet may take a variety of shapes as illustrated in figure 3.1.The wetting angle, θ, is given by the angle between interface of the droplet and the horizontal surface. The liquid is seen as wetting when $90<\theta<180$ degrees and non-wetting when $0<\theta<90$. $\theta=0$ and 180 degrees corresponds to perfect wetting and the drop spreads forming a film on the surface.

Figure 3.1 A liquid droplet in equilibrium with a horizontal surface surrounded by a gas. The wetting angle θ between the horizontal layer and the droplet interface defines the wettability of the liquid. To the left: A non-wetting fluid with $0<\theta<90$. To the right: A wetting fluid with $90<\theta<180$

Actually, the wetting angle θ is a thermodynamic variable that depends on the interfacial tensions of the surfaces. Let $\gamma_{l,g}$ denote the interfacial tension due to the liquid-gas surface, $\gamma_{s,l}$ refer to the interfacial tension due to the solid-liquid surface and $\gamma_{s,g}$ indicate the interfacial tension of the solid-gas surface. In thermodynamic equilibrium the wetting angle, θ, is given by Young's law

$$\gamma_{s,g} = \gamma_{s,l} + \gamma_{l,g} \cdot \cos\theta \tag{9}.$$

For two-phase flow in porous media the wetting angle influences the strength of the capillary pressure. Let θ denote the wetting angle between the interface and the pore wall, then the capillary pressure in a pore of size r becomes

$$p_c \approx \frac{2\gamma\cos\theta}{r} \tag{10}.$$

Drainage and imbibition

Depending on the wetting properties of the fluids, there are essentially two different types of displacements in two-phase flow in porous media. Drainage is usually defined as the process that occurs when a non-wetting fluid invades and displaces a wetting fluid. The opposite case, imbibition, occurs when a wetting fluid displaces a non-wetting fluid. The mechanisms of the two displacements in drainage and imbibition are quite different. Typically, slow drainage is characterized by piston-like motion inside the pores, where the invading non-wetting fluid only enters a pore if the capillary pressure is equal to or greater than the threshold pressure of that pore[1]. The threshold pressure corresponds to the capillary pressure in the narrowest part of the pore. However, in imbibition at low injection rates the invading fluid will enter the narrowest pores before any other is considered[1].

Capillary pressure as a function of saturation can be determined experimentally. The following definitions are used in this thesis:

Primary drainage

Primary drainage is the same as experimentally simulating first time invasion. The non-wetting phase is forced into the porous media originally saturated with the wetting fluid. The end point of the curve is often referred to as irreducible water saturation.

Spontaneous imbibition

Spontaneous imbibition is the positive side of the imbibition curve. I.e. the spontaneous response when releasing the forced energy applied to the system during primary drainage.

Forced imbibition

Forced imbibition is the negative side of the imbibition curve. I.e. the response caused by increasing an overpressure in the water phase. The end point on this curve is often referred to as residual oil or gas saturation.

Spontaneous re-drainage

This curve is the spontaneous response when releasing the energy applied to the system during forced imbibition. This curve might also be referred to as spontaneous oil imbibition.

Secondary drainage

Secondary drainage is obtained by performing re-drainage back to irreducible water saturation again.

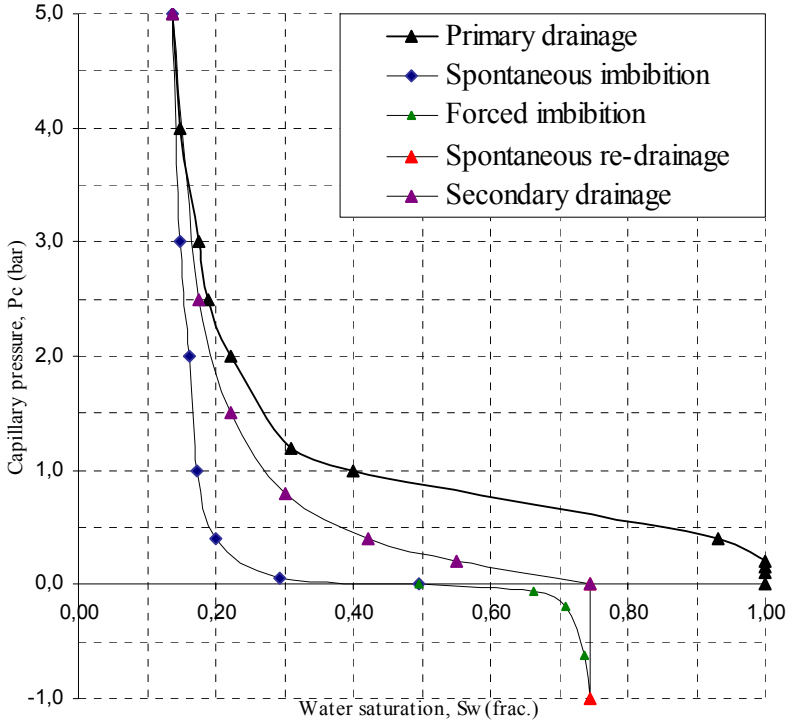

Figure 3.2 Illustration of experimental primary drainage, spontaneous imbibition, forced imbibition, spontaneous re-drainage and secondary drainage.

Drainage displacement

Drainage displacement is the process where a non-wetting fluid displaces a wetting fluid in a porous medium. In a continuous injection experiment the displacement process might provide pattern formations between the interface of the two fluids and the different structures obtained can be divided into three major flow regimes: viscous fingering, stable displacement and capillary fingering (invasion percolation). The properties of the different regimes are briefly discussed below.

Fluid forces

In two-phase fluid displacements there are three main types of force: viscous force in the invading fluid, viscous force in the defending fluid and capillary forces due to the interaction between them. This leads to dimensionless numbers that characterize the flow in porous media, the capillary number C_a and the viscosity ratio M.

The capillary number is a quantity describing the competition between capillary and viscous forces. Consider a porous medium of pores with average size a. Microscopically the pressure drop ΔP_v due to viscous forces across an average pore is obtained from Darcy's equation

$$\Delta P_V = \frac{u \cdot \mu \cdot a}{k} \tag{11},$$

where k is the local permeability of the pore, μ is the viscosity of the fluid and u denotes the flow velocity in the pore. Assume that the pore contains an interface between the liquids and that the curvature of the interface is approximately equal to the average pore size. The corresponding capillary pressure ΔP_c is proportional to γ/a where γ is the interfacial tension.

The capillary number may now be defined as the ratio of the viscous and capillary pressures

$$C_a = \frac{\Delta P_v}{\Delta P_c} = \frac{u \cdot \mu \cdot a^2}{\gamma \cdot k} \tag{12}.$$

The permeability of the pore is roughly given by a^2 and we obtain

$$C_a = \frac{\mu \cdot u}{\gamma} \tag{13}.$$

Thus, the capillary number becomes a ratio of viscous and capillary forces acting at the pore scale. In two-phase flow in a porous media, the capillary forces act across the fluids at all length

scales. Some of the sandstones investigated in this research are statistically homogeneous at large length scales but random on the pore scale due to the pore size distribution. It is not trivial to know how to measure the competition between these two forces. For instance, the above definition does not cover important properties such as pore size distribution and in two-phase flow it is not clear which viscosity should be inserted. Usually, authors tend to use maximum viscosity of the two liquids, under the assumption that the forces in the highest viscous fluid dominate the viscous forces. The viscosity ratio is defined as

$$M = \frac{\mu_2}{\mu_1} \qquad (14),$$

where μ_1 and μ_2 refer to the viscosity of the defending and invading fluid respectively.

Lenormand et al.[2] introduced the concept of the phase-diagram in 1988 for drainage displacements where various experiments and simulations were plotted in a plane with the capillary number C_a along the x-axis and the viscosity ratio M along the y-axis. The plot, reproduced in figure 3.3, clearly shows that the different structures they obtained divide into the major flow regimes whose region of validity in C_a and M space is given by the plot. The boundaries of the regions were qualitatively discussed and they concluded that the drainage displacements were fully characterized by C_a and M. However, it was stated that changing the pore size distribution of the simulation and experiments resulted in translations of the boundaries but that the general shape remained unchanged. The capillary number does not take into account the pore size distribution and careful analysis is required to understand better this effect before any complete phase-diagram can be drawn.

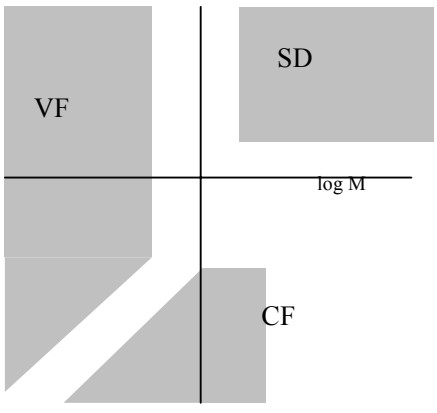

Figure 3.3 Lenormand's phase-diagram

Figure 3.3 illustrates Lenormand's phase-diagram on a logarithmic plot with viscosity ratio along the x-axis and the capillary number along the y-axis. The three regions bounded by gray color correspond to the three major flow regimes: viscous fingering (VF), stable displacement (SD) and capillary fingering (CF).

Major Regimes

In viscous fingering the principal force is due to viscous forces in the defending fluid. The process is obtained by injection of a low viscosity fluid into a medium containing high viscosity fluid, using a high injection rate. The capillary effects and the pressure drop in the invading fluid are negligible. The structures typically consist of fingers of invading fluid that propagate through the medium, with only a few small trapped clusters of defending fluid left behind.

Capillary fingering is executed by injection of the invading fluid at a very low injection rate. The low injection rate causes the viscous forces to vanish. Consequently, the principal force is due to capillary forces of the interface between the invading and the defending phases. The observed structures consist of a rough and wide front with trapped clusters of defending fluid ranging from the pore size to the length of the system. Due to the capillary pressure, the wetting properties of the two fluids become important. If the invader is non-wetting and the defending phase is strongly wetting the porous media, a piston-like motion on the pore scale level is observed. The hierarchy is to invade smaller and smaller pores at each time step.

In a stable displacement regime, the principal force is due to viscous forces in the invading fluid. Opposite to viscous fingering, the process is obtained by injection of a high viscosity fluid into a medium containing low viscosity fluid, using a high injection rate. Due to high injection rates, the capillary forces vanish and the pressure drop across the sample corresponds to the pressure over the invading fluid. The structures are characterized by an almost flat front between the invading and the defending phases and some clusters of defending fluid are observed. The cluster size is bounded by the roughness of the front and as a consequence only small clusters can develop.

Leverett j-function

Leverett[3] proposed a dimensionless form of the capillary drainage curve, which is referred to as the j-function by Rose and Bruce[4]

$$J(S) = \frac{P_c \sqrt{\frac{k}{\varphi}}}{\gamma \cdot \cos(\theta)} \qquad (15),$$

where k is the permeability and φ is the porosity. The j-function is used to correlate capillary pressure data within a reservoir. In addition, it is used to correlate measurements with different fluid pairs. The j-function does not take into account the pore architecture. Hence, it should only be used for correlation of rock within the same lithology group.

Thermodynamics of a capillary pressure experiment

A change in water volume ΔV_w in a porous medium is related to change in water saturation described by the expression

$$\Delta V_w = V_b \cdot \varphi \cdot \Delta S_w \qquad (16),$$

where V_b is the bulk volume, φ is the porosity and ΔS_w is the change in water saturation. The expression for external work[5] during drainage is

$$\Delta W_{external} = -\varphi \cdot V_b \int_{Sw_2}^{Sw_1} P_c \cdot dS_w \qquad (17).$$

The corresponding expression for imbibition is

$$\Delta W_{external} = \varphi \cdot V_b \int_{So_2}^{So_1} P_c \cdot dS_o \qquad (18).$$

The expressions are valid for reversible and immiscible displacement in the absence of gravity forces, magnetic forces and electric forces.

In reality, the process is not reversible, and is demonstrated by the hysteresis in capillary pressure measurements. Due to complex pore architecture with irregular shaped pore bodies and throats, Haines jumps[5], trapping mechanisms, and probably other mechanisms such as friction, will take place resulting in energy loss. In other words, a drainage curve and a spontaneous imbibition curve should be identical if there was no energy loss during the process.

4. PETROPHYSICAL EXPERIMENTAL TECHNIQUES

The determination of representative capillary pressure curves is of vital importance for the mapping of reservoir fluid distribution. The most frequently used techniques today are centrifugation, the porous plate and the mercury injection technique.

The centrifuge technique

The principle of the centrifuge technique is to invade water saturated core plug with a non-wetting fluid by centrifuging. The method is indirect and depends on models to calculate water saturation. The saturation distribution is non-uniform due to end-effects, which need to be taken care of by the model. The differential pressure across the core plug is calculated from the rotational speed at all stages. The reason for the popularity of this method is the fast turnaround time of the experiment. The disadvantage of the method is that it is impossible to obtain both drainage, spontaneous imbibition, forced imbibition and secondary drainage by centrifuging. In addition, maintaining plug integrity might be questionable due to the force acting on the grains while centrifuging. It is also difficult to combine other petrophyscial measurements, like resistivity index, in conjunction with centrifuging. Very often centrifuges do not have the opportunity to apply representative overburden pressure. In addition, the technique is not suitable for weakly or unconsolidated core material.

The mercury injection technique

The mercury injection method is also an indirect method, which must be converted to the actual fluid system. In a mercury injection experiment, mercury is injected stepwise while differential pressure and injected volume are recorded. In principle, it is possible to establish imbibition curves by reversing the injection pump. However, only the primary drainage curve is believed to be representative. The advantage of the method is that it is fast and simultaneously yields reliable pore size distribution curves due to the large interfacial tension between air and mercury. The method is therefore very useful and popular as a rock-typing tool in complex heterogeneous reservoir interpretations. Very often mercury injection rigs do not have the opportunity to operate with representative overburden pressure acting on the porous medium while injecting.

The porous plate technique

The traditional porous plate technique is very reliable but quite time consuming. The principle of the porous plate technique is to invade a water saturated core plug with a non-wetting fluid by applying a constant displacement pressure stepwise towards irreducible water saturation. The porous ceramic plate is coupled in series with the water saturated porous medium, like a composite core experiment.

History behind porous plate technique

The existence of connate water saturation in zones that produce clean oil was not readily accepted in the early days of petroleum engineering. An interesting review of Torray[21] provides early references to the subject. Schilthuis[22] provided conclusive evidence of the presence of connate water by analysis of cores cut using oil based mud with an extremely low water content. It also became clear that electric logging measurements depended on the presence of connate water. A theoretical reason for the presence of connate water in terms of balance between hydrostatic and capillary forces was first given by Garrison[23].

Once the presence of connate water in zones that produced clean oil was accepted, the problem of determination of connate water distribution in the reservoir by indirect means was addressed. The approach used first by Leverett[3] was to investigate the relationship between capillary pressure and water saturation in various unconsolidated sand packs.

The pressure membrane apparatus was first described by McCullough[24]. A few years later, Bruce and Welge[19] published the application to determine connate water in reservoirs.

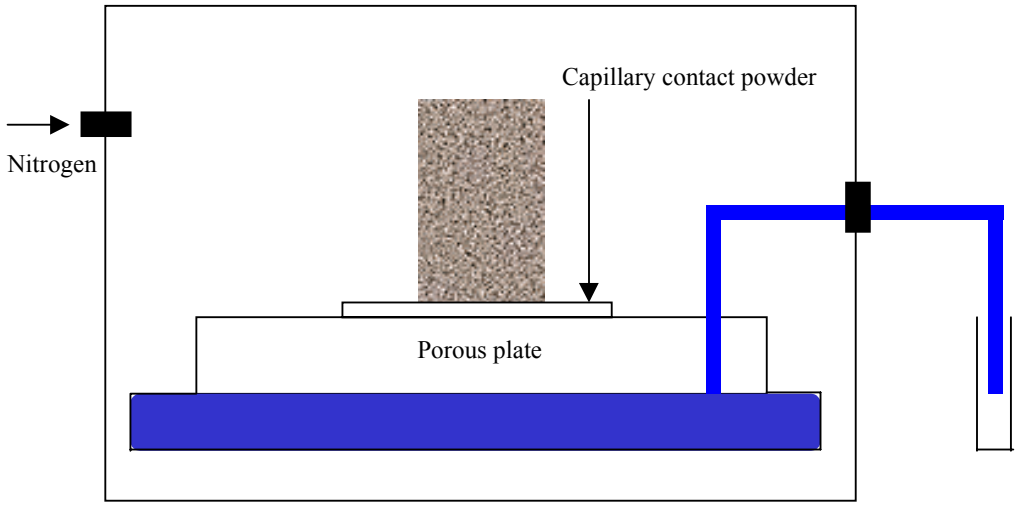

Figure 4.1 Gas-brine capillary pressure measurements by restored state method

Figure 4.1 illustrates a water saturated porous medium coupled in series with a water saturated porous plate in a closed chamber. Capillary contact between the two porous mediums is obtained using a fine contact powder.

The mission of the porous plate is to prevent the non-wetting phase to break through the barrier at all stages of the experiment. This will not happen as long as the capillary pressure is kept

below the entry pressure of the ceramic plate. For incrementally higher pressures, the non-wetting phase will enter the water saturated ceramic plate and the experiment has to be terminated.

Several core plugs can be measured simultaneously inside the chamber. The accumulative expelled brine from core plugs is measured continuously until obtaining equilibrium, i.e. no measurable changes in accumulative water production at each capillary pressure step. Water saturation is therefore calculated by recording changes in weight for each core plug, at each capillary displacement pressure, after taking the samples out of the chamber for a short period.

The effect of wettability on connate water distribution and electrical resistivity is a complex subject. In the early eighties the porous plate method was gradually modified to handle other fluid pairs at more realistic conditions. Longeron[25] transformed the restored state technique to handle net reservoir overburden stress by adopting the principles into individual core holders.

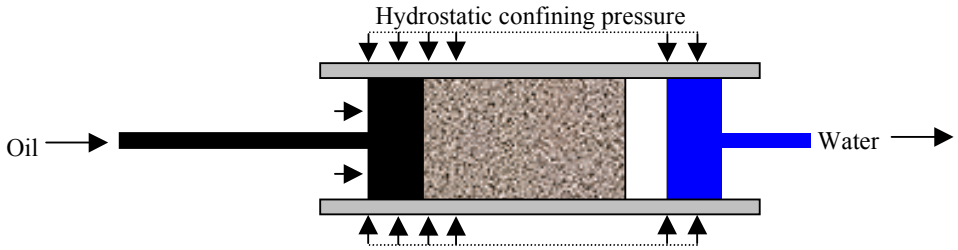

Figure 4.2 Modified restored state method

Figure 4.2 illustrates the principles of the modified restored state technique, known as the porous plate technique today. An individual water saturated ceramic porous plate is mounted in series with the rock, inside a hydrostatic core holder, allowing the measurements to be performed with at representative overburden pressure.

The strength of the porous plate technique is the possibility to establish both primary drainage, spontaneous imbibition, forced imbibition and secondary drainage without changing set up, conditions or method. The method has been used under different conditions since the late eighties[26,27]. If a full cycle curve is required, a hydrophobic version of the ceramic porous plate needs to be mounted in the opposite end of the core plug. The reason for this is to prevent the wetting phase breaking through during all stages of forced imbibition.

Another reason for the popularity of the technique is that its possible to combine experimental capillary pressure curves with other petrophysical measurements such as resistivity or NMR measurements. In addition, the experiment is free of end effects. The disadvantage is that it is

very time consuming. A reliable and representative full cycle capillary pressure curve might take as long as 1-2 years to establish using this method. Due to its reliability, all other techniques are using the porous plate technique as a reference in comparison studies.

During recent decades, different techniques like the membrane technique[6], the continuous injection technique[7], and recently the semi dynamic method[8] have been developed to reduce the amount of time required.

The membrane technique

The membrane technique[6,28,29,30,31] is a fruitful improvement to reduce the experimental turnaround in a capillary pressure experiment. The technique, which is analogous to the standard porous plate technique, has been reported[6] to be more than 30 times faster than the standard porous plate technique. However, the membranes itself seems to have problems in enduring mechanical stress and resisting wettability change when exposed to crude or live oil.

The technique has never been completely accepted in the industry as a replacement for the porous plate technique. The technique requires a special core holder in order to seal the membrane, to prevent fluid from passing around its edge and to protect it from being penetrated by the rough surface of the core sample. This is reported[28,29,30] to be solved by introducing a protecting membrane between the micropore and the rock surface. The core is not exposed to hydrostatic confining pressure.

The continuous injection technique

In the early nineties, a new technique called the continuous injection technique was introduced to the industry as a fast and reliable replacement technique for the porous plate technique. This technique is identical to the traditional porous plate technique except that the experiment is performed using an ultra low constant injection or withdrawal rate instead of using a stepwise constant differential pressure.

When the continuous injection technique was introduced to the industry, it was well accepted. One of the reasons for this is that it frequently showed curved S_w-RI relationships instead of linear relationships, which is often observed for equilibrium data from porous plate technique. It was reported[15] to have the potential for measuring reliable capillary pressure curves simultaneously with reliable and representative S_w-RI relationships. In addition, it was suggested that the method could be used to simultaneously establish representative relative permeability curves. Throughout this research, the potential of the method[11] has been gradually reduced.

5. POROUS PLATES CHARACTERISATION

The reported potential of the membrane tachnique[6] gave birth to the original idea behind this research study. By constructing a layered ceramic porous plate, with customized pore throat morphology, it might be possible to minimise flow restriction, simultaneously with increasing or maintaining threshold pressure. In addition, it has the potential to avoid the reported restrictions observed from the membrane technique.

Pre-study

Keranor, which is a material engineering company in Oslo, were hired to construct a hydrophobic and hydrophilic prototype of layered porous plate, customized for the core laboratory industry. The author's role at this early stage was to experimentally test all the different productions of layered prototypes and report back necessary adjustments prior to modifications.

The main problem the first year was to produce a ceramic substrate with mechanical properties similar to the traditional homogeneous porous plate. After 8 attempts to establish hydrophilic and hydrophobic prototypes, it was finally managed to test reproducible prototypes with high flux and high threshold pressure in conjunction with high mechanical strength.

All prototypes were experimentally tested using the following procedures at Reslab's laboratory:

Testing procedure, hydrophilic prototypes

All batches of produced prototypes were first visually inspected and optically described in a microscopy in order to look for production anomalies. Then, the layered porous plate production was pre-screened by measuring variations in gas permeability. The prototypes were saturated with distilled water (wetting fluid) in vacuum saturator, then mounted into core holders and exposed to confining pressure of 200 bar. Flooding with 100% distilled water was carried out against a low backpressure, until possible gas was removed. This was checked with temperature corrected resistivity measurements with continued distilled water throughput. At this stage water permeability was measured while flooding degassed distilled water through the samples using a multi-flow rate technique.

Differential pressure, flow rate and water temperature were recorded during an initial flooding rate of no more than 120ml/hour. The flow rate was then reduced to 75% of the original and differential pressure, flow rate and water temperature again recorded when stable. This was repeated for a flow rate of 50% and 25% of the original. Using a linear regression analysis of Q/A vs $\Delta P/L$ pairs, Kw was then calculated from Darcy's law.

After measuring water permeability, the saturated prototype was connected to a synthetic oil reservoir on the inlet tubing of the core holder. The pressure on the oil phase was then increased in steps. By measuring expelled water volume in a fine graduated pipette parallel with resistivity measurements across the layered porous plate, we could accurate determine the entry pressure of the oil. The used oil was an Isopar-L (non-wetting fluid) with an IFT of 35.0 mN/m at 20° C.

After detecting the oil-water entry pressure, the layered porous plate were cleaned in a traditional Soxhlet apparatus and dried in a conventional oven at 90 ° C. As a final check, the prototype was screened for gas permeability again followed up by visual inspection and description.

Testing procedure, hydrophobic prototypes

The same testing procedure as described for the hydrophilic-layered porous plate above was used when testing the hydrophobic-layered porous prototypes. The only difference from the above procedure was that we changed the fluid. I.e. using Isopar-L as the wetting fluid and distilled water as the non-wetting fluid.

Homogeneous porous plate

The Soil Moisture type is well known as a homogeneous porous plate with different threshold pressures. The 15 bar (gas/water) version with a diameter of 38.1 mm (1.5”) is the most popular porous plate for use in core analysis. The thickness of this type is 9.5mm. Water flux for a 100% water saturated Soil Moisture 1.5” diameter plate given by the manufacturer to be 0.13 ml/h at 1 bar differential pressure.

It should be noted that Soil Moisture product is originally designed for the soil industry. The core analysis industry has just adopted it for use in special core analysis. This plate is therefore not available in hydrophobic version. Different laboratories use different in-house chemical treatment procedures in order to transform an originally water wet soil moisture version to an oil wet version. The flux properties of standard oil wet porous plates may therefore vary from laboratory to laboratory. Furthermore, the plates needs to be cleaned after use and have therefore a tendency of alternate wettability back to original over time.

Layered porous plate prototype parameters

The layered porous prototypes are called KeraFlux. The structure of this porous plate is shown in Figure 5.1. The layered porous plates have a highly permeable and homogeneous substrate structure with large pore size. This substrate is approximately 4.8 mm thick. On top of the substrate is a top layer with smaller pore size. This layer is constructed as a graded layer with respect to pore size, porosity and composition. Due to the low thickness (0.2 mm) and the

graded nature of this layer, the flux is much higher (about 15-150 times) than the Soil Moisture plate. The total porosity of the prototype is measured to be 32 %.
Table 5.1 presents threshold pressure and flux for the layered hydrophilic and hydrophobic prototypes. Corresponding Soil Moisture data is reported by the manufacturer.

Table 5.1: Porous plate parameters

Parameter	**Layered** Hydrophilic	**Layered** Hydrophobic	**Homogeneous** Hydrophilic	**Homogeneous** Hydrophobic
Diameter	38.1mm	38.1mm	38.1mm	38.1mm
Thickness/length	5 mm	5 mm	9.5 mm	9.5 mm
Average pore size	100nm/4micron	100nm/4micron	160nm	160nm
Pc-max g/w	12 bar	-	15 bar	-
Pc-max o/w	26 bar	-	14 bar	-
Pc-max w/o		18 bar	-	>5 bar
Flux using water	10ml/h @ 1 bar	-	0.13ml/h @ 1bar	-
Flux using oil	-	20ml/h @ 1 bar	-	<0.13ml/h @ 1 bar

Figure 5.1 Layered porous plate constructions

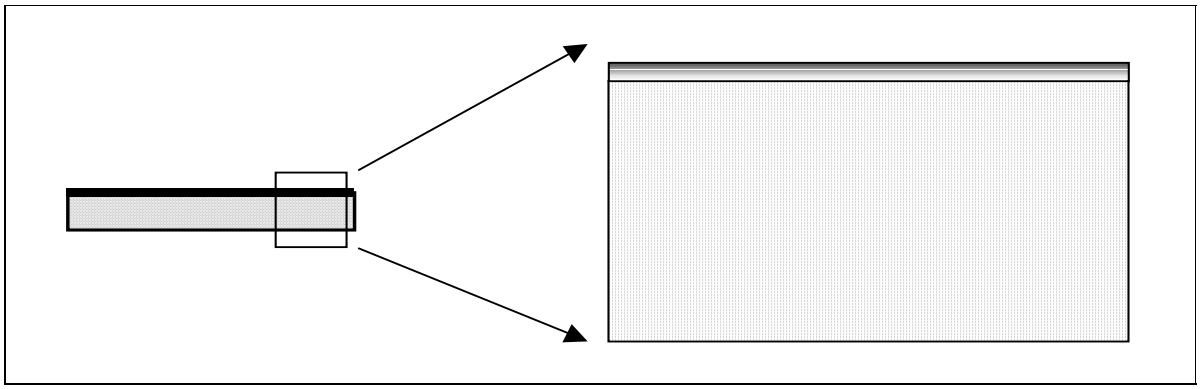

Characterisation of layered porous prototypes

In order to characterise the nature of the final hydrophilic and hydrophobic versions of the prototypes it was decided to use Mercury intrusion and digital SEM image. The digital SEM image in figure 5.2 illustrates the top layer (capillary layer). This is the layer, which will be exposed to the investigated porous media. Figure 5.3 illustrates the graded architecture in the middle of the layered porous plate.

The Mercury injection data in figure 5.4 and figure 5.5 shows that the capillary nature of the layered porous plates can in principle be divided in 3 distinguish layers. Figure 5.4 and 5.5 presents measurements performed on a hydrophilic version of the layered porous plate. The hydrophobic plate is an originally hydrophilic plate, which is treated by the manufacturer.

Figure 5.2 Top layer of a hydrophilic-layered porous plate from SEM

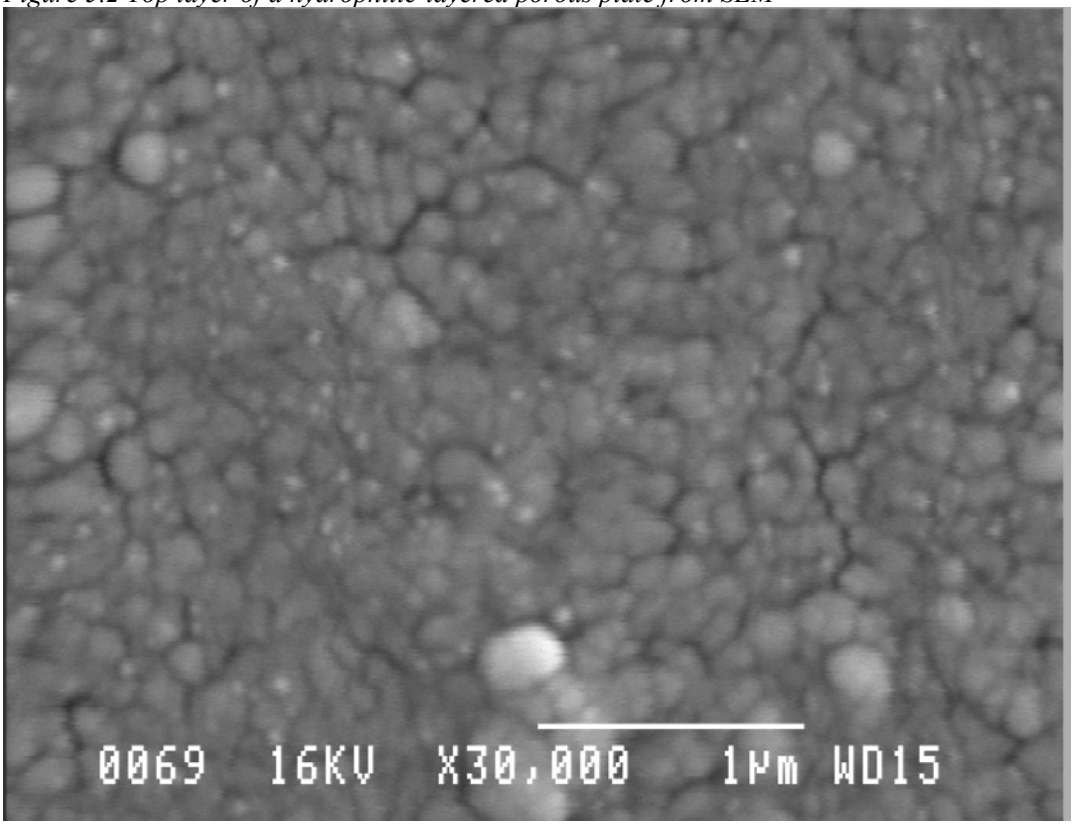

Figure 5.3 Graded layer of a hydrophilic-layered porous plate from SEM

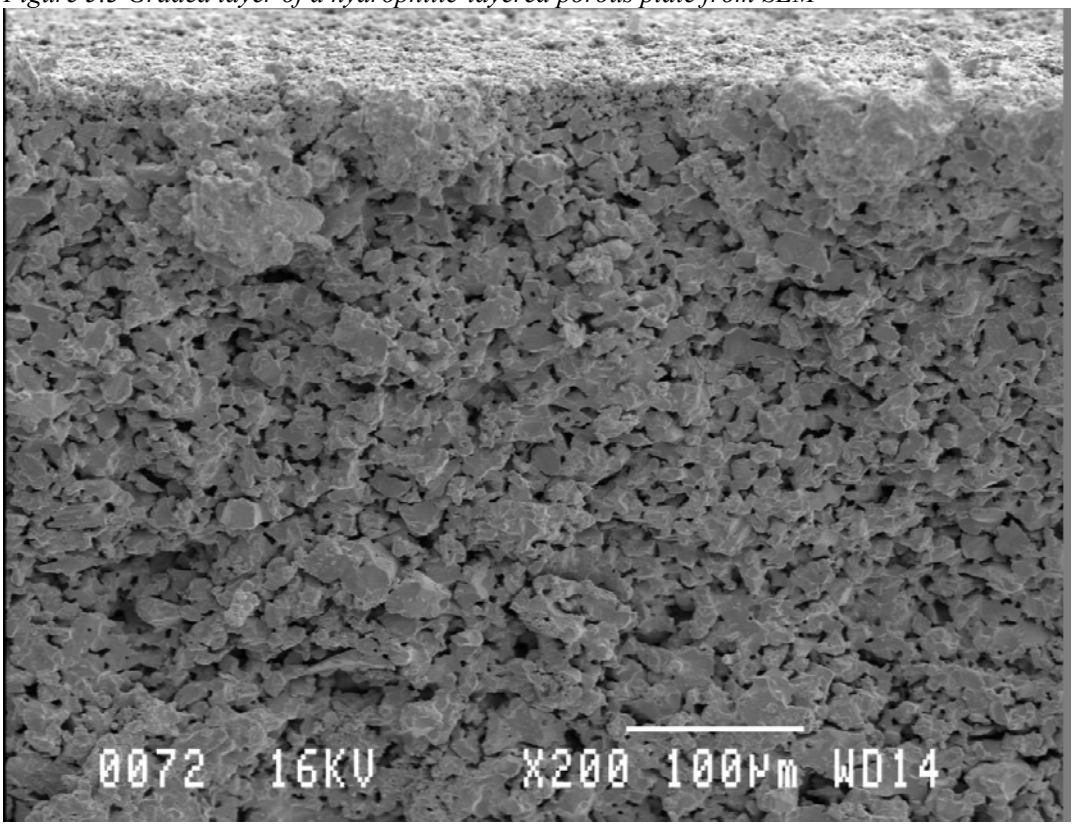

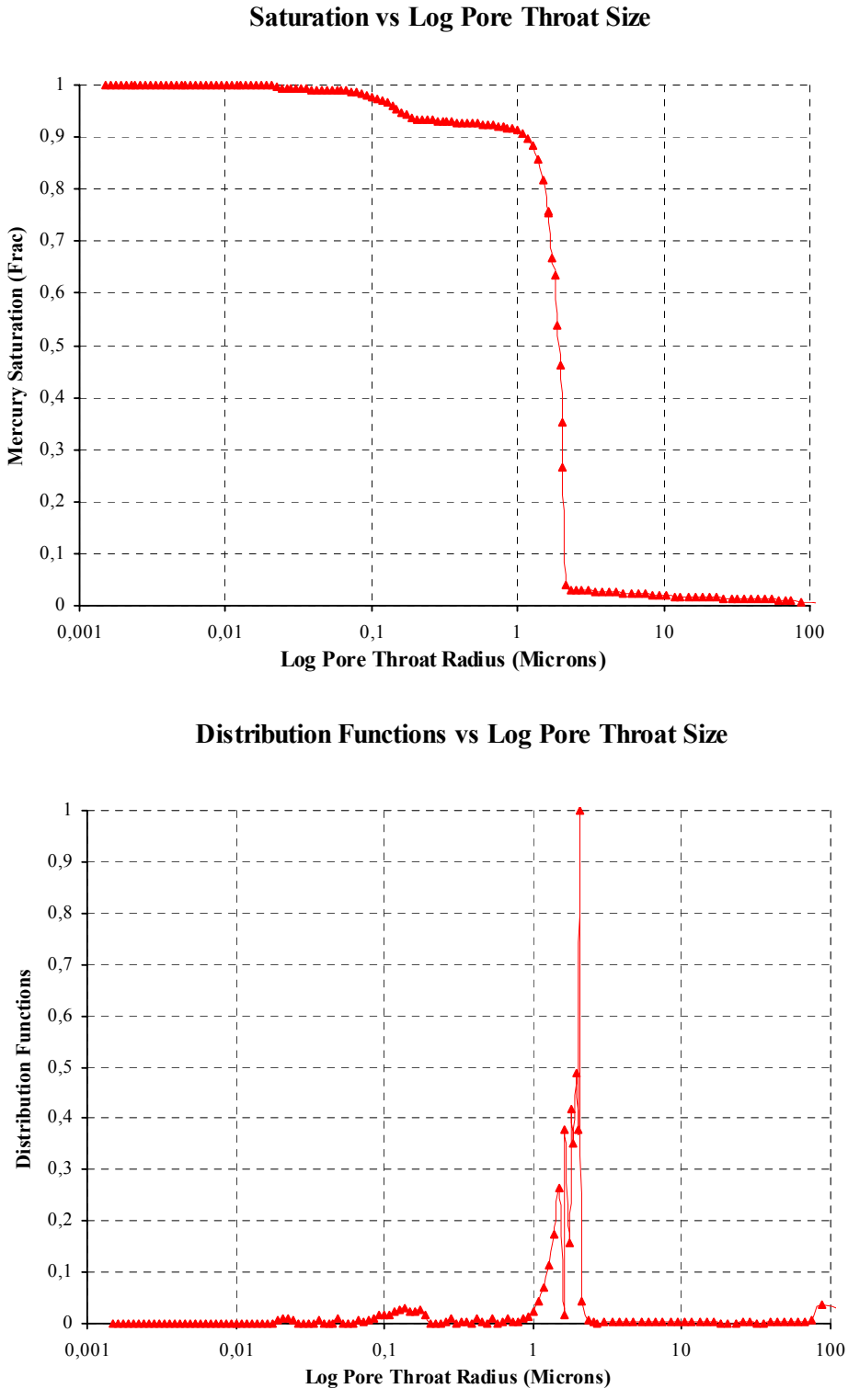

Figure 5.4 Mercury injection data on layered porous hydrophilic prototype

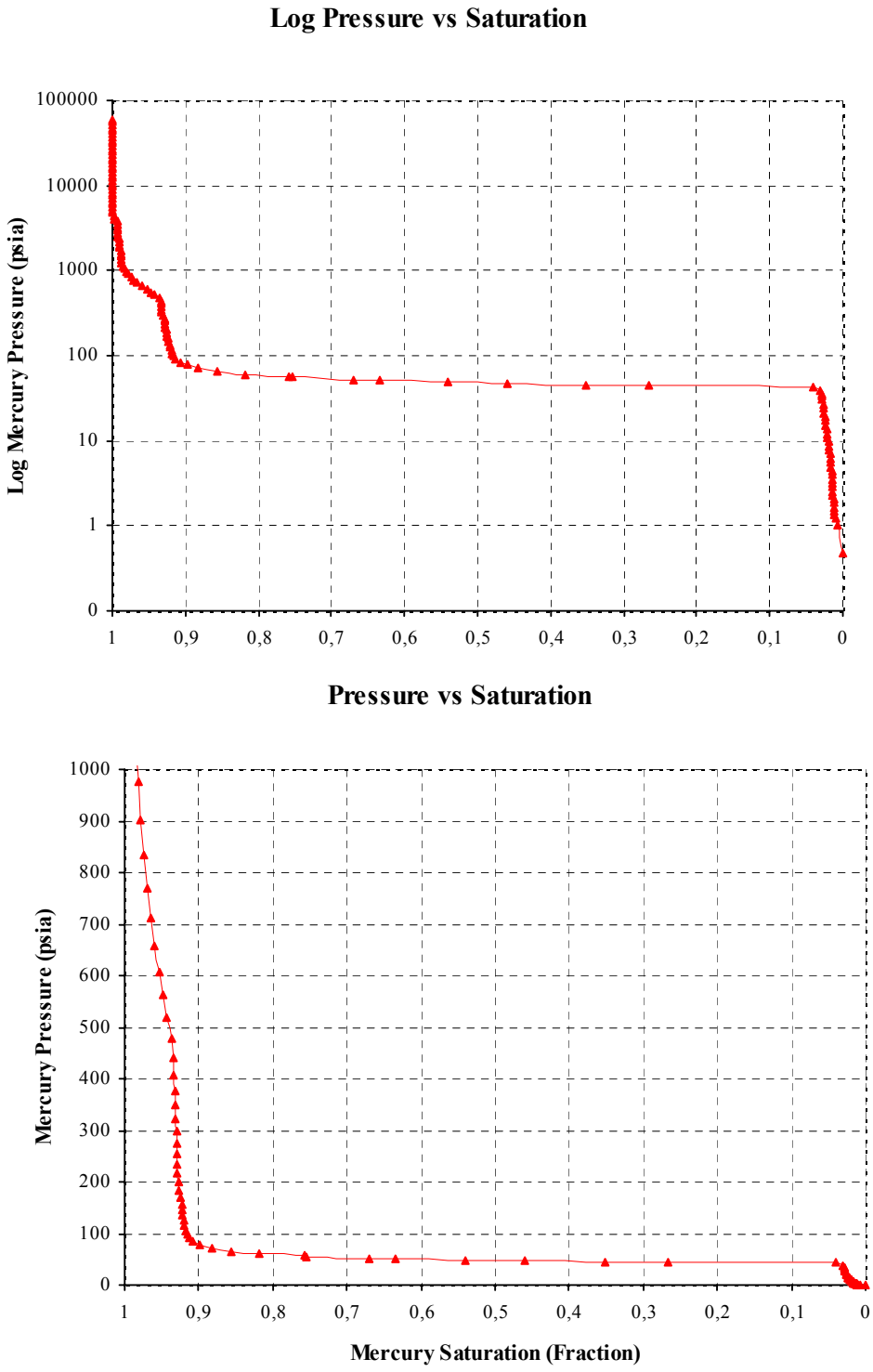

Figure 5.5 Mercury injection data on layered porous hydrophilic prototype

Homogeneous 1 bar porous plates

Ceramic Welterop plates, with a g/w threshold pressure of 1 bar, were used in Program A for the Bentheimer study reported in Chapter 7. This ceramic membrane has a relatively high flux and is normally not suitable for use in special core analysis due to the low threshold pressure. However, in order to study small incremental pressure steps below 450 mbar, which is approximately equivalent to 1 bar gas-water, these plates are suitable.

The petrophysical properties for these plates are reported in table 5.2.

Table 5.2 Petrophysical properties of 1 bar homogeneous plates.

Plug no.	L (cm)	D (cm)	V_{grain} 20°C (cm^3)	V_{bulk} 20°C (cm^3)	V_{pore} 20 bar/20°C (cm^3)	Φ_{He} 20 bar/20°C (frac.)	GD 20°C (g/cm^3)	K_L 20 bar/20°C (mD)
1	0.75	3.81	4.25	8.51	4.26	0.501	3.77	11.9
2	0.78	3.79	4.43	8.84	4.41	0.499	3.77	12.1
3	0.79	3.80	4.44	8.89	4.45	0.501	3.77	12.3
4	0.78	3.80	4.37	8.83	4.46	0.505	3.77	12.5
5	0.74	3.80	4.23	8.49	4.26	0.502	3.77	12.0
6	0.75	3.80	4.25	8.47	4.22	0.498	3.77	11.6
7	0.76	3.80	4.27	8.59	4.32	0.503	3.77	12.3
8	0.78	3.80	4.40	8.80	4.40	0.500	3.77	12.2
9	0.76	3.80	4.30	8.63	4.33	0.502	3.77	12.0
10	0.78	3.80	4.40	8.75	4.35	0.497	3.77	12.1

6. PREPARATION AND BASIC PETROPHYSICAL PROSEDURES.

Standard industry procedures have been used in this study for plug preparation and measurement of basic petrophysical properties of fluids and core material. Below follows a detailed description of the experimental procedure used in this work:

Cleaning procedure

The samples were cleaned using a miscible mixture of 75% toluene and 25% methanol. The samples were then flooded with alternating sequences of toluene and methanol, at a temperature of 70°C, until no discolouration in the effluent was observed. Silver nitrate was added to the methanol effluent in order to verify that all chloride ions were extracted from the plugs.

Saturation procedure

Methanol was displaced from the core plugs by flooding with 100% simulated formation water. Flooding with simulated formation water was carried out against a low backpressure, until ionic equilibrium was reached. This was checked with temperature corrected resistivity measurements after each 50 cc of formation water throughput.

A temperature of 20°C and a backpressure of 5 bar were maintained throughout flooding sequences.

Drying

The core plugs were dried in a heating cabinet at 90 ° C. Plug weights were checked throughout the drying processes to ensure the plugs were completely dry.

Resistivity analysis

The resistivity cell is designed to measure the resistivity of brine at ambient and elevated temperature, with or without pore pressure. Resistivity analysis is carried out in a 55 mm resistivity cell, with a volume of approximately 5 cm^3, using a HP 4276 A LCZ meter.

The resistivity cell is calibrated with a series of KCl standard solutions from 0.01 M up to 4 M in order to establish the cell constant, which is a function of concentration.

Resistivity of the synthetic brine at ambient conditions is performed on the degassed and filtered brine. Resistivity at full reservoir conditions was performed using methane to pressurize the brine up to net pore pressure. After obtaining equilibrium impedance, phase angle and temperature were recorded and resistivity calculated as a function of pore pressure up to net reservoir pore pressure.

Critical point drying

The petrophysical project illustrating application to a gas-brine system for the layered porous plate technique, is from a North Sea gas reservoir with high fibrous illite content. In order to maintain plug integrity, the core plugs needed special treatment with respect to drying.

The cleaned core plugs saturated with methanol were placed in a heating cabinet. The following illustration shows the experimental set-up used for critical point drying and saturation:

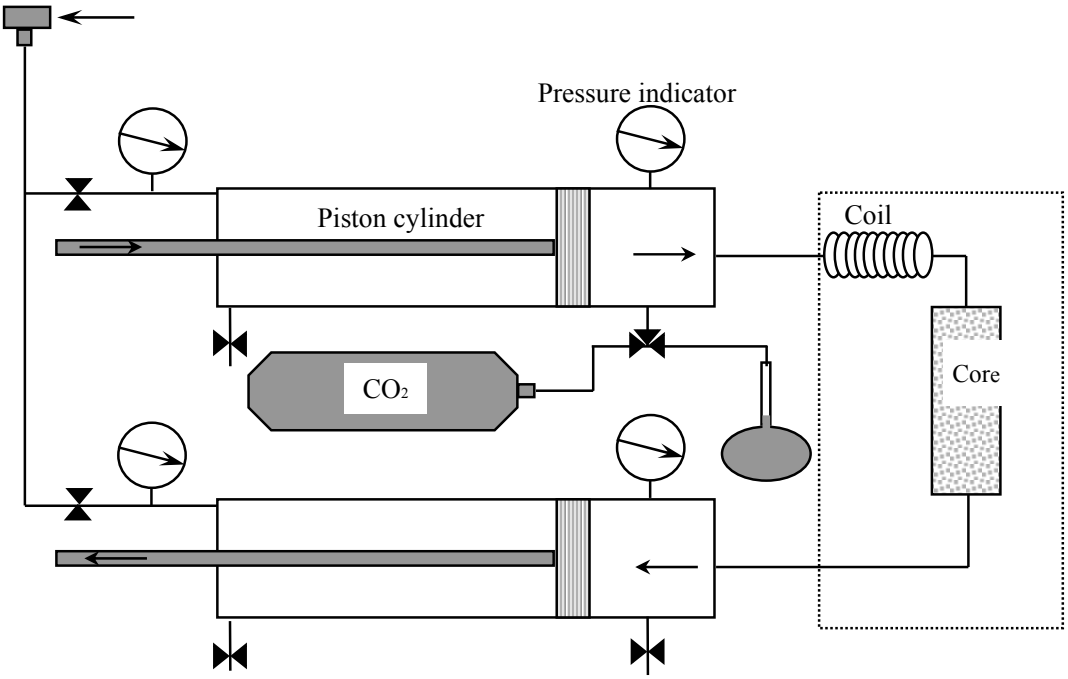

Figure 6.1 Experimental set-up for critical point drying and saturation

Pore and confining pressure were gradually increased until the pore pressure reached 85 bar. Miscible displacement of methanol with liquefied CO_2 was then performed. This was done by increasing the liquid pressure on the inlet piston cylinder, while maintaining constant pressure on the other piston cylinder. Each core plug was flooded with 5 pore volumes of liquefied CO_2. The temperature was then increased to 37° C. This temperature is over the critical point for CO_2. The pore pressure was then gradually decreased to atmospheric pressure, while bleeding gas on the outlet piston cylinder.

Critical point saturation

After measuring basic petrophysical properties, the dried core plugs were saturated with CO_2 gas at 20° C and atmospheric pore pressure. Test temperature was then increased to 37° C. Then the pore pressure was gradually increased to 85 bar. The test temperature was then decreased to 20° C, while maintaining the pore pressure constant. Miscible displacement of liquefied CO_2

with methanol was then performed. Each core plug was flooded with 5 pore volumes of methanol.

Basic petrophysical measurements

Porosity was determined by helium injection using a Boyle's law porosimeter. Pore volume and grain volume were measured. Pore volume was measured while the core plug was installed in the core holder, exposed to a confining pressure of 20 bar NCP. The grain volume was determined with the core plug in a matrix cup, i.e. no confining pressure was applied. Grain density was calculated from the recorded weight of the core plug.

Klinkenberg corrected gas permeability.

Klinkenberg corrected gas permeability was calculated from measurements of gas permeability at four different mean gas pressures. At each mean gas pressure, gas flow rate, backpressure and differential pressure were recorded. Nitrogen gas was used at moderate flow rates, in order to be within a laminar flow regime. The readings were taken at steady state conditions. A net confining pressure of 20 bar NCP and ambient temperature were applied during the measurements.

Liquid permeability.

Water permeability was measured while flooding degassed and filtered simulated formation water through the samples at a constant flow rate. At steady state conditions, differential pressure, flow rate and water temperature were recorded. The measurements were performed against two backpressures. At each backpressure two different flow rates were used, yielding equal permeabilities. A net confining pressure of 20 bar and a temperature of 20° C were applied during the measurements.

Formation resistivity factor

Formation resistivity factor was determined using a two-electrode configuration. The steel end pieces in the core holder were used as electrodes and the plug resistivity was determined from measurements of impedance and phase angle. A current frequency varying from 1-10 kH_z was used in the different measurements.

Water resistivity was determined from measurements of the synthetic formation water in a conductivity cell with platinum electrodes, using a current frequency 1-10 kH_z. The cementation exponent, m, was calculated from Archie's equation using least squares method, given by the expression

$$FF = \frac{R_o}{R_w} = \frac{a}{\Phi^m} \qquad (19),$$

where R_O is the resistivity of the water saturated core plug, R_W is the resistivity of simulated formation water, Φ is fractional porosity, m is the forced fit cementation exponent.

Confining pressure measurements of porosity, permeability and formation resistivity factor.

The following general illustration shows the experimental set-up used for confining pressure measurements:

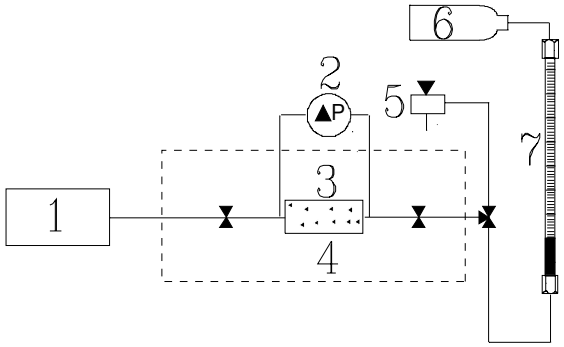

Where: 1. Constant rate water pump.
2. Differential pressure transmitter.
3. Core plug.
4. Heating cabinet.
5. Back pressure regulator.
6. Back pressure.
7. Fine graduate pipette.

Figure 6.2 Experimental set-up for overburden measurements

Confining pressure measurements were carried out in 5 steps from 20 bar up to net reservoir overburden pressure. The first confining pressure is assumed to yield equal porosity to that determined with the Boyle's law helium porosimeter. When increasing the confining pressure up to the next confining pressure, the pore volume reduction was recorded by collecting the expelled water in a fine graduated pipette.

Stability time at each confining pressure was 1 hour before recording the expelled water and repeat measurements of water permeability and formation resistivity factor. A typical example of overburden measurements is illustrated in figure 6.3.

Depth: 4220.47 m.

C.P.	Porosity		Water permeability		Formation factor	
(bar)	(frac)	F.O.O.	(mD)	F.O.O.	FF	F.O.O.
20	0,198	1,000	275	1,000	21,9	1,000
50	0,197	0,995	266	0,969	22,6	1,032
75	0,196	0,990	265	0,965	22,7	1,037
100	0,195	0,985	263	0,956	22,9	1,046
150	0,194	0,980	261	0,948	23,1	1,055
200	0,194	0,980	260	0,944	23,2	1,059

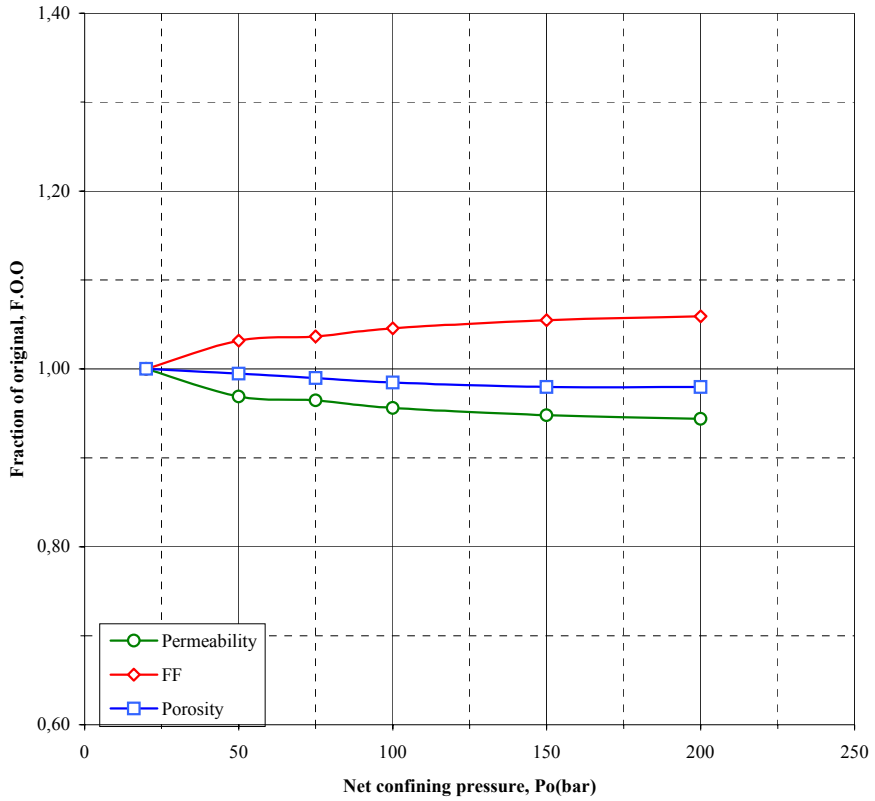

Figure 6.3 Typical example of confining pressure measurement data.

Procedure for mounting porous plates

After measuring the effect of overburden on K_w, FF and Φ, the hydrostatic confining pressure was released back to atmospheric pressure again in order to mount saturated porous plates against the plug ends. Pores and throats expand during this process. A water reservoir was therefore connected to the inlet end of the core holder, allowing external water to imbibe and compensate for the pore volume expansion. The core plugs were then left to equilibrate for 2 days before mounting the saturated ceramic plates.

In order to study porous plate influence on effective drainage and imbibition rates, it was decided to have one ceramic plate present at each capillary sequence. Water wet ceramic plates were therefore first mounted in the opposite end to oil invasion, prior to capillary drainage. For the experiments undergoing forced imbibition in this report, the water wet ceramic plates were dismounted after completing spontaneous imbibition and replaced by saturated oil wet ceramic plates, in the opposite plug end.

For the full reservoir condition experiments, where imbibition is included, the above procedure for mounting ceramic plates is impossible due to the nature of live oil. Live oil will expand and form free gas if pore pressure is released. In this case, both saturated hydrophilic and hydrophobic porous plates need to be mounted prior to initiating capillary drainage. The oil-wet plate was first saturated with stock tank oil and then left to equilibrate towards a live oil reservoir at full reservoir condition prior to capillary drainage.

An oil wet porous plate is an electric isolator. For all experiments performed with such plates, bypassing electrodes were mounted allowing for resistivity index measurements.

After mounting saturated porous plates, the requested conditions were re-established and formation resistivity factor reproduced. This was checked with reistivity measurements with and without porous plates installed. The core plugs are then left to equilibrate at the requested conditions for a minimum of 1 week before initiating capillary drainage. During this aging period resistivity was continuously measured.

Experimental set-up for capillary pressure measurements at ambient and pseudo reservoir condition

The following illustration shows the experimental set-up used for capillary pressure measurements at ambient or pseudo reservoir condition:

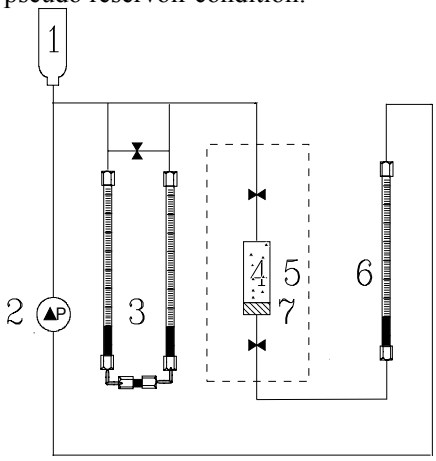

Where: 1. Differential pressure regulator.
2. Differential pressure transmitter.
3. Reservoir for humidified gas, laboratory oil or stock tank oil.
4. Core plug with water wet porous plate.
6. Graduated separator.
7. Porous plate.

Capillary drainage and imbibition

At each pressure step, the drained water was recorded and the impedance measured. Stability criteria at each capillary pressure were no changes in both resistivity and water production over a period and minimum 2-4 days for the different experiments.

For the experiments performed at pseudo reservoir condition, recorded water production is measured at ambient temperature. These measurements are therefore density corrected when calculating saturation.

At irreducible water saturation, the capillary pressure is gradually decreased in steps back to Pc=0 bar again allowing water to spontaneously imbibe into the porous media. The porous plates are then changed in order to describe forced imbibition by lowering the capillary pressure, on the negative side, in steps to Pc=-1 bar. Then, the pressure is increased back to Pc=0 allowing for possible spontaneous re-drainage.

For the investigated Berea samples, it was decided to perform secondary drainage back to irreducible water saturation again. The oil wet porous plates were therefore changed and replaced by water wet ceramic plates again before initiating secondary drainage.

Saturation exponent.

The saturation exponent, n, was calculated using the Archie's equation

$$RI = \frac{R_t}{R_o} = S_w^{-n} \qquad (20),$$

where R_t is the resistivity of the core plug partially water saturated, R_O is the resistivity of the water saturated core plug, S_W is fractional water saturation, and n is saturation exponent.

Karl Fisher titration for saturation determination

At the end of the capillary pressure tests, at ambient or pseudo reservoir condition, the ceramic plates were dismounted from the core holders prior to second cleaning. Then, the core plugs were flooded with toluene and methanol. The effluents from each core plug was analysed for water content using the Karl Fischer titration method.

Capillary pressure measurements at full reservoir condition

A petrophysical study at full reservoir condition requires advanced equipment in order to measure water saturation at high pore pressures. One way of doing this is to use in situ saturation monitoring, from x-ray or gamma ray attenuation, instead of the traditional separator measurements. Below follows the procedures used in the layered porous plate experiment at full reservoir condition using gamma ray:

In order to calculate porosity and saturation variations versus position in the core plug, reliable attenuation coefficients were established with low uncertainty. The attenuation coefficients are conversion factors for the fluid system used, relative to air.

Reliable attenuation coefficients can be established directly in a system when it is saturated with air, brine or oil at representative conditions. These coefficients are unaffected by rock type, sleeve type, core holder etc. as long as these remain constant throughout the scanning period. In order words, reliable attenuation coefficients depend on a constant position, temperature, pressure and counting time when the system is filled with the respective fluids and air. Attenuation coefficients can be determined directly in the core holders when the core plug is dry, water saturated and oil saturated at the required conditions. Or it can be determined in a separate attenuation chamber when this is filled with the same fluids at representative conditions. The result will be exactly the same as long as the test conditions do not change.

Attenuation coefficients were in this study determined directly in a 50 mm diameter attenuation chamber of composite carbon. Then, the following procedure was used to establish attenuation coefficients:

The chamber was first installed in the heating cabinet. Then the test temperature was brought up to reservoir temperature. At stable conditions the dry scan was initially measured and then repeated five times over a period of two days, using 1 hour as the counting time. The gamma position was kept constant throughout each repeated scan. The chamber was then filled with doped brine at reservoir pressure, using a constant pressure Quizix pump. Water saturated scans at reservoir conditions were then established in the same positions, using the same counting time.

Live oil at reservoir conditions was then introduced from the upper end using two Quizix pumps to maintain the reservoir pressure. At stable conditions, oil saturated scans were established in the attenuation chamber in the same positions using the same counting time.

Attenuation coefficients were calculated from the expression

$$\mu_i = \ln(\frac{I_{air}}{I_i}) \cdot \frac{1}{id} \quad (21),$$

where I_{air} is the gamma count when the chamber is filled with air over a period of one hour, I_i is the gamma count when the chamber is filled with a fluid over a period of one hour, and id is the diameter of the attenuation chamber.

In situ saturation monitoring

Below follows a brief description when establishing in situ saturation at reservoir conditions.

Porosity distribution can be calculated as a function of position using the expression

$$\Phi = \frac{\ln(\frac{I_{air}}{I_{water}})}{d \cdot \mu_{water}} \quad (22),$$

where I_{water} is the gamma count on water saturated core plug at reservoir conditions, I_{air} is the gamma count on dry core plug at reservoir conditions, d is the diameter of the rock, and μ_{water} is the attenuation coefficients of water.

Water saturation can then be determined using the expression

$$\ln\left[I(S_w)\right] = \ln(I_{air}) - d\left[\Phi S_w(\mu_{water} - \mu_{oil}) + \Phi\mu_{oil}\right] \quad (23).$$

By solving this equation with respect to S_w and substituting the expression for porosity (18), we obtain the in situ saturation expression

$$S_w = \frac{\ln(\frac{I_{air}}{I}) \cdot \mu_{water}}{\ln(\frac{I_{air}}{I_{water}})} - \frac{\mu_{oil}}{(\mu_{water} - \mu_{oil})} \quad (24),$$

where I is the gamma count on core plug at reservoir conditions at any saturation level.

Procedures for continuous injection technique at ambient conditions

A continuous injection experiment is a very fruitful method with respect to giving fast resistivity data at a significantly reduced experimental turnaround time. The concept behind the technique is to perform the experiment at conditions similar to a capillary-fingering regime.

In order to achieve reliable I-Sw relationships, the most important factor is to perform CI in a completely incompressible environment. In addition, the measurement has to be performed at stable temperature and stress conditions. This is achieved by including following steps when performing continuous injections:

i. Volume flux conservation.

This is obtained by measuring both the volume of the invading fluid and the volume of the expelled defending fluid. The volume of the invading fluid is calculated from cylinder position calibrations. The volume of the expelled water phase is calculated from a calibrated separator.

ii. Injection rate control.

The relationship between the volume injected and the position of the piston in the cylinder is essential in order to calculate saturations based on the volume of the invading phase. This is only achieved by having reliable calibration curves for each cylinder. By monitoring date, hours and minutes relative from the start point of the continuous injection, an effective injection rate can be calculated from volumes and experimental time. This rate should match the set point rate on the ultra-low flow displacement pump. In other words, a quality indicator on the calibration curves.

iii. Constant backpressure.

It is easy to induce small amounts of gas to the composite porous media, i.e. water saturated core plug, slurry and porous ceramic plate, at the different pre-stages prior to injection. It is also easy to induce small amounts of gas when the cylinders are refilled. This is hard to detect without measuring volume flux conservation during measurements. In order to detect all possible incompressibility problems prior to injection, in either the porous media or in the oil cylinders, the backpressure was increased from atmospheric to approximately 2 bar pressure in the total system.

During this procedure it is possible to measure both resistivity and separator changes. If measurable changes on one of the core plugs are detected, it is possible to reject the plug from further analysis and start all over again. If this happens, resistivity changes indicate compressibility problems in the porous composite and separator changes indicate compressibility problems with either the composite or the external oil reservoir in the cylinder.

iiii.Temperature.

To obtain a stable temperature environment of +/- 0.2 degree Celsius, the core plugs have to be installed in a heating cabinet. The core plugs were therefore installed in a heating cabinet at 30° C. The oil cylinders are located outside the heating cabinet. Therefore, a heating cap was built for each of the five cylinders, to yield the same stable temperature on the pump.

Experimental set-up for continuous injection

The following picture shows the experimental set-up used for continuous injection measurements:

The unit basically consists of five Hydratron single shot ultra low flow-metering pumps. The pumps are mounted within a fabricated steel framework together with one central stepper motor, gearbox and an electronic controller mounted remotely from the pump unit.

The controller controls the speed at which the stepper motor revolves. The stepper motor drives up to five pumps via the two 100:1 gear units. Each individual pump has an outer screwed drive nut, which is held within bearings and then in turn drives a screwed shaft either forward or backward. The screwed shafts are in turn connected to hydraulic pistons, which either displace or take in fluid through the inlet or outlet ports. Each of the five singles shot pumps is fitted with Newall linear scales, allowing the piston position to be read digitally.

Each metering pump is surrounded by a heating cap, in order to maintain constant temperature on the inlet fluid reservoir. I. e. the oil phase inside each metering pump.

Calibration routines, continuous injection

Prior to any new continuous injection project, calibration curves for each oil cylinder must be established in the following way:

The relationship between oil pressure versus relative cylinder position is established for each of the five cylinders. This calibration is performed in the pressure interval between atmospheric and 10 bar oil pressure. These curves reflect the compressibility in each cylinder when the total oil volume is largest. The criteria for approval is a minimum three time reproducible curve and at the same time the total compressibility in the system must be less than 0.05 ml in a total volume of 30 ml. I.e. less than 0.2 %.

After mounting the porous plates and the reduction in pore volume measured, the total composite compressibility is checked frequently at room temperature by measuring resistivity with and without backpressure. This is followed by flooding sequences of the composite until resistivity measurements with and without backpressure are negligible. I.e. less than 0.2%

The resistivity of the porous plate itself is also calculated by evaluating the difference between resistivity of 100% water saturated core plugs compared to 100% water saturated composite. The criteria for approval is a total porous plate resistivity contribution less than 5% of the resistivity of 100% water saturated core plug. The derived resistivity index during continuous injection is corrected for porous plate resistivity.

The water saturated composite is installed in the heating cabinet and connected to the injection cylinders. The total composite compressibility between atmospheric pressure and 10 bar is then controlled. Then, the temperature is increased from room temperature to 30° C. The resistivity is controlled against room conditions, the position counter is reset and continuous injection initiated.

During continuous injection the following parameters are continuously recorded at each time step:

i. Oil pressure on the cylinders
ii. Temperature
iii. Water pressure on the separators
iiii. Piston position.
iiiii. Water volume on the separators
iiiiii. Backpressure on the defending phase.

iiiiii. Resistivity of the composite
iiiiiii. Zero point resistivity in the LZR instrument.

Below follows a description of the calculation steps.
i. Pseudo-capillary pressure is calculated as the pressure difference between the two respective fluid phases using the expression

$$P_o - P_W \tag{25}.$$

ii. Volume of oil injected is calculated from the expression

$$(\nabla_o \cdot (\lambda_n - \lambda_0) \cdot \rho(t)) - V_L - C_o(P_o) \tag{26},$$

where ∇_o is the volume gradient of each cylinder, λ_n is the position of the cylinder at time step n, λ_0 is the initial set point position prior to injection, $\rho(t)$ is the density of the invading fluid at the measured temperature divided by the same density at reference temperature, V_L is the dead volume in the inlet end piece of the core holders initially filled with the defending fluid, and $C_o(P_o)$ is the compressibility value as a function of the pressure at time step n.

iii. Volume of expelled water is calculated from the expression

$$(\nabla_w \cdot (h_n - h_0) \cdot \rho(t)) - V_L \tag{27},$$

where ∇_w is the volume gradient of each separator, h_n is the water level in the separator at time step n, h_0 is the reference water level in the separator prior to injection, $\rho(t)$ is the density of the defending fluid at the measured temperature divided by the same density at reference temperature, and V_L is the dead volume in the inlet end piece of the core holders initially filled with the defending fluid.

iiii. Mass balance is calculated as the volume difference

$$V_o - V_w \tag{28},$$

where V_o is the calculated volume of invaded fluid, and V_w is the calculated volume of defending fluid.

iiiii. Effective drainage rate are calculated from the expression

$$((\nabla_o \cdot (\lambda_n - \lambda_0) \cdot \rho(t)) - C_o(P_o)) / (24 \cdot \Delta t) \quad (29),$$

where Δt is the cumulative experimental time.

iiiiii. Continuous resistivity is Arp's corrected from the expression

$$(Z_n - Z_s) \cdot \frac{t + 21.5}{t_{ref} + 21.5} - Z_p \quad (30),$$

where Z_n is the resistivity measured at time step n, Z_s is the zero set point resistivity, t is the temperature at time step n, t_{ref} is the reference temperature, and Z_p is the resistivity of the porous plate including the kaolin slurry.

iiiiiii. Water saturation, resistivity index and saturation exponent are calculated from the expressions

$$S_w = 1 - \frac{V_o}{V_p} \text{ and } RI = \frac{R_t}{R_o} \text{ and } I = S_w^{-n} \quad (31),$$

where V_o is the cumulative volume of invading fluid, V_p is pore volume at net overburden confining pressure, R_t is the corrected resistivity of the porous media at time step n, and R_o is the corrected resistivity at of the 100% water saturated porous media.

7. CAPILLARY DRAINAGE AND IMBIBITION ON BENTHEIMER OUTCROPS.

A study on 10 Bentheimer outcrops has been performed in several stages. Bentheimer is known as a homogeneous outcrop. Unlike other reference outcrops, there is little or no structural clay in these rocks.

The idea behind using this rock type was to form a platform with data by using them in different types of experiments, in several programs. Clay rich rock types might not be comparable if they are used several times in different programs. In addition, results might not be reproducible for the same experiment.

The 10 Bentheimer outcrops have been used in 3 different programs. In the first program, it was decided to investigate the influence of the amount of incremental capillary pressure steps on derived water saturation and resistivity index. This was investigated by using the standard porous plate method. Experiment 1 was drained in ten steps from Pc=15 mbar up to P_c=230 mbar, while experiment 10 was drained in one step at P_c=230 mbar

After cleaning and re-saturating the ten core plugs, it was decided to initiate capillary drainage and resistivity index by the continuous injection method. Rate influence on Sw-RI relationship was investigated by applying different injection rates. Eight experiments were initiated with layered porous plates, while the remaining two experiments were initiated with homogeneous porous plates in order to investigate the diaphragm influence on continuous injection data.

In the third program it was decided to compare the layered porous plate technique with the homogeneous porous plate technique for capillary drainage, imbibition and secondary drainage process.

At the end of the third experimental study, pore size distribution from mercury intrusion was established on end trims.

Basic petrophysical properties of outcrops

Basic petrophysical properties of the Bentheimer outcrops were established prior to capillary drainage and imbibition by using the technical standard procedures described in section 6.

Table 7.1 Porosity on Bentheimer rocks determined by helium injection

Plug no.	L (cm)	D (cm)	V_{grain} 20°C (cm^3)	V_{bulk} 20°C (cm^3)	V_{pore} 20 bar/20°C (cm^3)	Φ_{He} 20 bar/20°C (frac.)	GD 20°C (g/cm^3)
1	7.35	3.75	61.42	80.15	18.73	0.234	2.64
2	6.89	3.76	56.56	74.81	18.25	0.244	2.64
3	6.25	3.75	51.94	67.92	15.98	0.235	2.63
4	6.09	3.76	50.71	66.28	15.57	0.235	2.63
5	5.84	3.75	49.55	63.79	14.24	0.223	2.63
6	5.76	3.75	47.75	62.69	14.94	0.238	2.63
7	5.68	3.75	47.00	61.57	14.57	0.237	2.63
8	5.68	3.76	47.25	61.83	14.58	0.236	2.63
9	5.07	3.75	42.22	54.95	12.73	0.232	2.63
10	4.83	3.75	39.74	52.06	12.32	0.237	2.63

Table 7.2Permeabilities and formation resistivity factors on outcrops

Plug no.	L (cm)	D (cm)	K_W 20 bar/20°C (mD)	K_L 20 bar/20°C (mD)	FF 20 bar/20°C	FF 200 bar/20°C
1	7.35	3.75	1921	3280	12.4	13.1
2	6.89	3.76	2767	5210	11.2	11.8
3	6.25	3.75	2641	4100	11.6	12.6
4	6.09	3.76	1803	3360	12.5	13.0
5	5.84	3.75	1769	2650	13.3	14.1
6	5.76	3.75	2289	4580	11.6	12.2
7	5.68	3.75	1773	3690	12.1	12.5
8	5.68	3.76	3024	4160	11.7	12.2
9	5.07	3.75	2714	3760	12.5	12.9
10	4.83	3.75	3031	4220	11.8	12.3

20 bar NCP		
no.:	Φ(frac.)	KL(mD)
1	0,234	3280,0
2	0,244	5210,0
3	0,235	4100,0
4	0,235	3360,0
5	0,223	2650,0
6	0,238	4580,0
7	0,237	3690,0
8	0,236	4160,0
9	0,232	3760,0
10	0,237	4220,0

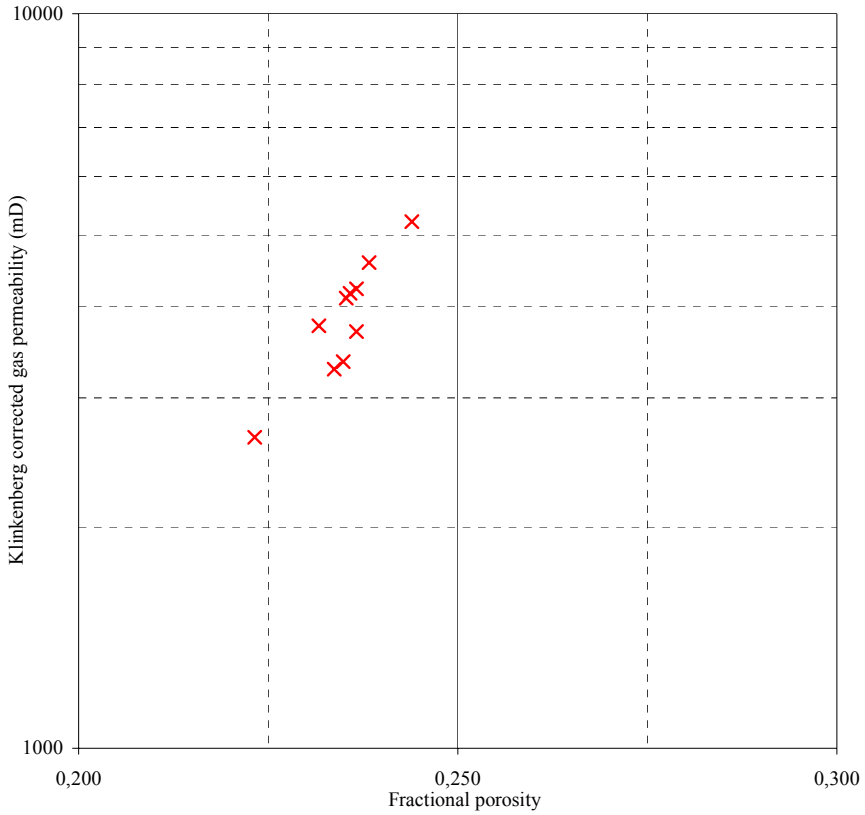

Figure 7.1 Klinkenberg corrected gas permeability versus porosity, Bentheimer samples.

20 bar NCP		
no.:	K_w(mD)	K_L(mD)
1	1921	3280
2	2767	5210
3	2641	4100
4	1803	3360
5	1769	2650
6	2289	4580
7	1773	3690
8	3024	4160
9	2714	3760
10	3031	4220

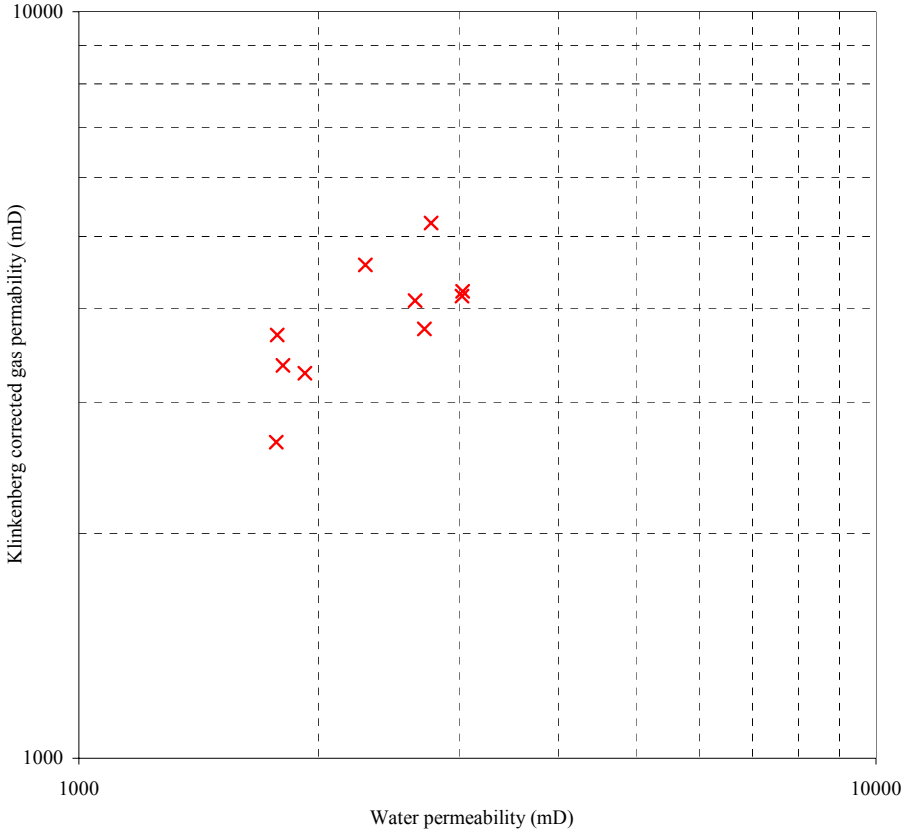

Figure 7.2 Water permeability versus Klinkenberg corrected gas permeability, Bentheimer samples.

m: 1.76
20 bar NCP

no.:	Φ(frac.)	FF
1,0	0,234	13,05
2,0	0,244	11,81
3,0	0,235	12,61
4,0	0,235	12,86
5,0	0,223	14,11
6,0	0,238	12,43
7,0	0,237	12,52
8,0	0,236	12,78
9,0	0,232	12,92
10,0	0,237	12,56

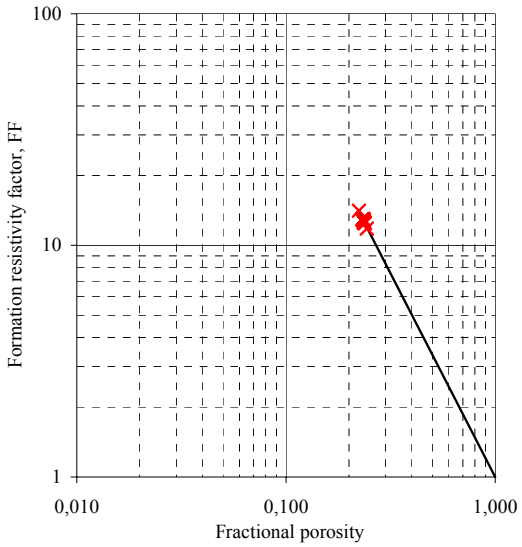

m: 1.78
200 bar NCP

no.:	Φ(frac.)	FF
1	0,226	14,13
2	0,235	12,93
3	0,227	13,56
4	0,227	14,02
5	0,216	15,55
6	0,230	13,64
7	0,229	13,63
8	0,228	13,92
9	0,224	14,13
10	0,229	13,82

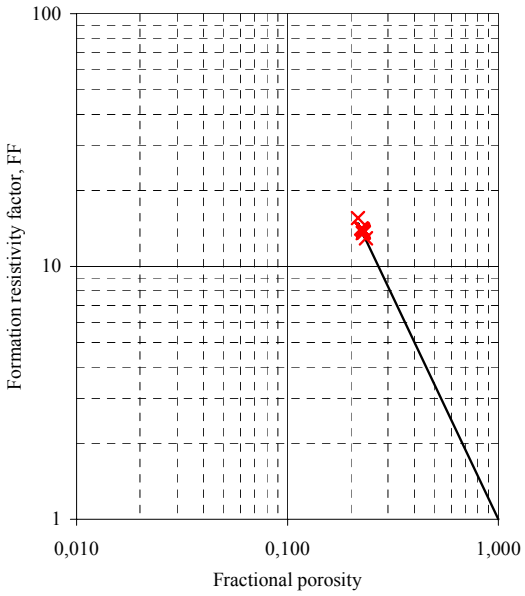

Figure 7.3 Cementation exponents, Bentheimer samples.

Experimental program on Bentheimer outcrops

In order to maintain focus on the main aim of this study, it was decided to design the experimental program, on Betheimer rocks, in 3 stages.

Program A was designed to study the influence of incremental capillary pressure steps on achieved saturation and resistivity behaviour. Prior to a sophisticated relative permeability programs at reservoir conditions, irreducible water saturation is often established by using a single stage porous plate method. I.e. applying oil-water capillary pressure of Pc=5 bar directly, without going in steps.

As an alternative to the continuous injection technique, a new technique called the FRIM method[9] has been introduced to the industry. This method is a fast method to establish Sw-RI relationships. This method applies constant capillary pressure steps instead of using a constant injection rate for establishing the Sw-RI relationship. The capillary pressure is increased in three steps towards irreducible water saturation, without waiting for equilibrium.

Program B was designed to study the influence of injection rate on Sw-RI relationships, subsequently investigating porous plate type influence on experimental data.

After performing primary drainage in program A and B, spontaneous imbibition was checked by lowering the capillary pressure down to P_c=0 mbar directly without going in steps or waiting for equilibrium.

Program C was designed to study porous plate influence on capillary drainage, imbibition and secondary drainage by using traditional and layered porous plate methods.

At the end of program C, mercury injection was performed on a selection of end trims, in order to establish pore size distribution.

The following experimental program was undertaken:

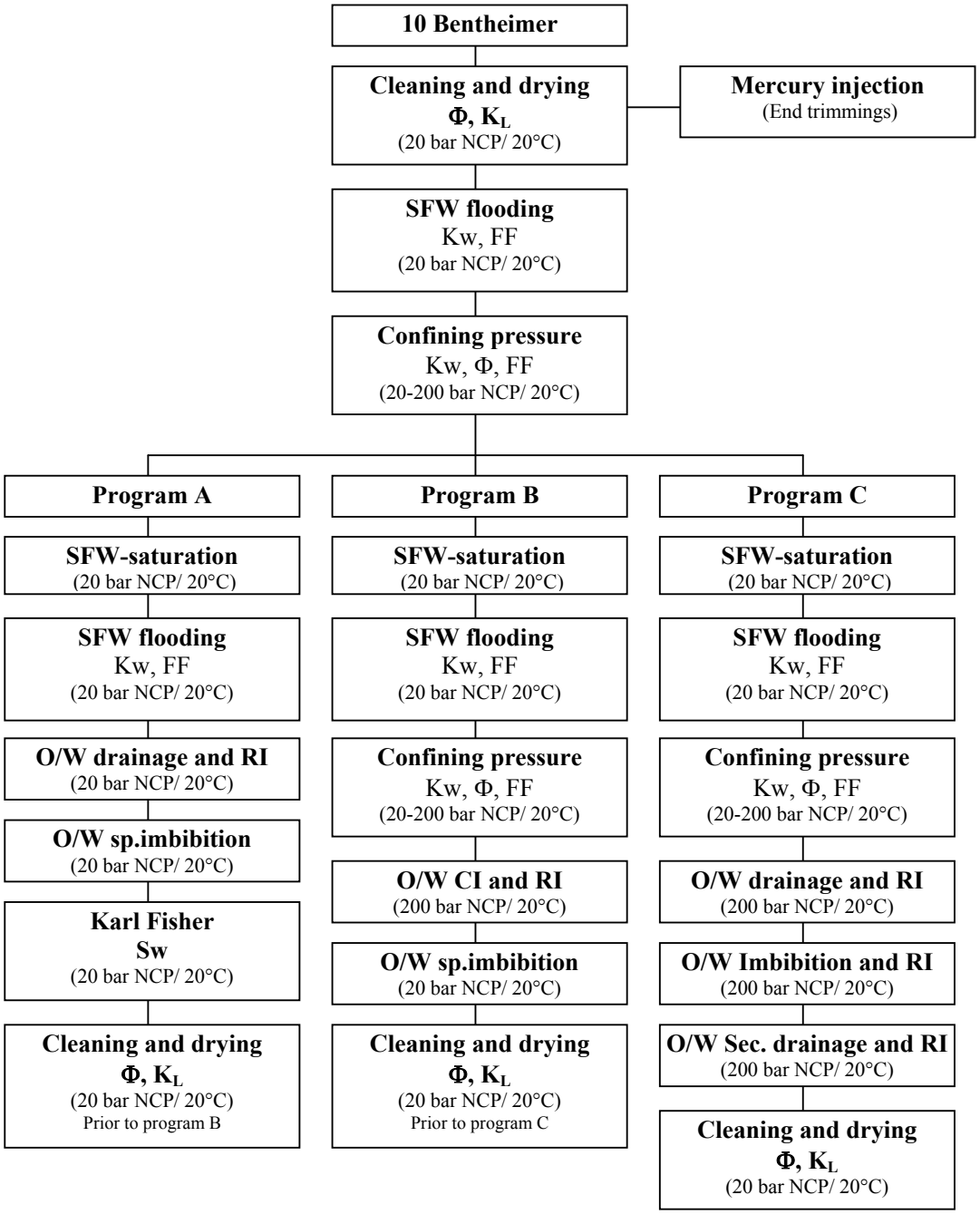

Figure 7.4 Experimental programs on Bentheimer rocks.

Program A

Program A was designed to study the plateau level of the L-shaped primary drainage capillary pressure curve, where most of the de-saturation occurs. A summary of the capillary pressure data obtained in program A is reported in table 7.3 and in Appendix A.

Table 7.3 Summary of capillary pressure data, program A

Plug no.	P_c Steps 20 bar NCP (no.)	Φ_{He} 20 bar NCP (frac.)	K_L 20 bar NCP (mD)	K_W 20 bar NCP (mD)	S_{wi} 20 bar NCP Production (frac.)	$S_{w(Pc=0)}$ 20 bar NCP Production (frac.)	$S_{w(Pc=0)}$ 20 bar NCP Karl Fisher (frac.)	n 20 bar/20°C
1	10	0.234	3280	1921	0.163	0.641	0.641	1.91
2	9	0.244	5210	2767	0.112	0.630	0.629	1.86
3	8	0.235	4100	2641	0.111	0.634	0.634	1.76
4	7	0.235	3360	1803	0.107	0.632	0.632	1.78
5	6	0.223	2650	1769	0.115	0.665	0.664	1.84
6	4	0.238	4580	2289	0.106	0.657	0.658	1.75
7	4	0.237	3690	1773	0.121	0.631	0.631	1.79
8	3	0.236	4160	3024	0.119	0.624	0.623	1.81
9	2	0.232	3760	2714	0.144	0.629	0.629	1.87
10	1	0.237	4220	3031	0.123	0.626	0.625	1.83

It was decided to use homogeneous porous plate types with a gas-water threshold pressure of 1 bar in Program A. These plates are normally not suitable for use in special core analysis due to the low threshold pressure. However, in order to study small incremental pressure steps below 450 mbar, which is approximately equivalent to 1 bar gas-water, these plates are suitable.

The capillary pressures were selected individually for each core plug in order to generate different drainage rates. The following capillary pressures were selected for the core samples:

Core plug no. 1 : 15-25-50-60-80-115-140-160-190-230 mbar
Core plug no. 2 : 25-35-50-80-115-140-160-190-230 mbar
Core plug no. 3 : 50-60-80-115-140-160-190-230 mbar
Core plug no. 4 : 80-115-140-160-190-210-230 mbar
Core plug no. 5 : 115-140-160-190-210-230 mbar
Core plug no. 6 : 140-160-190-230 mbar
Core plug no. 7 : 160-190-210-230 mbar
Core plug no. 8 : 190-210-230 mbar
Core plug no. 9 : 210-230 mbar.
Core plug no. 10: 230 mbar

Experimental set-up, program A

It was decided to use a simple set up for the first experimental stage of this study. Small variations in reference height inside the oil and water separators, pay an impact on applied effective capillary pressure bellow Pc=230 mbar. Individual oil reservoirs, with a large volume gradient, were therefore built in order to apply individual capillary pressure steps for each of the core plugs.

Figure 7.5 shows the core holders and reservoirs used for program A. The capillary pressure was increased by adjusting the height of the oil reservoir relative from the reference level of the water reservoir.

The following picture shows the experimental set-up used for capillary pressure measurements:

Figure 7.5 Experimental set-up, program A.

Bentheimer sample no.	: 1
Porous plate type	: Homogeneous 1 bar plate
Water permeability at 20 bar NCP (mD)	: 1921
Porosity at 20 bar NCP (frac.)	: 0.234
Water saturation at Pc=230 mbar	: 0.163
n exponent	: 1.91

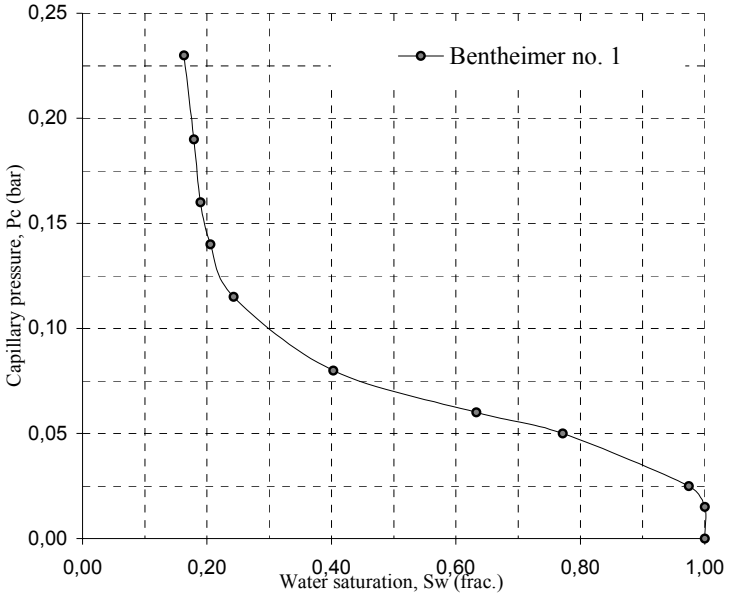

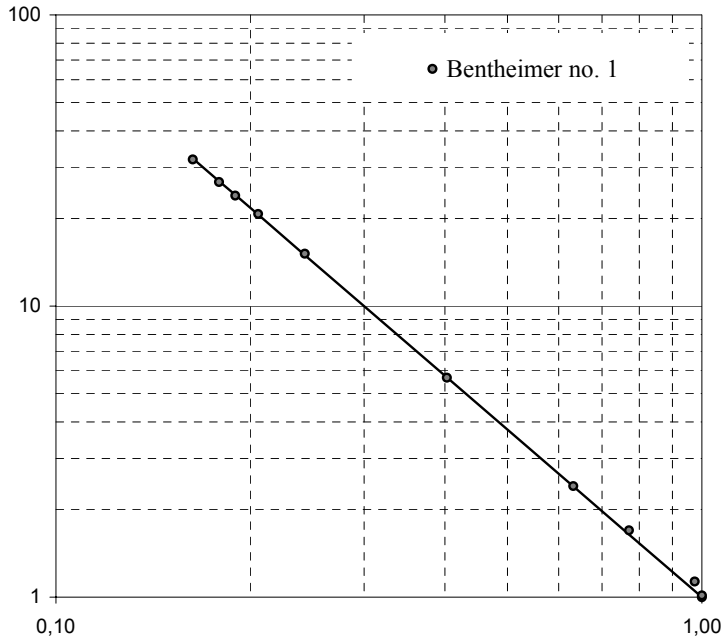

Figure 7.6 Primary drainage and resistivity index, program A, Bentheimer no.1.

Bentheimer sample no.	: 2
Porous plate type	: Homogeneous 1 bar plate
Water permeability at 20 bar NCP (mD)	: 2767
Porosity at 20 bar NCP (frac.)	: 0.244
Water saturation at Pc=230 mbar	: 0.112
n exponent	: 1.86

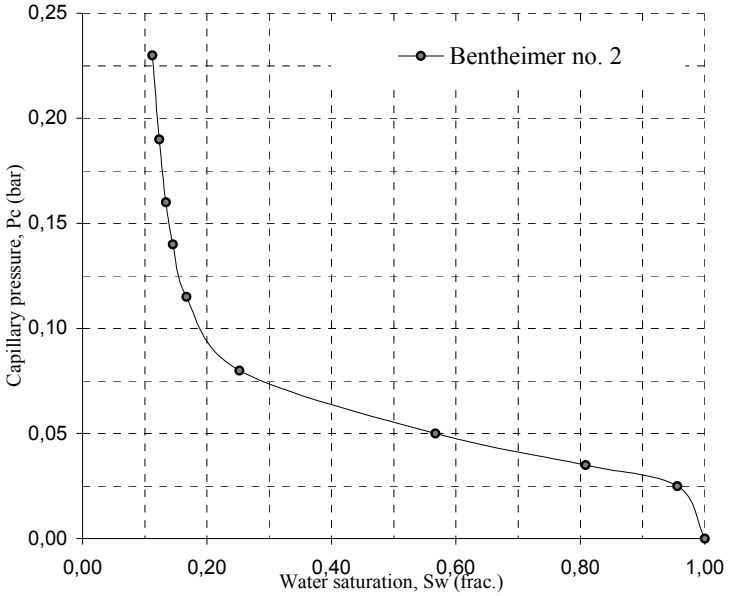

Figure 7.7 Primary drainage and resistivity index, program A, Bentheimer no.2.

Bentheimer sample no.	: 3
Porous plate type	: Homogeneous 1 bar plate
Water permeability at 20 bar NCP (mD)	: 2641
Porosity at 20 bar NCP (frac.)	: 0.235
Water saturation at Pc=230 mbar	: 0.111
n exponent	: 1.76

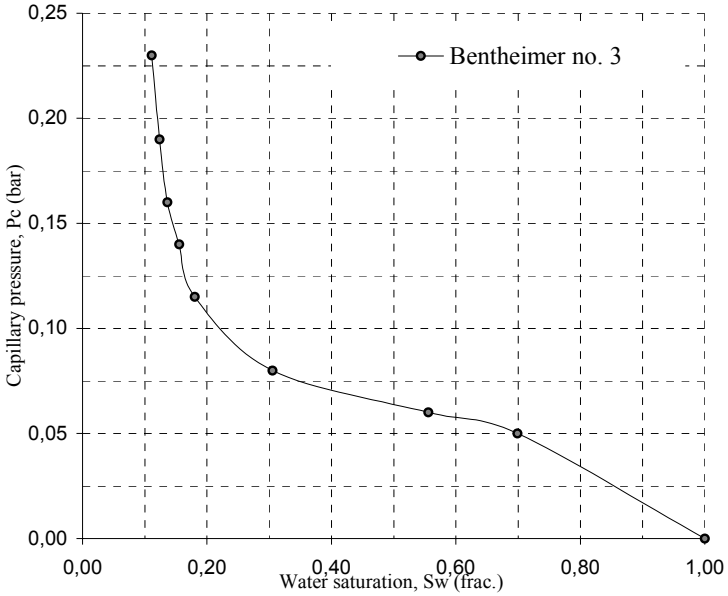

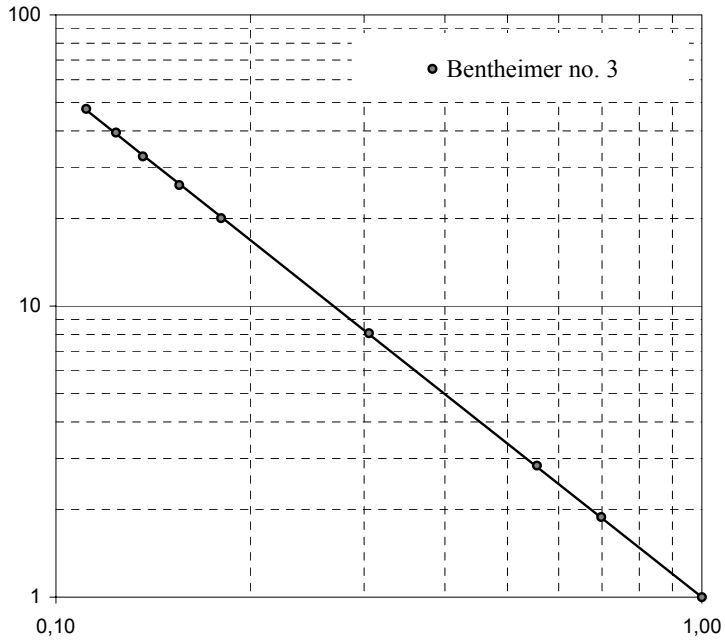

Figure 7.8 Primary drainage and resistivity index, program A, Bentheimer no.3.

Bentheimer sample no.	: 4
Porous plate type	: Homogeneous 1 bar plate
Water permeability at 20 bar NCP (mD)	: 1805
Porosity at 20 bar NCP (frac.)	: 0.235
Water saturation at Pc=230 mbar	: 0.107
n exponent	: 1.78

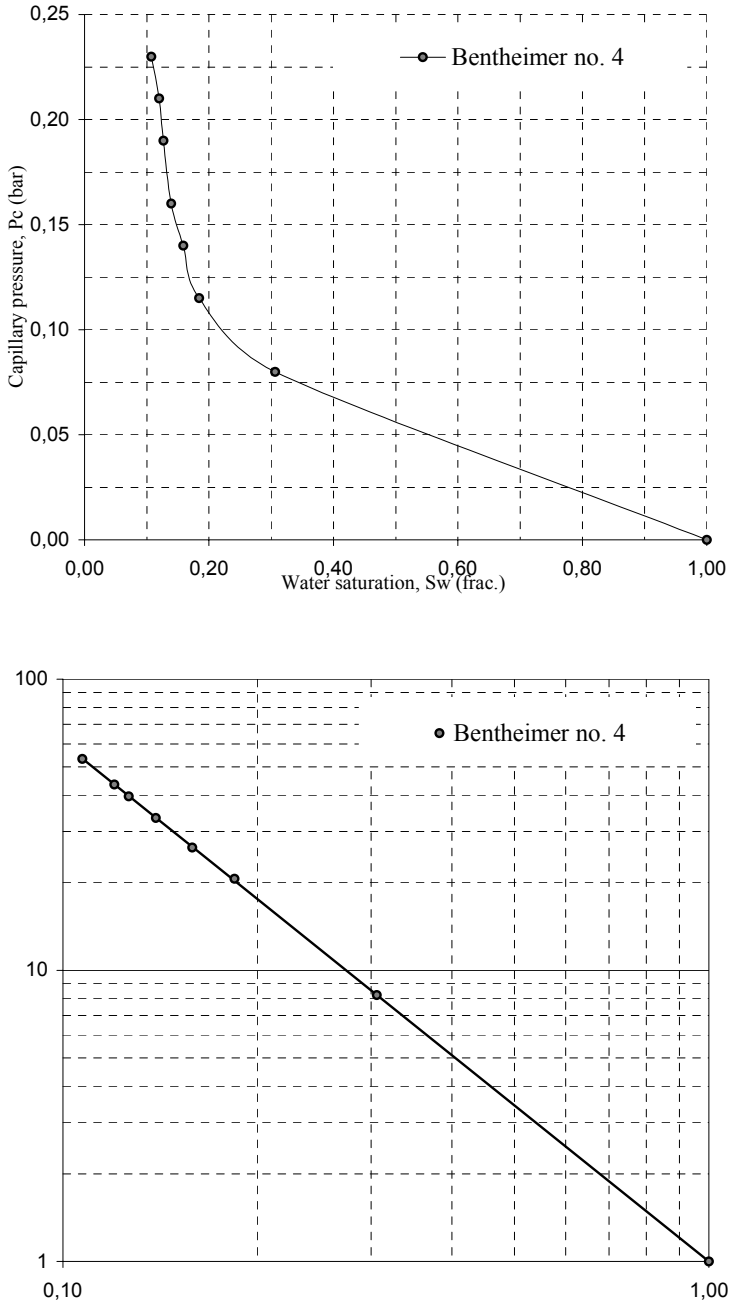

Figure 7.9 Primary drainage and resistivity index, program A, Bentheimer no.4.

Bentheimer sample no.	: 5
Porous plate type	: Homogeneous 1 bar plate
Water permeability at 20 bar NCP (mD)	: 1769
Porosity at 20 bar NCP (frac.)	: 0.223
Water saturation at Pc=230 mbar	: 0.115
n exponent	: 1.84

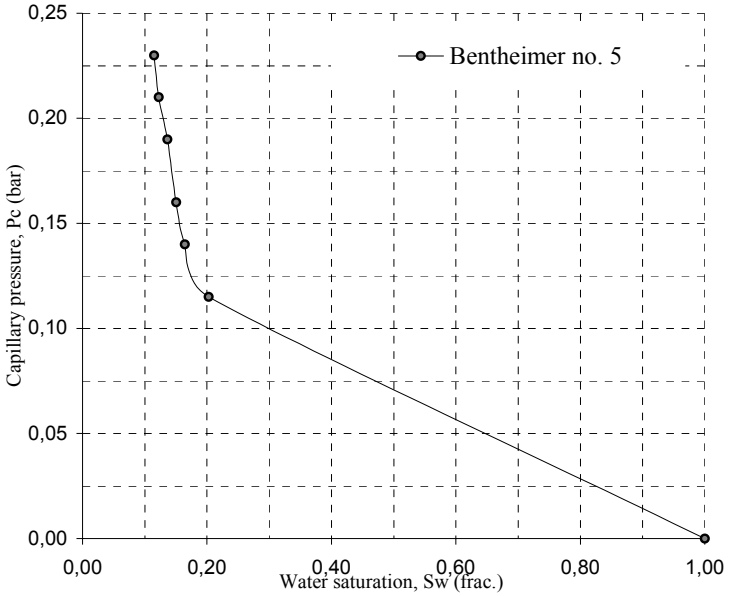

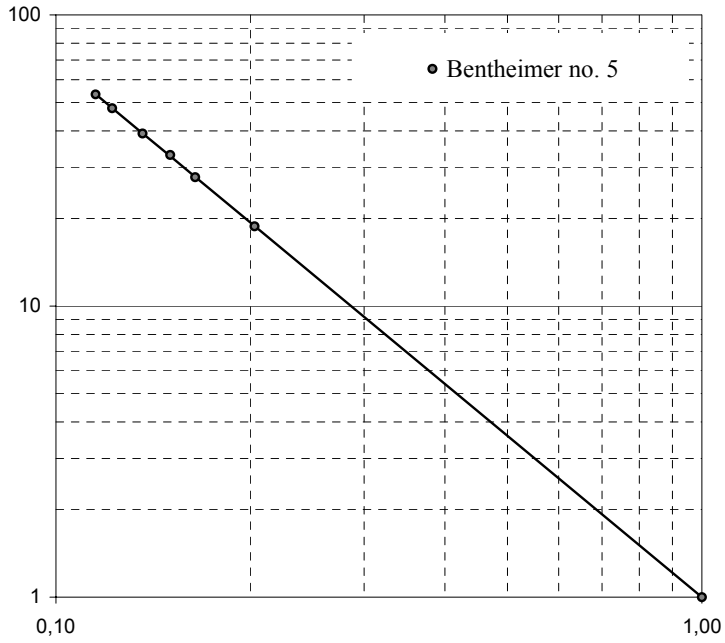

Figure 7.10 Primary drainage and resistivity index, program A, Bentheimer no.5.

Bentheimer sample no.	: 6
Porous plate type	: Homogeneous 1 bar plate
Water permeability at 20 bar NCP (mD)	: 2289
Porosity at 20 bar NCP (frac.)	: 0.238
Water saturation at Pc=230 mbar	: 0.106
n exponent	: 1.75

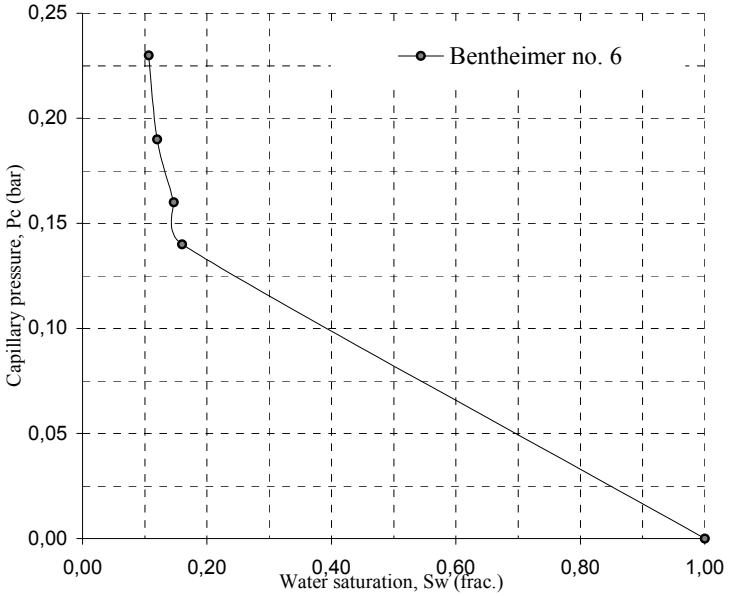

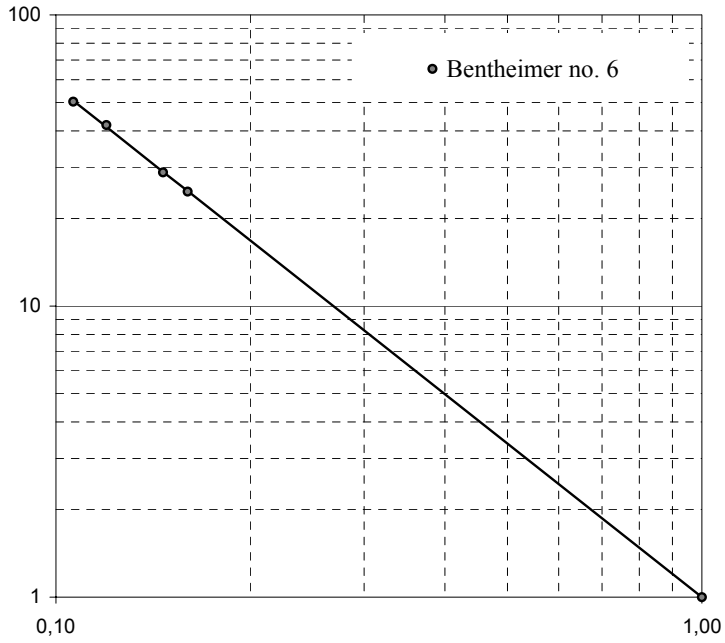

Figure 7.11 Primary drainage and resistivity index, program A, Bentheimer no.6.

Bentheimer sample no.	: 7
Porous plate type	: Homogeneous 1 bar plate
Water permeability at 20 bar NCP (mD)	: 1773
Porosity at 20 bar NCP (frac.)	: 0.237
Water saturation at Pc=230 mbar	: 0.121
n exponent	: 1.79

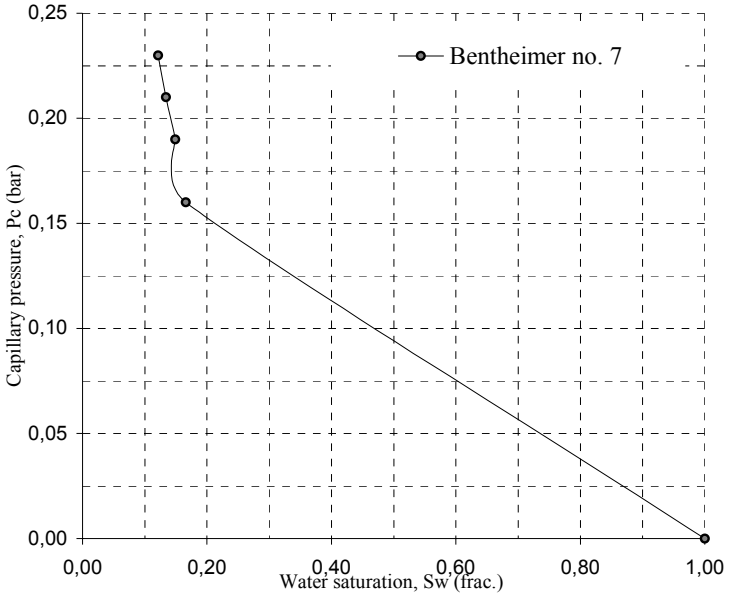

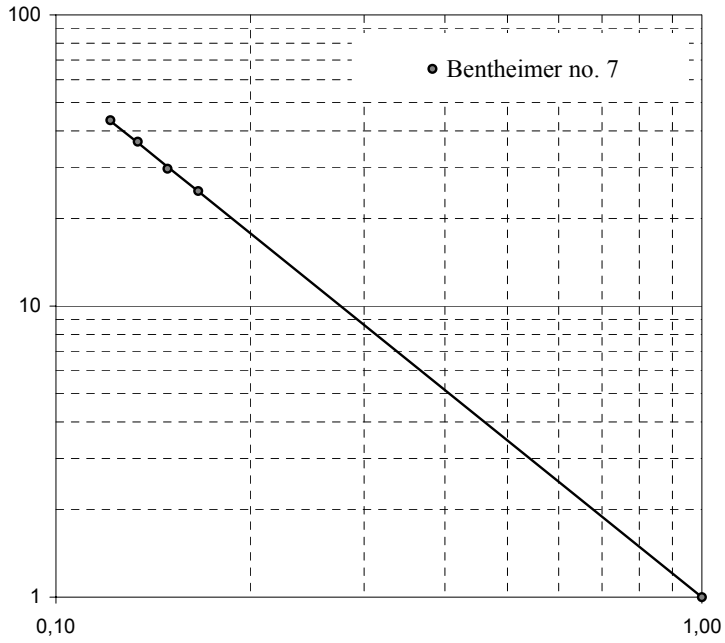

Figure 7.12 Primary drainage and resistivity index, program A, Bentheimer no.7.

Bentheimer sample no.	: 8
Porous plate type	: Homogeneous 1 bar plate
Water permeability at 20 bar NCP (mD)	: 3024
Porosity at 20 bar NCP (frac.)	: 0.236
Water saturation at Pc=230 mbar	: 0.119
n exponent	: 1.81

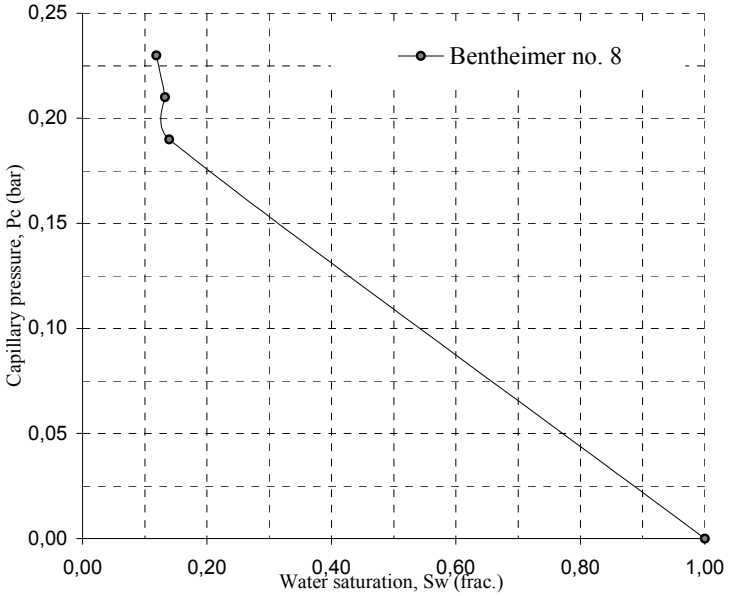

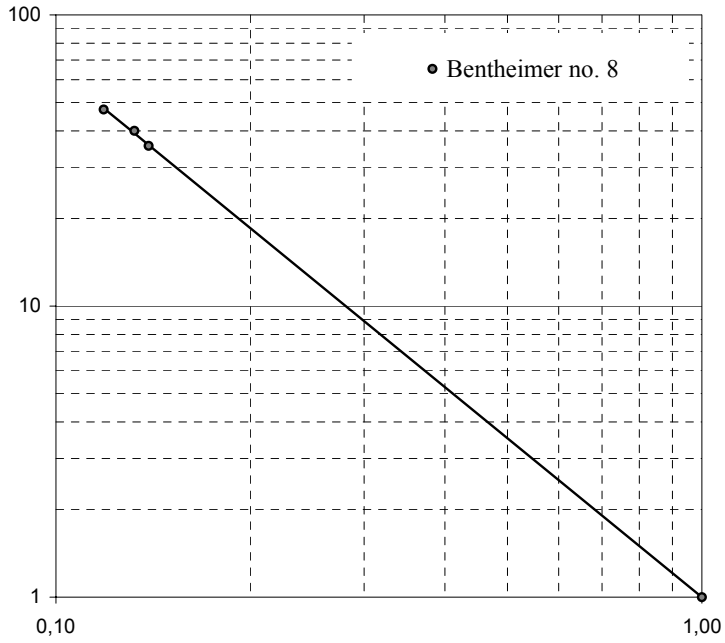

Figure 7.13 Primary drainage and resistivity index, program A, Bentheimer no.8.

Bentheimer sample no.	: 9
Porous plate type	: Homogeneous 1 bar plate
Water permeability at 20 bar NCP (mD)	: 2714
Porosity at 20 bar NCP (frac.)	: 0.232
Water saturation at Pc=230 mbar	: 0.144
n exponent	: 1.87

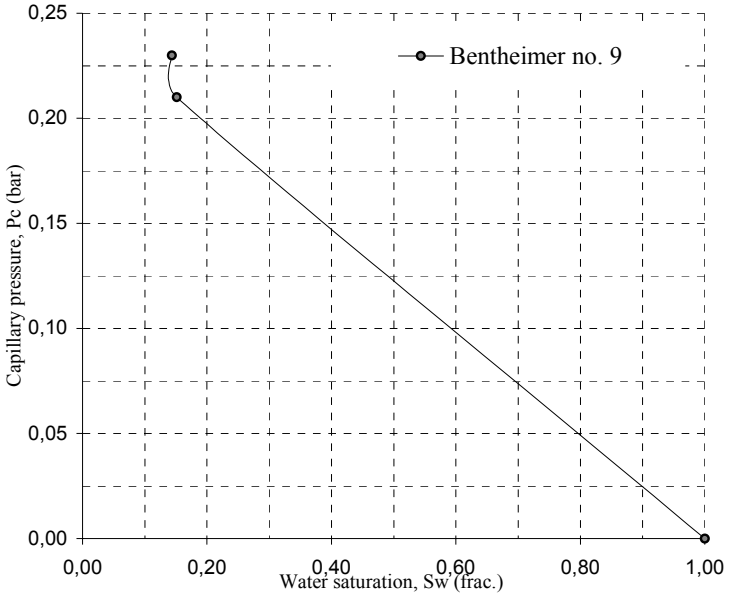

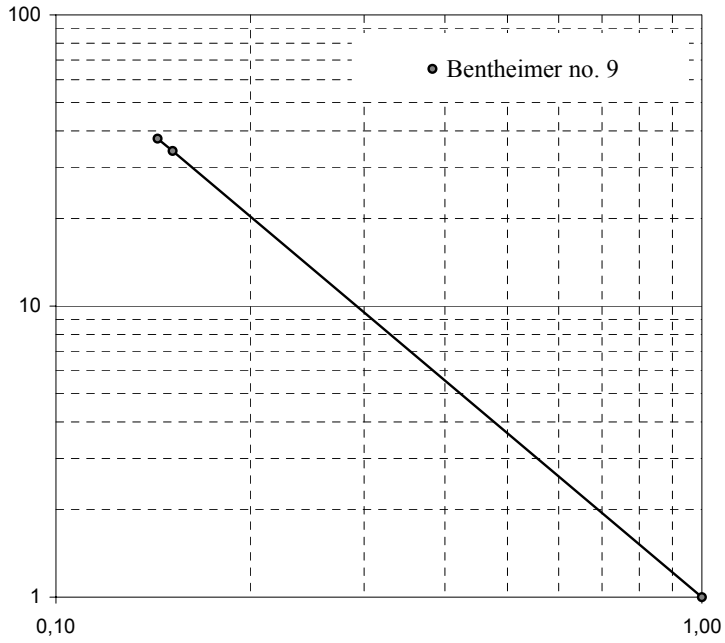

Figure 7.14 Primary drainage and resistivity index, program A, Bentheimer no.9.

Bentheimer sample no.	: 10
Porous plate type	: Homogeneous 1 bar plate
Water permeability at 20 bar NCP (mD)	: 3031
Porosity at 20 bar NCP (frac.)	: 0.237
Water saturation at Pc=230 mbar	: 0.123
n exponent	: 1.83

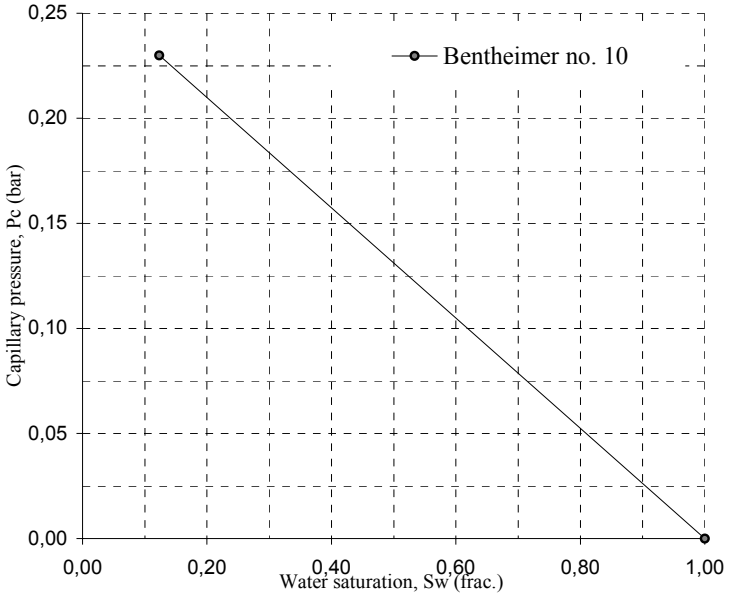

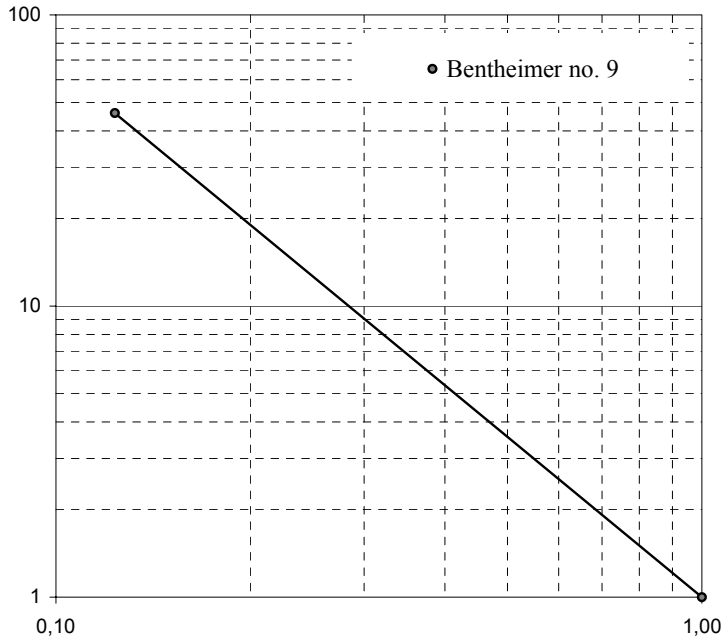

Figure 7.15 Primary drainage and resistivity index, program A, Bentheimer no.10.

Bentheimer sample no. : 1-10

n exponent : 1.81

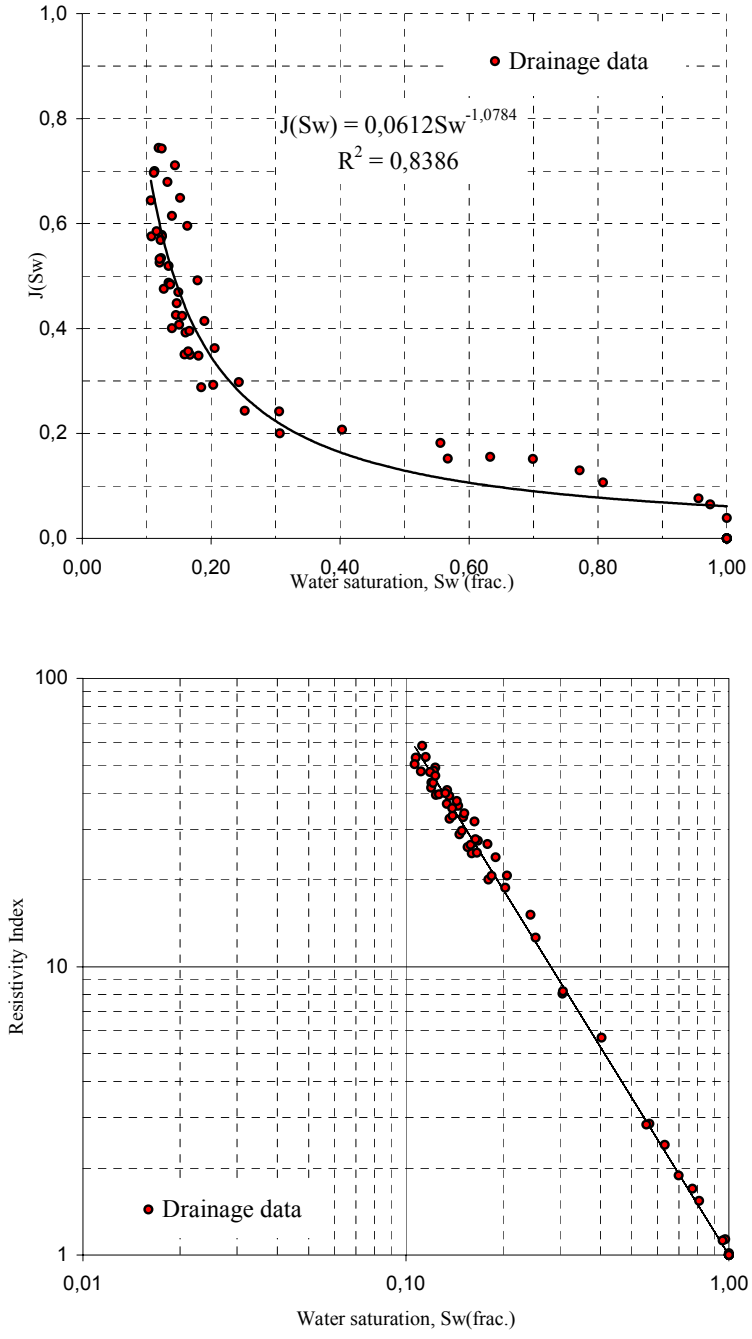

Figure 7.16 J(Sw) and Sw-RI relationship, program A.

Reproducibility, program A

Program A was performed 3 times. After completing the program for the first time, the rocks were cleaned and the effluent analysed for water content. When trying to reproduce the program, there was a huge difference between first and reproduced results. The Karl Fisher results for the first performance did not match material balance from production data. The third attempt matched the second results with an accuracy of +/- 0.5 %. I.e. in line with acceptable uncertainty in readings.

In the first attempt to perform program A, no material balance was achieved and it was observed a curved Sw-RI relationship near 230 mbar. I.e. the changes in saturation changes without observing a corresponding response in resistivity changes. This indicates a break through in the porous plate or slippage effect between the sleeve and the porous plate. In addition, no spontaneous imbibition occurred which indicates an oil wet tendency behaviour or breaking discontinuity between the porous plate and the porous rock.

In the second attempt we therefore modified the high flux 1 bar porous plate with an L-shaped seal ring in order to avoid slippage. The Sw-RI relationship showed a linear trend and we obtained material balance in the system. In addition, water spontaneously imbibed.

Observations and discussions, program A

By looking at the achieved water saturation at P_c=230 mbar, for experiments 1-10 in table 7.3, it appears that achieved water saturation is a function of the amount of applied capillary pressure steps prior to P_c=230 mbar. However, experiment no. 1 and no. 5 deviate from the observation. In order to study this closely, different partial derivatives were calculated and plotted for the transient data matrix in program A.

The following partial derivatives were plotted and investigated:

$$\frac{dS_w}{dt} \text{ and } \frac{dS_w}{dP_c} \qquad (32).$$

The partial derivatives were plotted against each other and towards S_w, P_c, and t. No clear tendency was observed.

The observed water saturation at P_c=230 mbar varies from 0.106 to 0.163. However, the variation in basic petrophysical properties is also relatively large. It was therefore decided to calculate and plot the partial derivative

$$\frac{dS_w}{dJ} \qquad (33),$$

where dJ is the partial derivate of the dimensionless J-function.

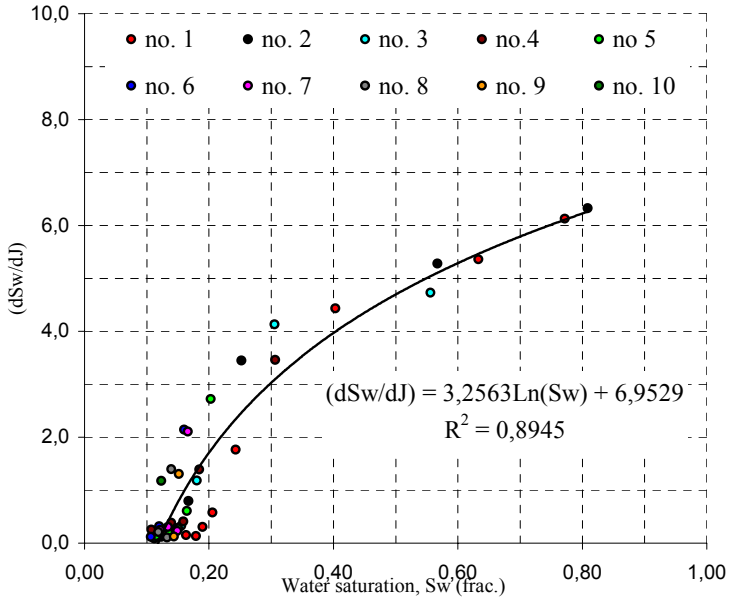

Figure 7.17 (dS_w/dJ) versus water saturation.

Figure 7.17 expresses the changes in water saturation caused by an incremental increase in capillary pressure. The petrophyscial variance is taken into consideration by the dimensionless capillary pressure J. (dS_w/dJ) is large and corresponds to a capillary pressure level right above the threshold pressure of the homogeneous Bentheimer rock which will cause a relatively large de-saturation.

The observed pattern is probably not correct due to stopping the drainage at P_c=230 mbar, which is far from irreducible water saturation. Taking this into consideration, an S-shaped curve is expected if the program was performed in steps down to P_c=5 bar instead of P_c=230 mbar. However, it clearly forms some kind of pattern which points in the direction that obtained water saturation is independent of the amount of pressure steps performed prior to the final destination, which in this case is P_c=230 mbar.

The observed pattern indicates that the S-shape is a function of pressure steps. By reducing the amount of pressure steps it seems that the behaviour is described by a logarithmic relationship.

Experiment no. 1 is the only experiment that clearly deviates from the observed pattern. This might be explained in terms of local pore size distribution. Early invasion data for this experiment fits the pattern in line with the other experiments.

Conclusion, program A

It seems that establishing water saturation in single or multi stages does not influence the distribution as long as a strict equilibrium criteria is used. No evidence has been found that achieved saturation is a function of the amount of increasing incremental capillary pressure steps towards this destination.

However, further studies should be initiated in order to verify the observation in this study by for instance initiating:

- Experimental studies using in situ saturation monitoring from gamma ray or X ray attenuation or NMR distributions in order to study local variations.

- Synthetic studies by the use of dynamic network simulators.

Program B

In order to investigate porous plate influence on Sw-RI relationships, a continuous injection study was initiated on the same 10 Betheimer rocks. Five experiments were imitated with layered porous plates, while the remaining five experiments were imitated with homogeneous porous plates.

Experimental set-up, program B

We used a standard set up for continuous injection experiments, described in Chapter 6 in this thesis. In order to compare the result as a function of injection rate, it was decided to initiate two experiments, each run with layered and homogeneous plates respectively.

Figure 7.18-7.27 presents the injection results.
Composite plots are presented in figure 7.28-7.31.
Numerical data is presented in Appendix B.

Table 7.4 Summary of continuous injection data

Plug (no.)	Porous plate (type)	$Q_{injection}$ 20 bar NCP (ml/h)	S_{wi} 20 bar NCP (frac.)	n 20 bar NCP	P_i (S_{wi}) 20 bar NCP (bar)	$S_{wi(Pc=0)}$ 20 bar NCP Production (frac.)	$S_{wi(Pc=0)}$ 20 bar NCP Karl Fisher (frac.)
1	Layered	0.2000	0.231	1.68	11.92	0.642	0.640
2	Layered	0.0339	0.123	1.82	14.23	0.631	0.632
3	Homogeneous	0.0339	0.146	1.74	14.50	0.633	0.633
4	Homogeneous	0.2000	0.266	1.63	10.13	0.629	0.630
5	Layered	0.0605	0.144	1.79	11.95	0.678	0.675
6	Homogeneous	0.0605	0.184	1.76	10.96	0.674	0.675
7	Layered	0.1027	0.180	1.65	11.67	0.631	0.631
8	Homogeneous	0.1027	0.228	1.66	10.16	0.626	0.624
9	Layered	0.1838	0.408	1.57	8.16	0.635	0.634
10	Homogeneous	0.1838	0.432	1.47	14.10	0.629	0.626

Bentheimer sample no.	: 1
Porous plate type	: Layered porous plate
Water permeability at 20 bar NCP (mD)	: 1921
Injection rate at 20 bar NCP (ml/h)	: 0.2000
Water saturation at Pinjection=5 bar	: 0.268
n exponent	: 1.68

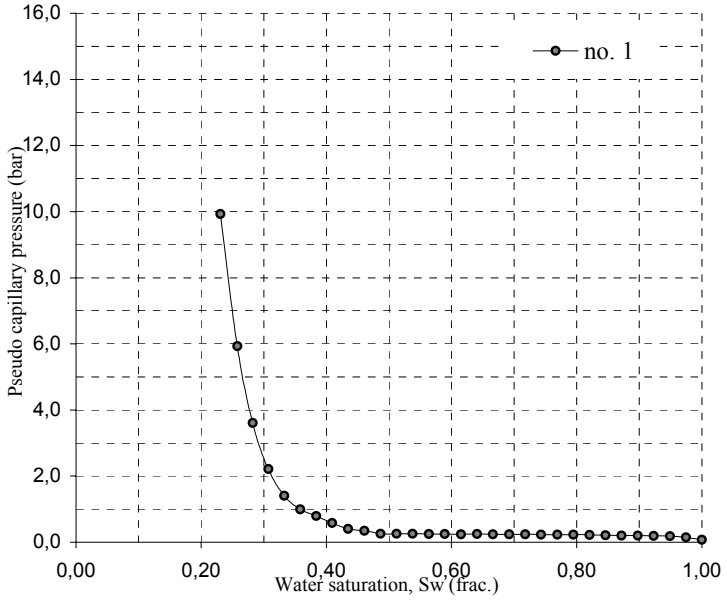

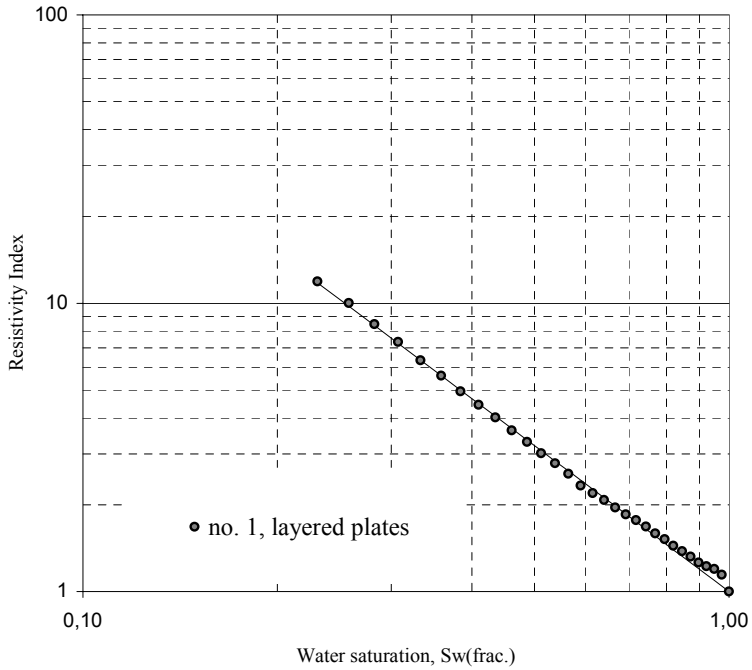

Figure 7.18 Continuous injection, Bentheimer no. 1.

Bentheimer sample no.	: 2
Porous plate type	: Layered porous plate
Water permeability at 20 bar NCP (mD)	: 2767
Injection rate at 20 bar NCP (ml/h)	: 0.0339
Water saturation at Pinjection=5 bar	: 0.155
n exponent	: 1.82

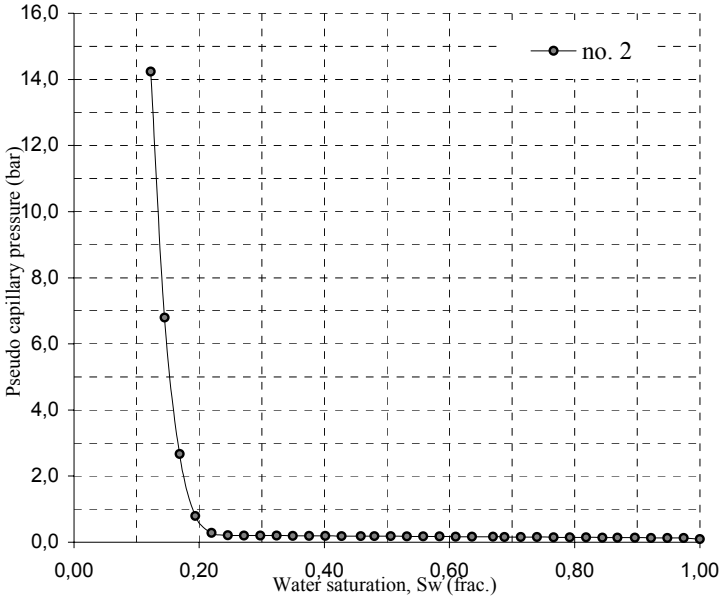

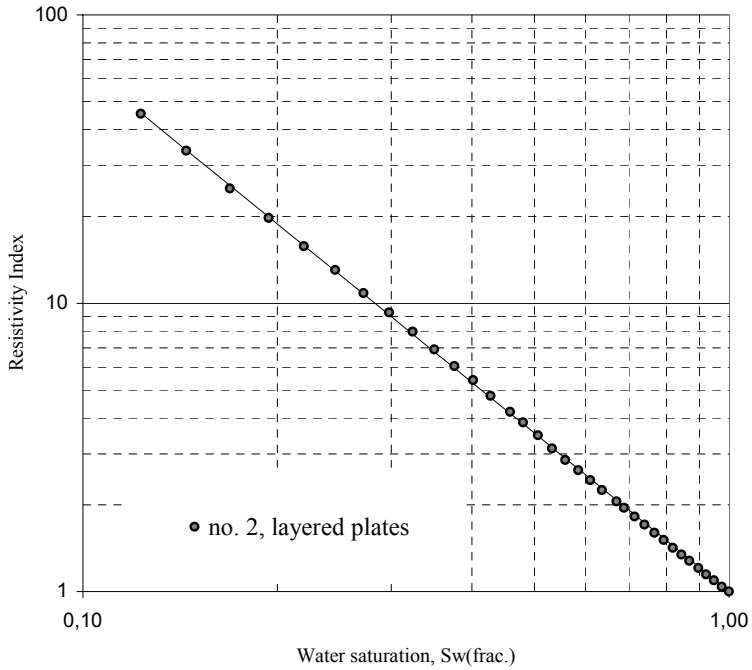

Figure 7.19 Continuous injection, Bentheimer no. 2.

Bentheimer sample no.	: 3
Porous plate type	: Homogeneous porous plate
Water permeability at 20 bar NCP (mD)	: 2641
Injection rate at 20 bar NCP (ml/h)	: 0.0339
Water saturation at Pinjection=5 bar	: 0.192
n exponent	: 1.74

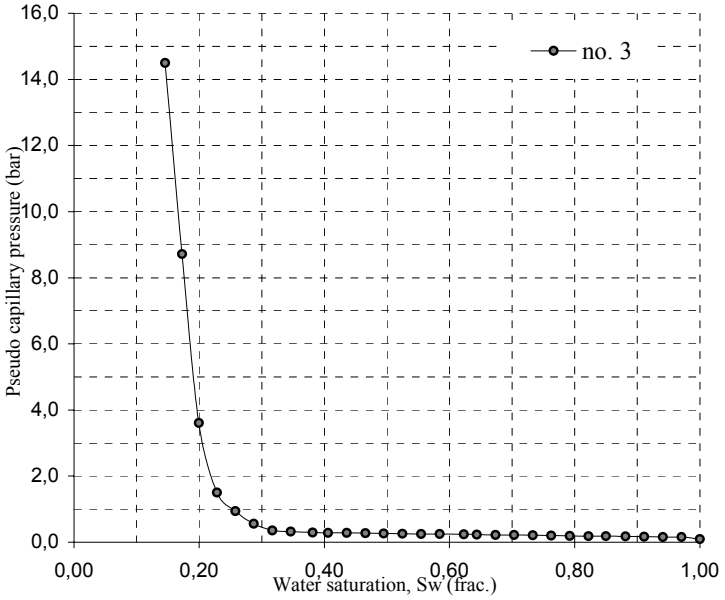

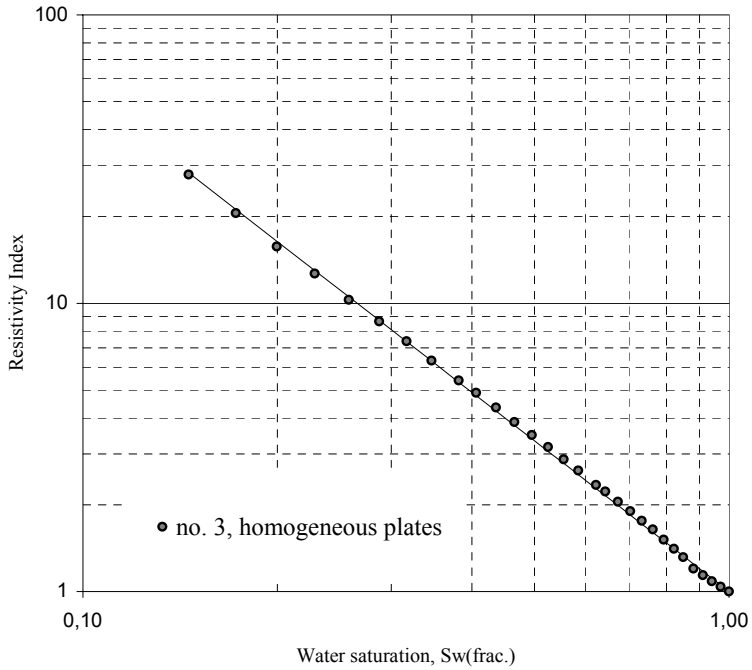

Figure 7.20 Continuous injection, Bentheimer no. 3.

Bentheimer sample no.	: 4
Porous plate type	: Homogeneous porous plate
Water permeability at 20 bar NCP (mD)	: 1803
Injection rate at 20 bar NCP (ml/h)	: 0.0605
Water saturation at Pinjection=5 bar	: 0.222
n exponent	: 1.63

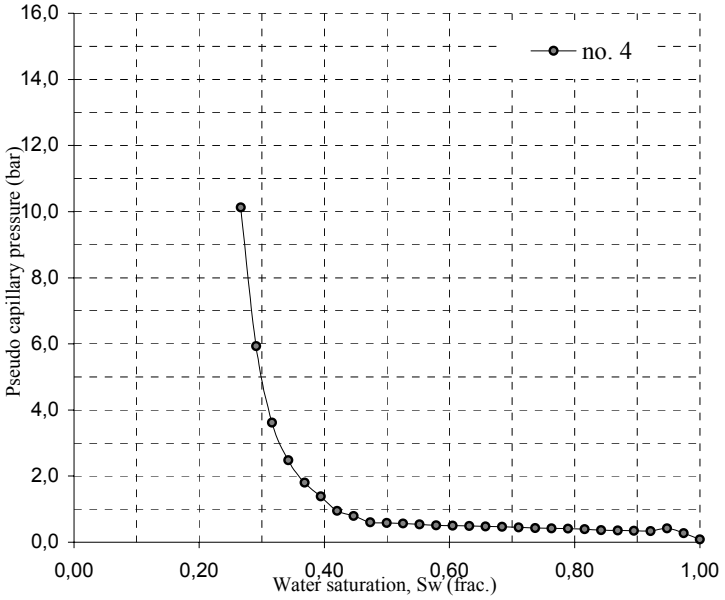

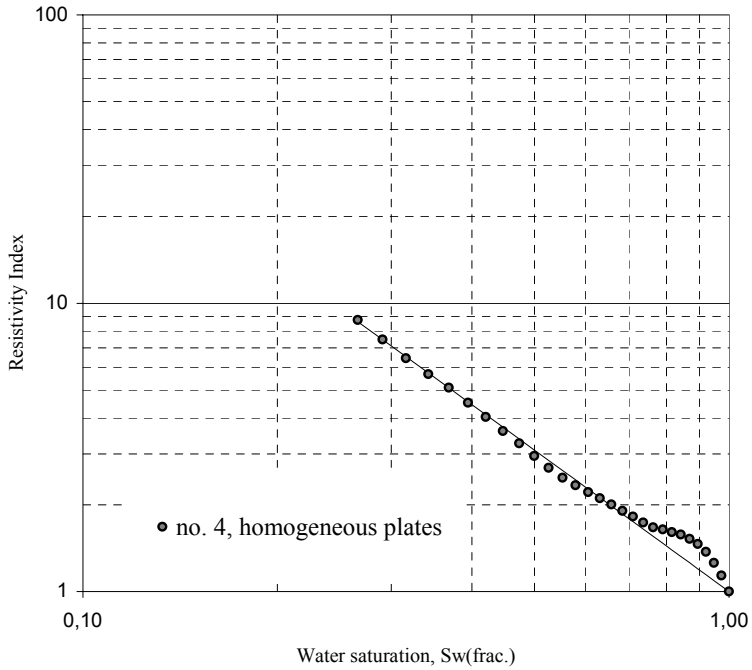

Figure 7.21 Continuous injection, Bentheimer no. 4.

Bentheimer sample no.	: 5
Porous plate type	: Layered porous plate
Water permeability at 20 bar NCP (mD)	: 1769
Injection rate at 20 bar NCP (ml/h)	: 0.0605
Water saturation at Pinjection=5 bar	: 0.177
n exponent	: 1.79

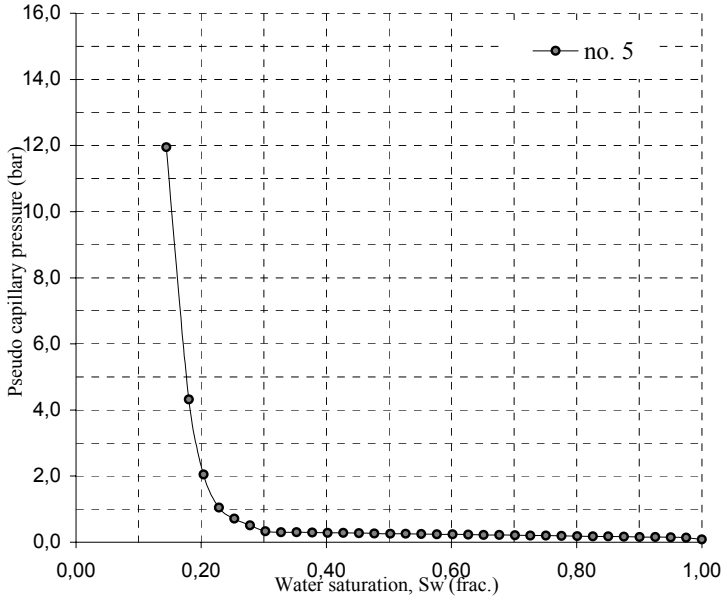

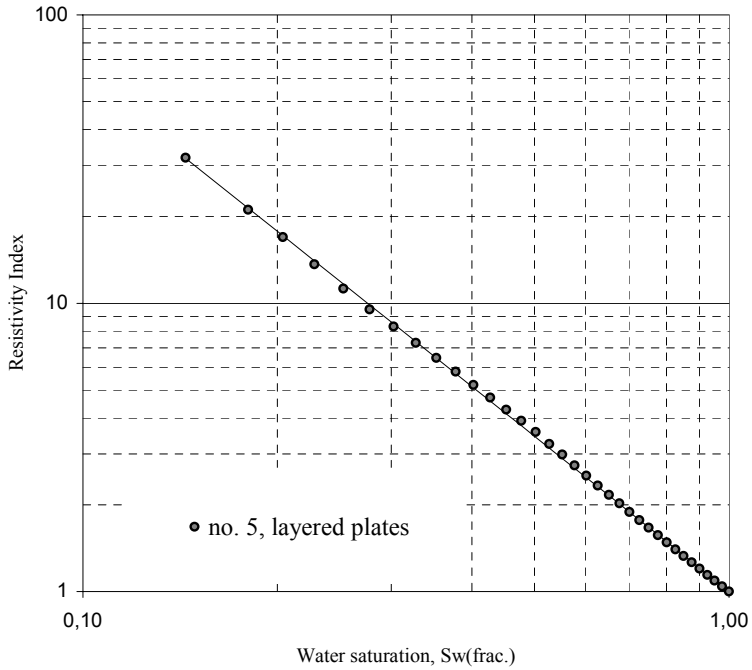

Figure 7.22 Continuous injection, Bentheimer no. 5.

Bentheimer sample no.	: 6
Porous plate type	: Homogeneous porous plate
Water permeability at 20 bar NCP (mD)	: 2289
Injection rate at 20 bar NCP (ml/h)	: 0.1027
Water saturation at Pinjection=5 bar	: 0.257
n exponent	: 1.76

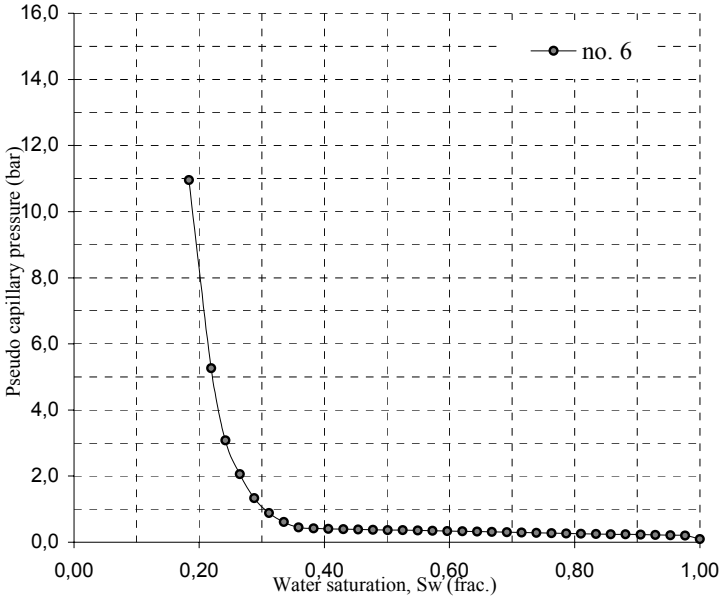

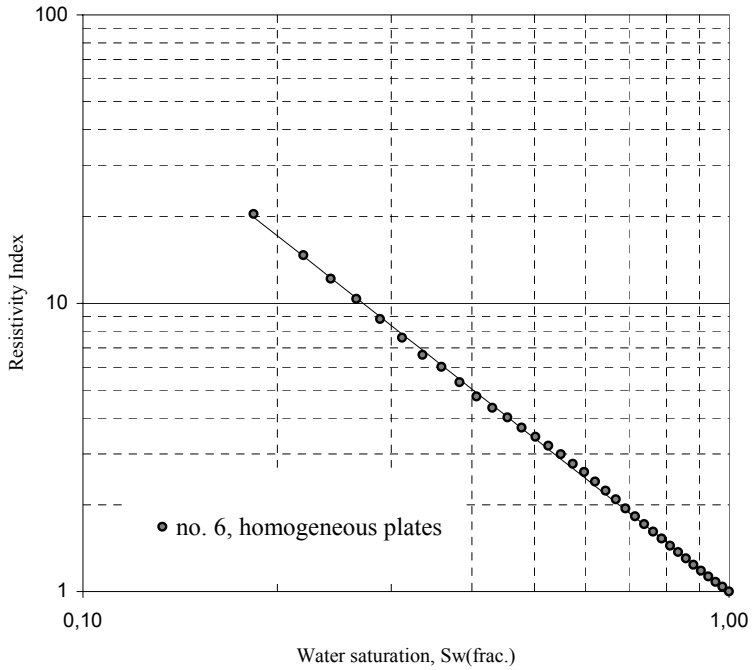

Figure 7.23 Continuous injection, Bentheimer no. 6.

Bentheimer sample no.	: 7
Porous plate type	: Layered porous plate
Water permeability at 20 bar NCP (mD)	: 1773
Injection rate at 20 bar NCP (ml/h)	: 0.1027
Water saturation at Pinjection=5 bar	: 0.216
n exponent	: 1.76

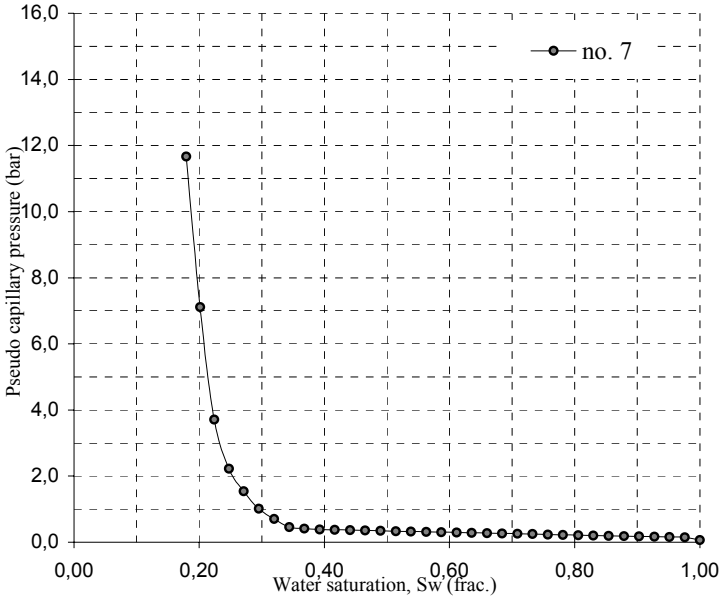

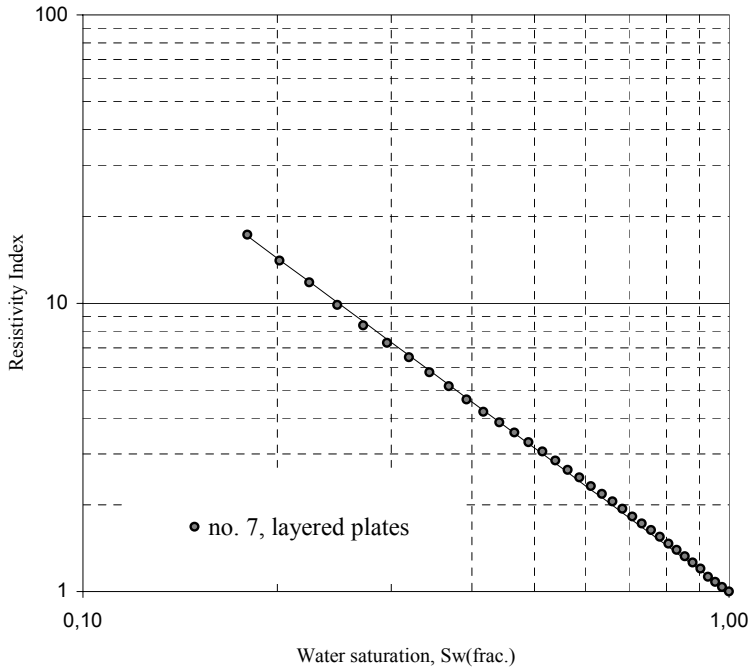

Figure 7.24 Continuous injection, Bentheimer no. 7.

Bentheimer sample no.	: 8
Porous plate type	: Homogeneous porous plate
Water permeability at 20 bar NCP (mD)	: 3024
Injection rate at 20 bar NCP (ml/h)	: 0.2000
Water saturation at Pinjection=5 bar	: 0.301
n exponent	: 1.66

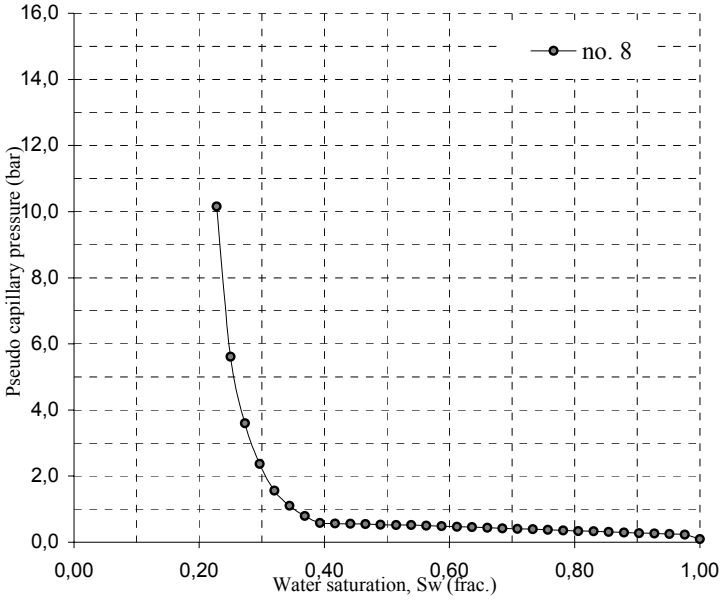

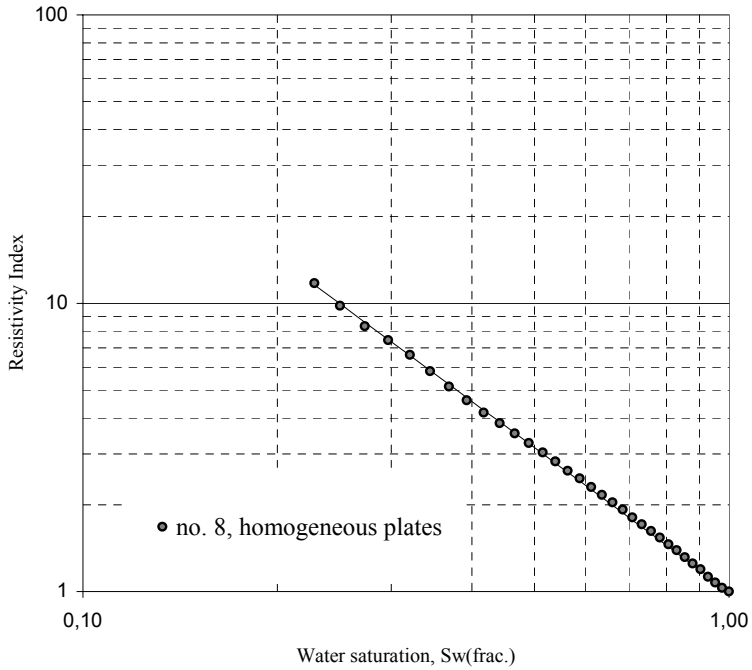

Figure 7.25 Continuous injection, Bentheimer no. 8.

Bentheimer sample no.	: 9
Porous plate type	: Layered porous plate
Water permeability at 20 bar NCP (mD)	: 2714
Injection rate at 20 bar NCP (ml/h)	: 0.1838
Water saturation at Pinjection=5 bar	: 0.439
n exponent	: 1.57

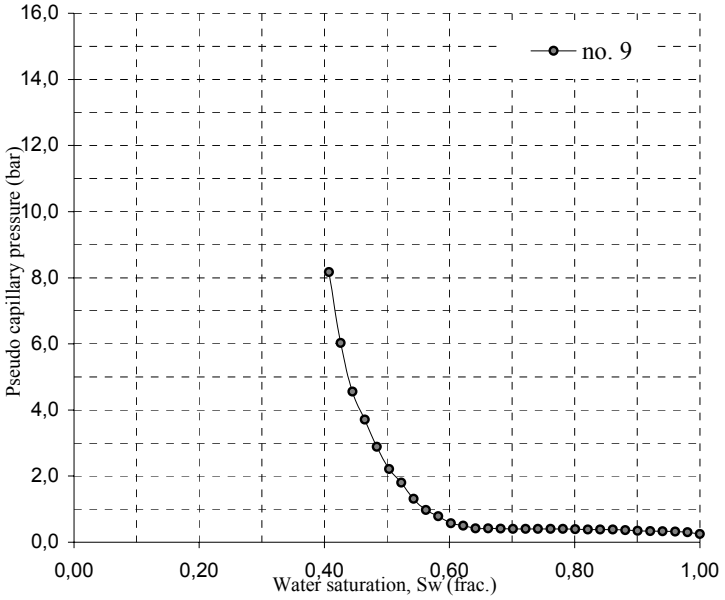

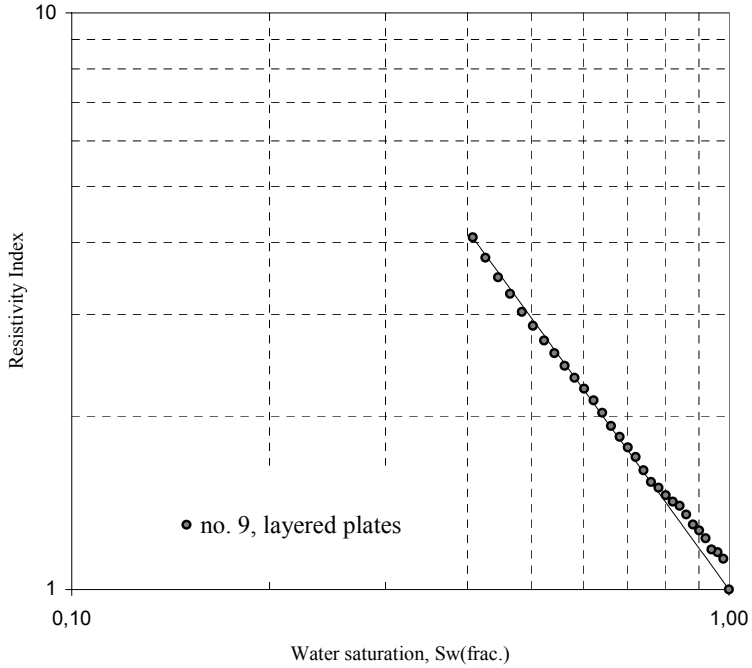

Figure 7.26 Continuous injection, Bentheimer no. 9.

Bentheimer sample no.	: 10
Porous plate type	: Homogeneous porous plate
Water permeability at 20 bar NCP (mD)	: 3031
Injection rate at 20 bar NCP (ml/h)	: 0.1838
Water saturation at Pinjection=5 bar	: 0.551
n exponent	: 1.47

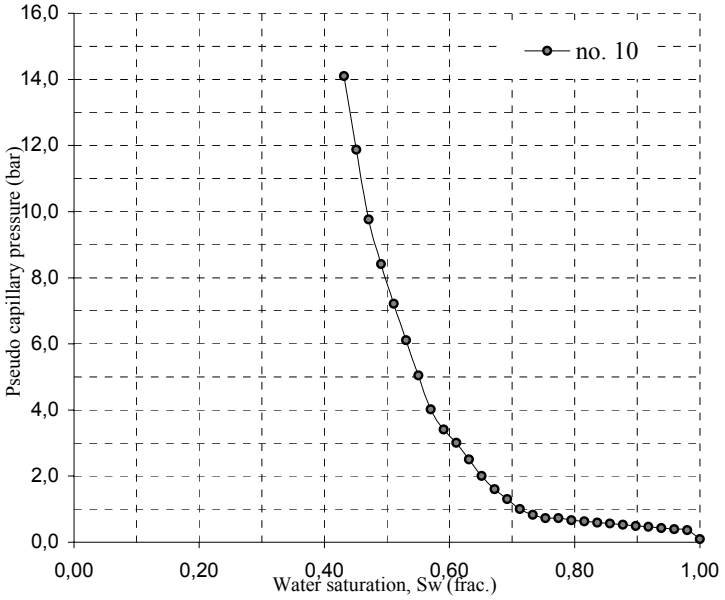

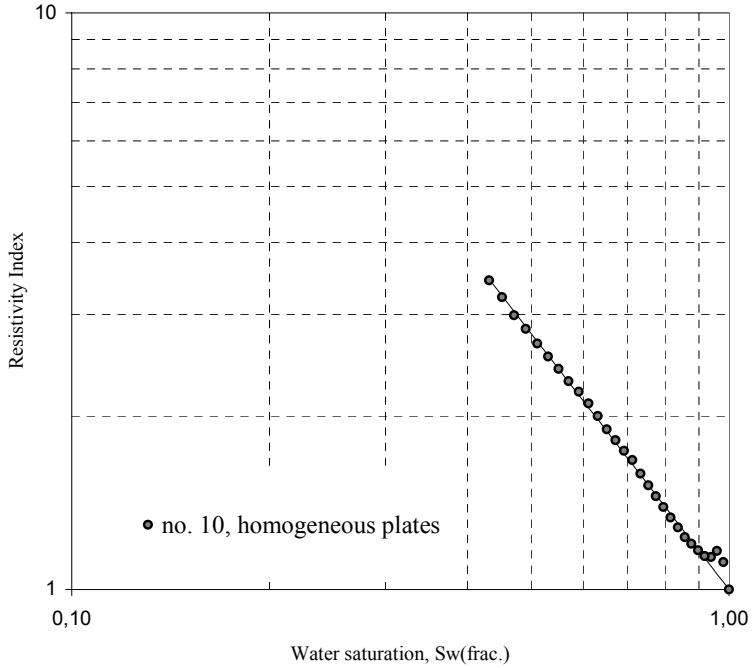

Figure 7.27 Continuous injection, Bentheimer no. 10.

Bentheimer sample no. : 1, 2, 5, 7 and 9

Porous plate type : Layered porous plates

n exponent : 1.74

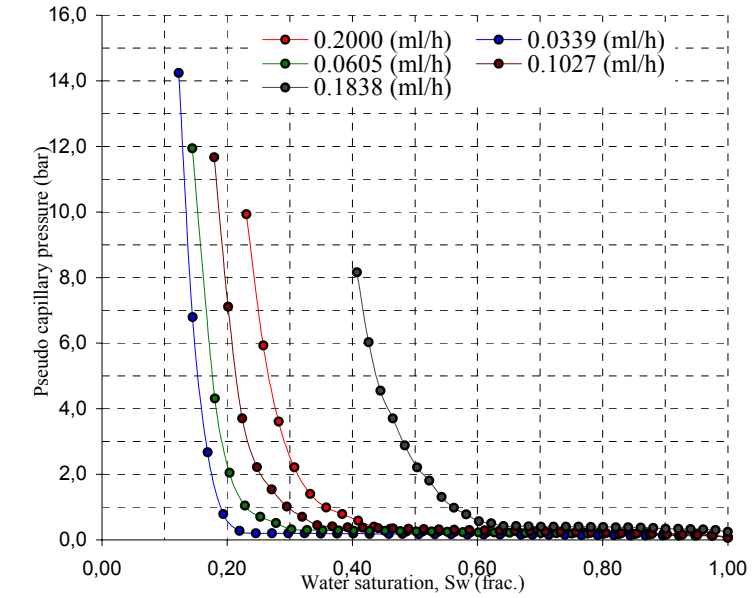

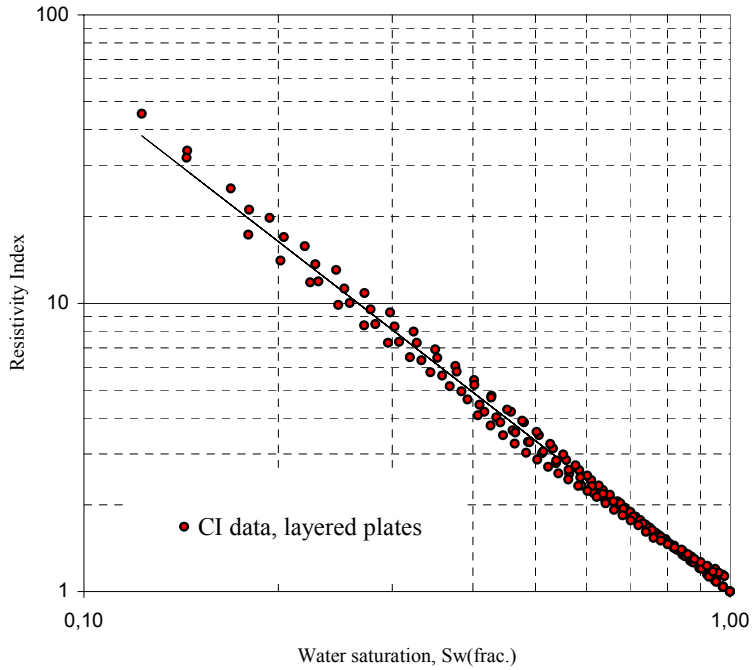

Figure 7.28 Continuous injection, Layered porous plate data.

Bentheimer sample no. : 3, 4, 6, 8 and 10

Porous plate type : Homogeneous porous plates

n exponent : 1.69

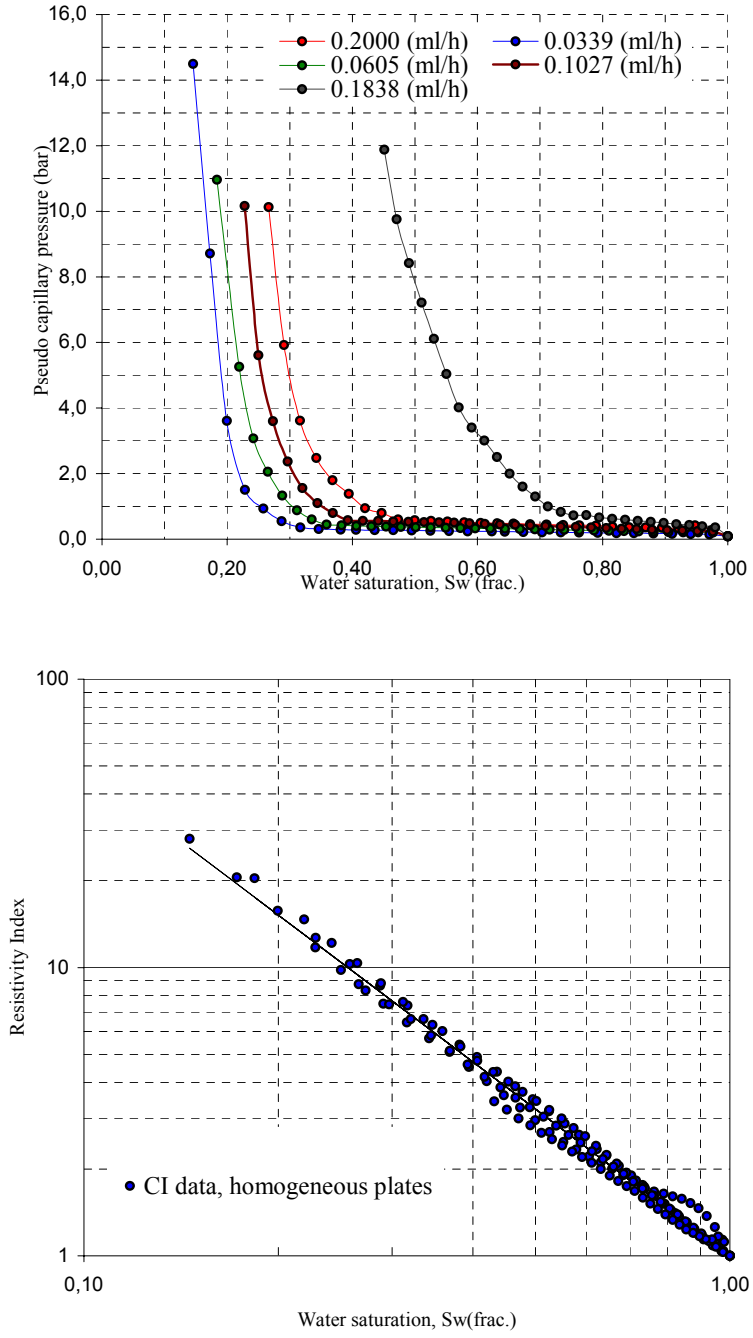

Figure 7.29 Continuous injection, homogeneous porous plate data.

Reproducibility, program B

Continuous injection was performed twice for this program. The first attempt failed. By following the procedures described in Chapter 6, no agreement between injected oil volume and expelled water volume was achieved. The most likely explanation is injection in an incompressible environment. The core plugs were therefore re-cleaned and saturated again in order to start all over again. Prior to second injection the compressibility of the oil cylinders were re-established.

The second attempt to perform continuous injection gave a good agreement between oil injected and expelled water. An agreement of +/- 0.004 ml difference between injected oil volume and expelled water volume was achieved.

Observations and discussions, program B

Several observations can be observed by studying the continuous injection plots. This can be summarised as follows:

Obtained water saturations from continuous injection data at high pseudo capillary pressure, P_c=5 bar, is much higher than obtained water saturation from porous plate results obtained at P_c=230 mbar in program A.

In general, it seems that decreasing injection rate yields lower water saturations. Hence, the pseudo capillary pressure curve is somehow related to injection rate. However, layered experiment no. 9 and corresponding homogeneous experiment no. 10 deviates from this observation.

The pressure level on the plateau of the pseudo capillary pressure curve seems to decrease for decreasing injection rates. Furthermore, it seems that the porous plate type influences the pressure plateau level. The layered experiments yields lower pressure at the plateau than corresponding experiments initiated with homogeneous porous plates.

Experiments initiated with layered porous plates yields a larger de-saturation than corresponding homogeneous porous plate experiments for the continuous injection technique.

The Sw-RI relationships for this rock type is more and less described by a linear relationship, except for early invasion data. However, it seems that obtained saturation exponent is a function of obtained water saturation. By taking into consideration that the injection rate influences achieved water saturation, it might be reasonable to investigate if the n exponent is also a function of injection rate.

Interpretation, program B

In a continuous injection set-up, pressure, injected volume, resistivity and temperature are digitally logged in fixed incremental time steps. The injection pressure at the end of the experiment will therefore vary from experiment to experiment. In order to compare achieved end point parameters, water saturation at exactly P_c=5 bar was calculated by a linear interpolation.

Injection rate does not take into consideration the size of the pore volume. The turnaround time in an experiment is therefore related to both injection rate and pore volume. Layered experiment no. 9 and corresponding homogeneous experiment no. 10 have much smaller pore volumes than the remaining core plugs in this study. It was therefore decided to introduce specific injection rate defined as

$$Q_s = \frac{Q_{injected}}{V_{pore}} \qquad (34).$$

Specific rates and interpolated water saturations at P_c=5 bar are presented in table 7.5.

Table 7.5 specific rates

Plug (no.)	Porous plate (type)	$Q_{injection}$ 20 bar NCP (ml/h)	V_{pore} 20 bar NCP (ml)	Q_s 20 bar NCP (ml/h)/(ml)	$S_{wi(Pc=5\ bar)}$ 20 bar NCP (frac.)
1	Layered	0.2000	18.73	0.0107	0.268
2	Layered	0.0339	18.25	0.0019	0.155
3	Homogeneous	0.0339	15.98	0.0021	0.192
4	Homogeneous	0.2000	14.94	0.0040	0.222
5	Layered	0.0605	14.24	0.0042	0.177
6	Homogeneous	0.0605	14.58	0.0070	0.257
7	Layered	0.1027	14.57	0.0070	0.216
8	Homogeneous	0.1027	15.57	0.0128	0.301
9	Layered	0.1838	12.73	0.0144	0.439
10	Homogeneous	0.1838	12.32	0.0149	0.551

It is now possible to plot water saturation at P_c=5 bar pseudo capillary pressure versus specific rate for experiments performed with the two different porous plates.

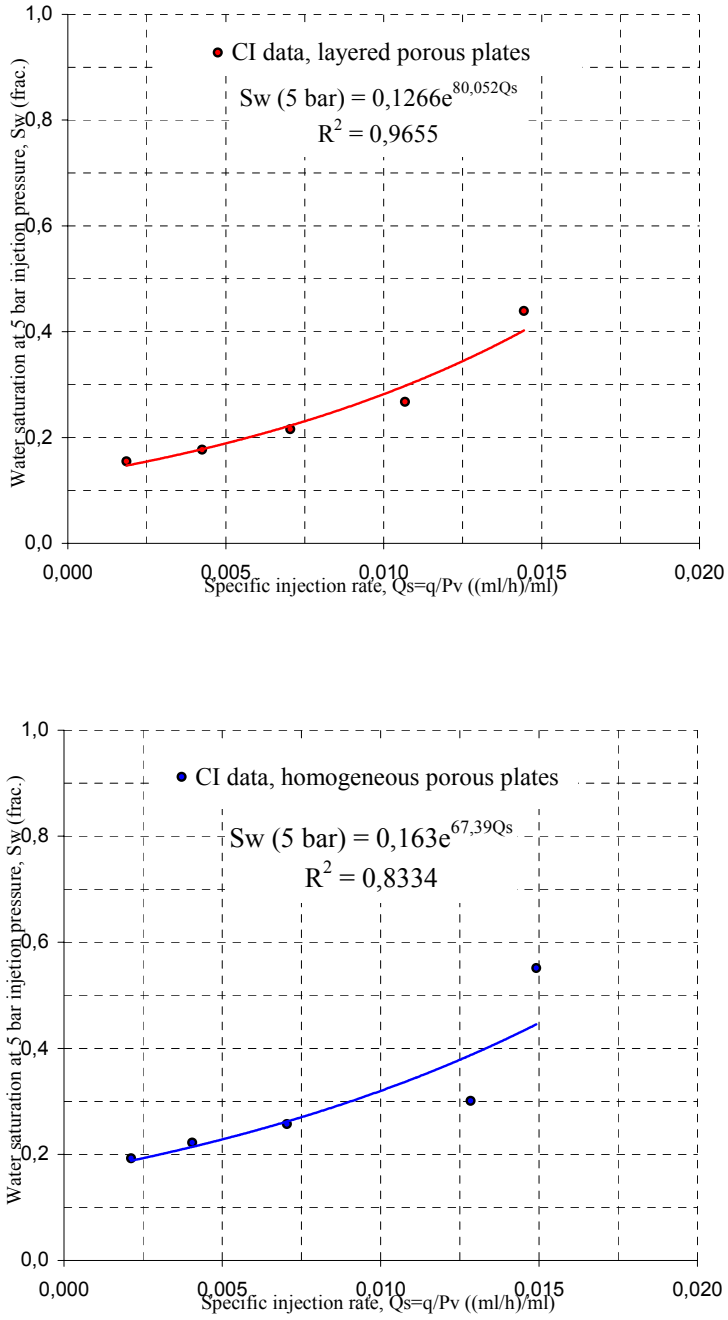

Figure 7.30 Continuous injection interpretation.

Figure 7.30 shows that achieved water saturation is a function of specific injection rate. Decreasing rates yield lower water saturation. For the investigated rock type it seems that this is described with a logarithmic relationship

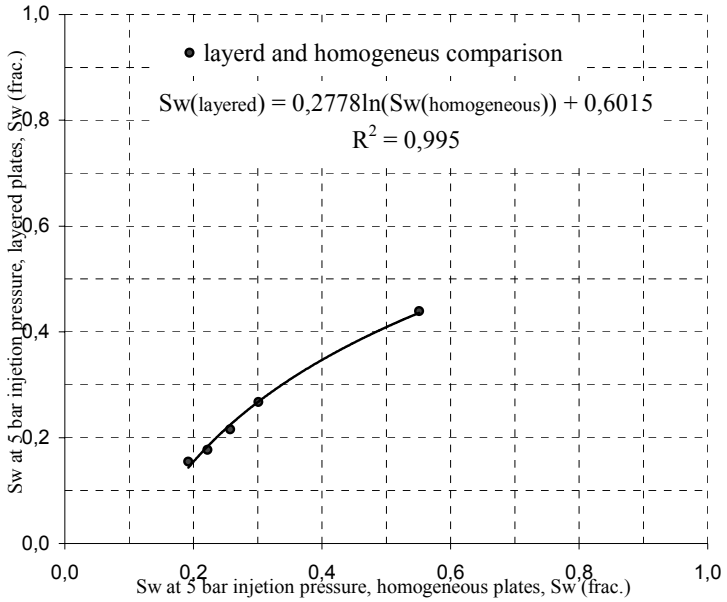

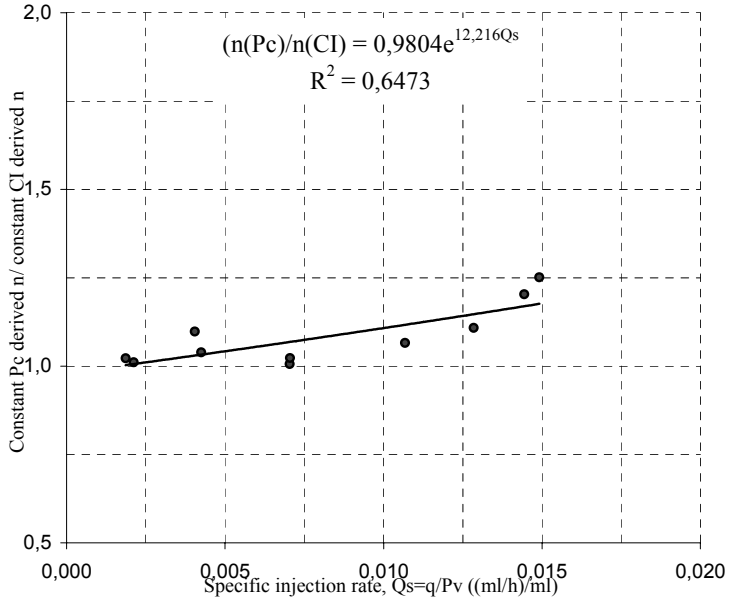

Figure 7.31Continuous injection interpretation.

The first plot in Figure 7.31 presents water saturation at P_c=5 bar pseudo capillary pressure for layered and homogeneous experiment respectively. The plot illustrates the relative influence of porous plate types on achieved water saturation.

The second plot in figure 7.31 illustrates the relative influence of drainage method on Sw-RI relationships for the investigated rock type and fluid pair. The figure illustrates that the specific injection rate needs to be kept lower than a certain value in order to be comparable with the porous plate method. This statement is in line with previous reported observasions[10]. It seems that the influence of method on Sw-RI relationship is described by a power law. However, further investigation is needed in order to verify this as a general tendency.

Considerations, program B

In order to explain some of the observations, we can simplify the observations by considering the following:

Two synthetic porous media, each represented by a two-dimensional square lattice of cylindrical tubes, are connected together like a composite core experiment. The first network has a different radius distribution than the other, which has a radius distribution analogous to a ceramic plate.

Initially, the system is filled with a defending fluid of viscosity μ1. We restrict the discussion to drainage displacement and let the invading fluid be non-wetting and the defending fluid be wetting. The fluids are immiscible and there is a well-defined interface between the two phases. The curvature of this interface gives rise to capillary pressure given by the interfacial tension. Moreover, we assume that the fluids are incompressible.

We restrict the discussion further to an area in the composite lattice where a single tube meets the restriction.

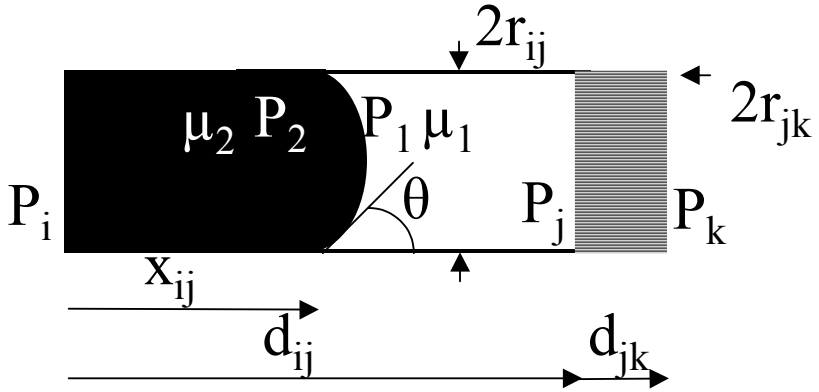

Figure 7.32 Flow in a cylindrical tube

The volume flux q_{ij} from node i to node j in the tube is found from the Washburn equation for capillary flow with two fluids present described by the equation

$$q_{ij} = \frac{\pi r_{ij}^{\,2} k_{ij}}{\mu_{eff}} \frac{1}{d_{ij}} \left(\Delta P_{ij} - P_c\right)^{+} \tag{35},$$

where $k_{ij} = \frac{r_{ij}^{\,2}}{8}$ is the permeability of a cylindrical tube, $\mu_{eff} = \mu_2 x_{ij} + \mu_1 (1 - x_{ij})$ is the weighted effective viscosity, $\Delta P_{ij} = P_i - P_j$ is the pressure difference between node i and node j, $P_c = P_2 - P_1$ is the capillary pressure in the tube, x_{ij} is the position of the pore-interface in the tube, r_{ij} is the radius of the tube, and $^{+}$ indicates that $(P_i - P_j) > P_c$ otherwise $q_{ij} = 0$.

The capillary pressure is derived under the assumption that the fluids are in static equilibrium, i.e. there is no flow in the tube and $\Delta P_{ij} = P_c$. The dynamics of the moving interface is still unsolved theoretically but at low velocities without turbulence it can be assumed that capillary pressure is given by the Young-Laplace equation.

For tubes completely filled with either the invading or the defending fluid, P_c=0 and the Washburn equation reduces to Hagen-Poiseuille flow in a cylinder. Hence, the volume flux q_{ij} from node j to node k in the tubes, illustrating the ceramic plate, for one of the tubes is

$$q_{jk} = \frac{\pi r_{jk}^{\,2} k_{jk}}{\mu_{eff}} \frac{1}{d_{jk}} (\Delta P_{jk}) \tag{36},$$

where $\mu_{eff} = \mu_1$.

The assumption of incompressible fluids leads to volume flux conservation at each node. Hence, The Kirchoff equations become

$$q_{ij} = q_{jk} \tag{37}.$$

The total pressure across the composite system is given by $\Delta P_{ik} = P_i - P_j$, which is the pressure difference between inlet and outlet. The pressure difference can be written

$$\Delta P_{ik} = (\Delta P_{ij} - P_c)^{+} + \Delta P_{jk} \Rightarrow (P_i - P_k) = \left[(P_i - P_j) - P_c\right]^{+} + (P_j - P_k) \tag{38}.$$

Initially, the composite is filled with the defending fluid and P_i=P_j=P_k. When a constant injection rate is initiated, there will be a rapid build up of pressure until (P_i-P_j)>P_c. Then the oil will start to invade the capillary. A traditional porous plate has a smaller flux compared with a

layered porous plate. In order words, for the same injection rate the flux restriction, ΔP_{jk}, will be smaller if the porous plate is a layered type instead of a homogeneous plate. This is exactly what is observed for the plateau level for the Bentheimer experiments during continuous injection. By reducing the injection rate the effect becomes smaller.

Lets now connect several tubes, with smaller radii, in parallel with the existing tube like a bundle of capillary tubes model. The pressure P_i-P_k will increase rapidly, due to the high injection rate, which will result in a larger amount of non-invaded tubes when P_i reach the limit of 5 bar overpressure. By reducing the rate it might be possible to drain several tubes at a lower pressure. This is in line with the experimental observations for the Bentheimer rocks. Increasing injection rate yields higher water saturation at the same injection pressure relative to injection with much lower rate.

Conclusions, program B

The pseudo capillary pressure function in a continuous injection experiment must under no circumstances be used as a capillary pressure function.

It seems that for each rock type and fluid pair, the injection rate must be lower than a certain value in order to yield a representative Sw-RI relationship. This will vary for rock type and probably fluid pair.

Layered porous plates have a positive impact on continuous injection data resulting in larger de-saturation.

Program C

In order to investigate porous plate influence on primary drainage, imbibition and secondary drainage, it was decided to perform a full cycle on the same 10 Bentheimer rocks. 8 experiments were initiated with layered porous plates, while the remaining two experiments were imitated with homogeneous porous plates.

Prior to capillary pressure measurements, overburden pressure was increased to 200 bar NCP. The effect of overburden was initially measured, following the procedure reported in Chapter 6.

Experimental set-up, program C

We used a standard set up for capillary pressure measurements, described in Chapter 6.

Figure 7.33-7.42 presents the results.
Composite plots are presented in figure 7.43-7.44.
Numerical data is presented in Appendix C.

Table 7.6 Summary of capillary pressure data, program C

Plug no.	Φ_{He} 200 bar NCP (frac.)	K_L 20 bar NCP (mD)	K_W 200 bar NCP (mD)	S_{wi} 200 bar NCP drainage (frac.)	S_{or} 200 bar NCP Production (frac.)	S_{wi} 200 bar NCP sec. drainage (frac.)	S_{wi} 20 bar NCP Karl Fisher (frac.)	n 20 bar/20°C
1	0.226	3280	1523	0.119	0.279	0.119	0.120	1.92
2	0.235	5210	2203	0.100	0.284	0.100	0.101	1.87
3	0.227	4100	2094	0.104	0.286	0.103	0.102	1.77
4	0.227	3360	1424	0.107	0.268	0.107	0.107	1.80
5	0.216	2650	1401	0.119	0.260	0.119	0.118	1.86
6	0.230	4580	1833	0.110	0.252	0.110	0.110	1.78
7	0.229	3690	1411	0.108	0.286	0.107	0.107	1.81
8	0.228	4160	2413	0.093	0.291	0.094	0.096	1.85
9	0.224	3760	2147	0.112	0.284	0.112	0.112	1.89
10	0.229	4220	2410	0.096	0.291	0.096	0.098	1.85

Bentheimer sample no.	: 1
Porous plate type	: Layered
Water permeability at 200 bar NCP (mD)	: 1523
Porosity at 200 bar NCP (frac.)	: 0.226
Irreducible water saturation, Pc=5 bar	: 0.119
Residual oil saturation, Pc=-1 bar	: 0.279
n exponent	: 1.92

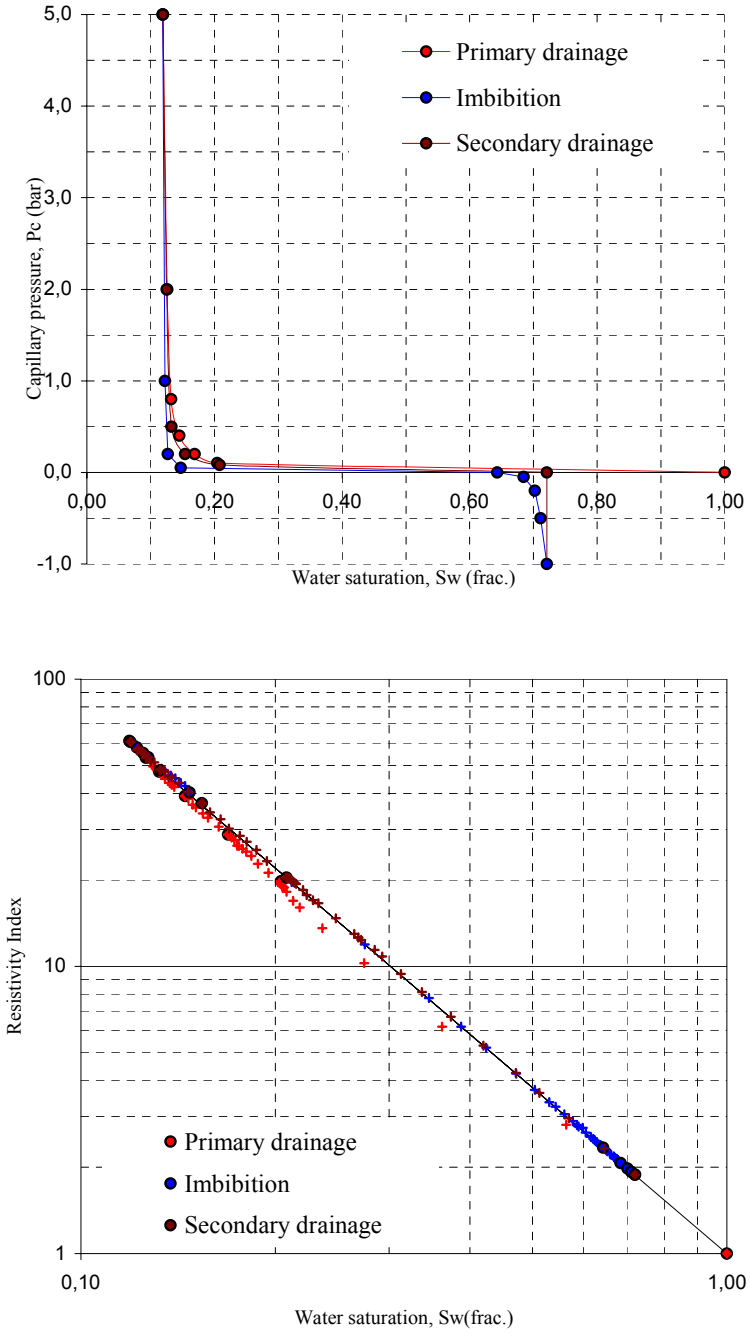

Figure 7.33 Full cycle capillary pressure and resistivity index, program C, Bentheimer no.1.

Bentheimer sample no.	: 2
Porous plate type	: Layered
Water permeability at 200 bar NCP (mD)	: 2203
Porosity at 200 bar NCP (frac.)	: 0.235
Irreducible water saturation, Pc=5 bar	: 0.100
Residual oil saturation, Pc=-1 bar	: 0.284
n exponent	: 1.87

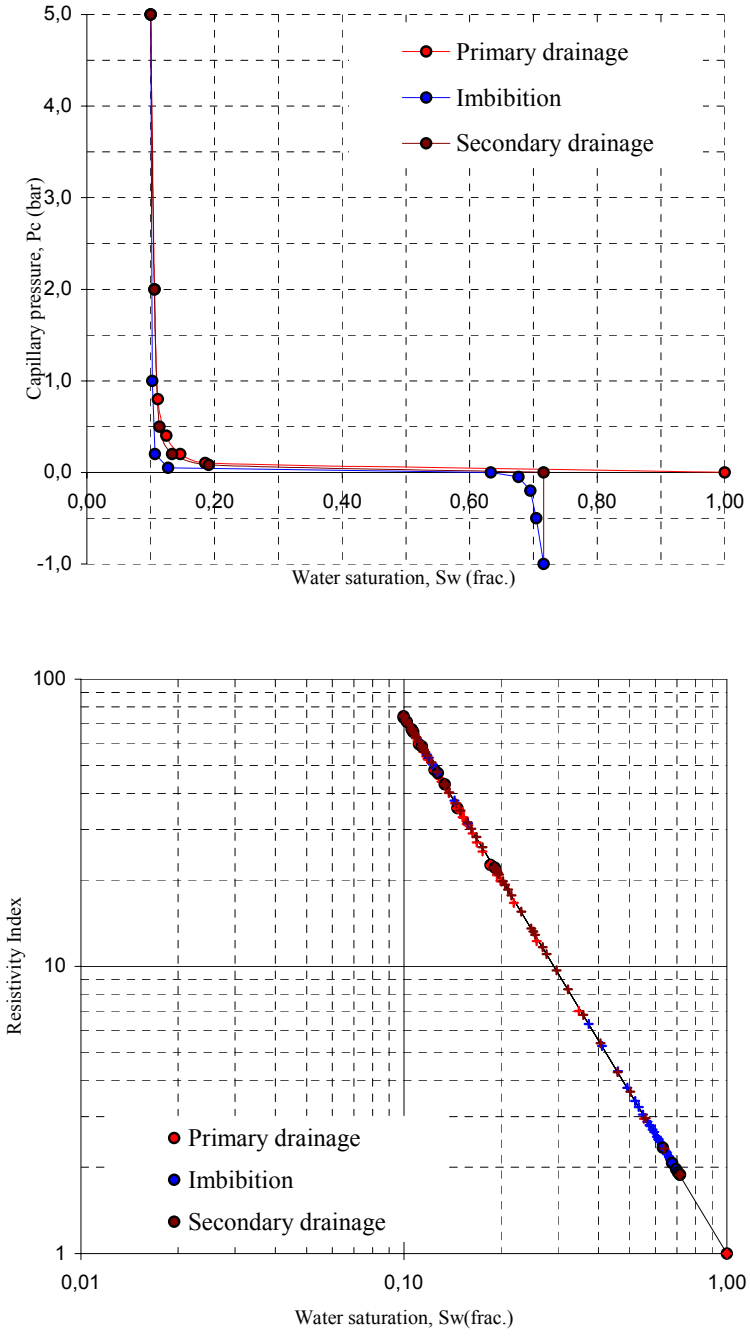

Figure 7.34 Full cycle capillary pressure and resistivity index, program C, Bentheimer no.2.

Bentheimer sample no.	: 3
Porous plate type	: Layered
Water permeability at 200 bar NCP (mD)	: 2094
Porosity at 200 bar NCP (frac.)	: 0.227
Irreducible water saturation, Pc=5 bar	: 0.104
Residual oil saturation, Pc=-1 bar	: 0.286
n exponent	: 1.77

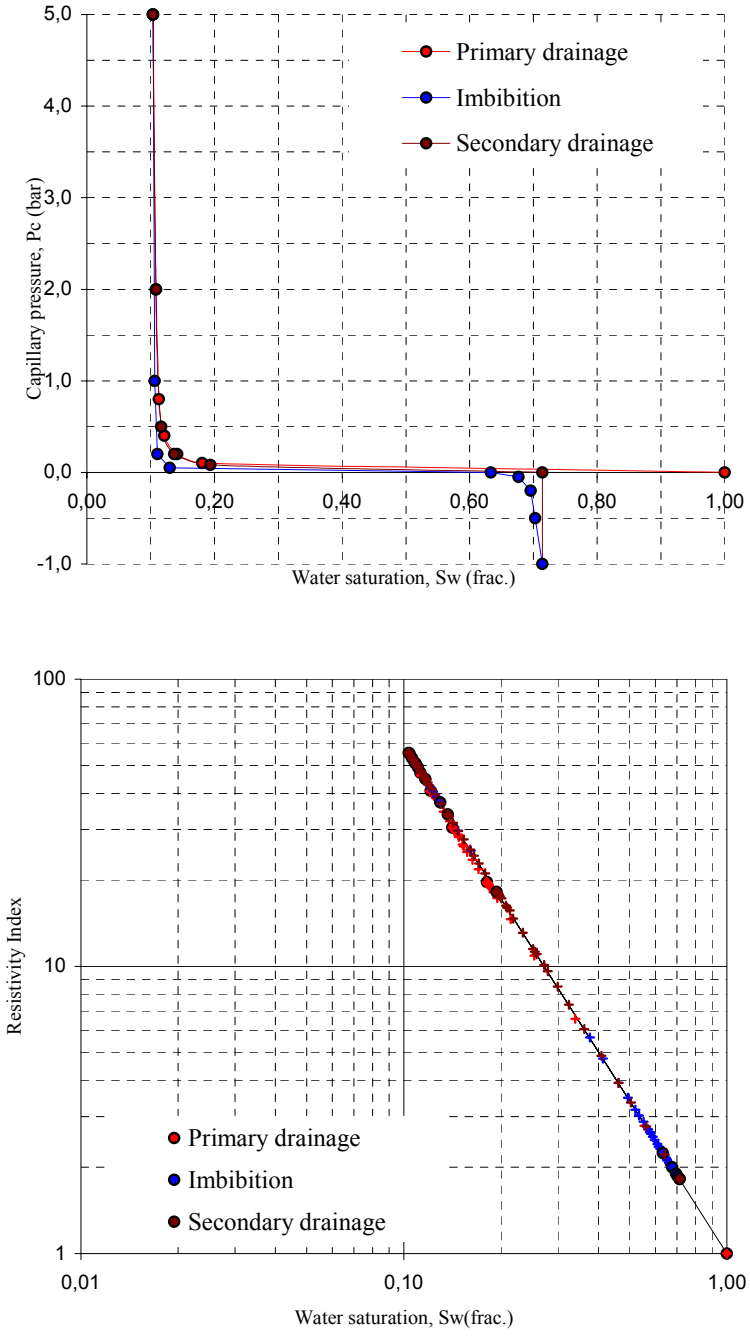

Figure 7.35 Full cycle capillary pressure and resistivity index, program C, Bentheimer no.3.

Bentheimer sample no.	: 4
Porous plate type	: Layered
Water permeability at 200 bar NCP (mD)	: 1424
Porosity at 200 bar NCP (frac.)	: 0.227
Irreducible water saturation, Pc=5 bar	: 0.107
Residual oil saturation, Pc=-1 bar	: 0.268
n exponent	: 1.80

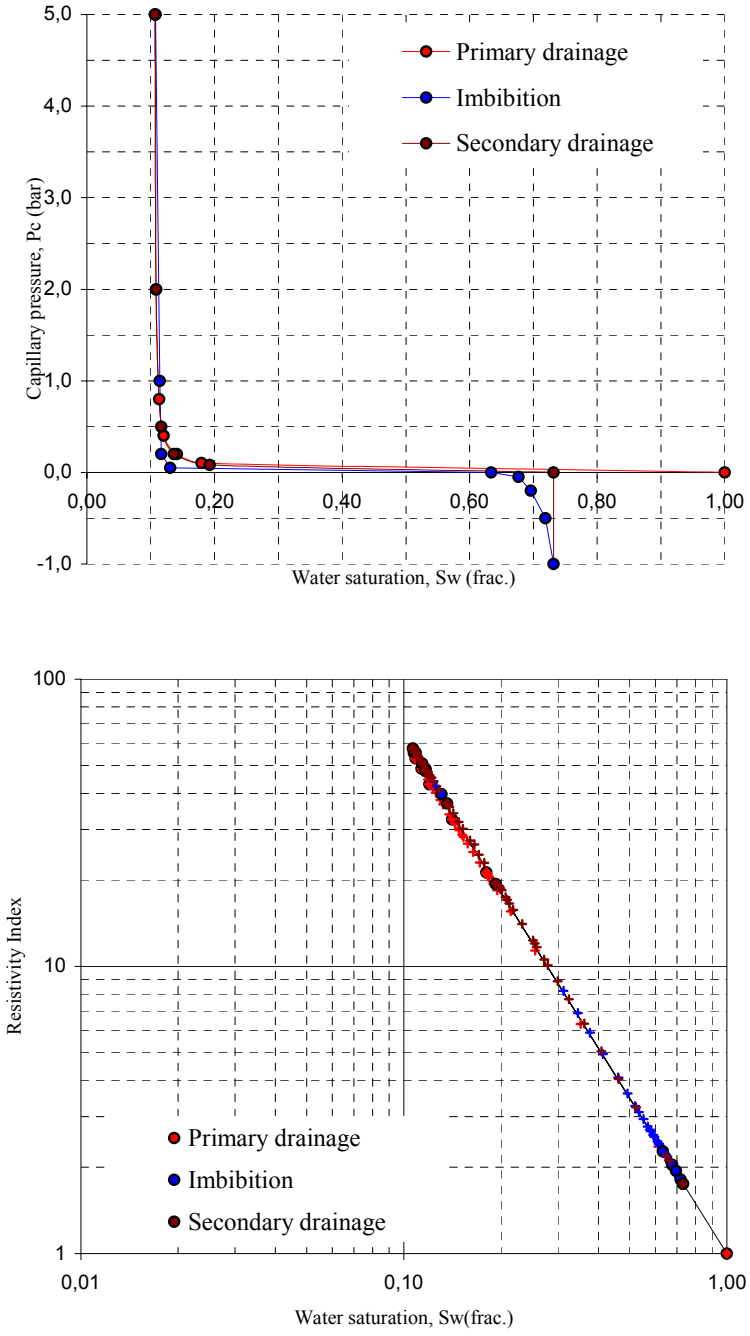

Figure 7.36 Full cycle capillary pressure and resistivity index, program C, Bentheimer no.4.

Bentheimer sample no.	: 5
Porous plate type	: Layered
Water permeability at 200 bar NCP (mD)	: 1401
Porosity at 200 bar NCP (frac.)	: 0.216
Irreducible water saturation, Pc=5 bar	: 0.119
Residual oil saturation, Pc=-1 bar	: 0.260
n exponent	: 1.86

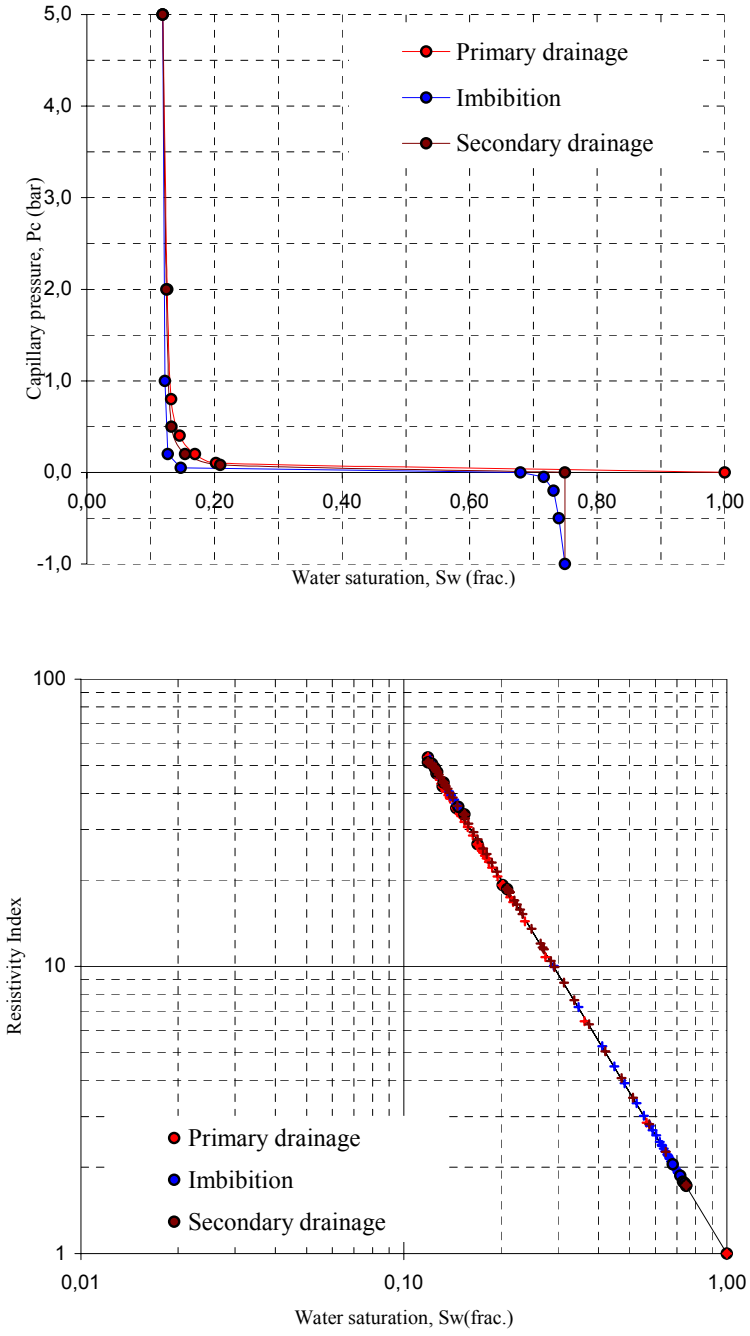

Figure 7.37 Full cycle capillary pressure and resistivity index, program C, Bentheimer no.5.

Bentheimer sample no.	: 6
Porous plate type	: Layered
Water permeability at 200 bar NCP (mD)	: 1833
Porosity at 200 bar NCP (frac.)	: 0.230
Irreducible water saturation, Pc=5 bar	: 0.110
Residual oil saturation, Pc=-1 bar	: 0.252
n exponent	: 1.78

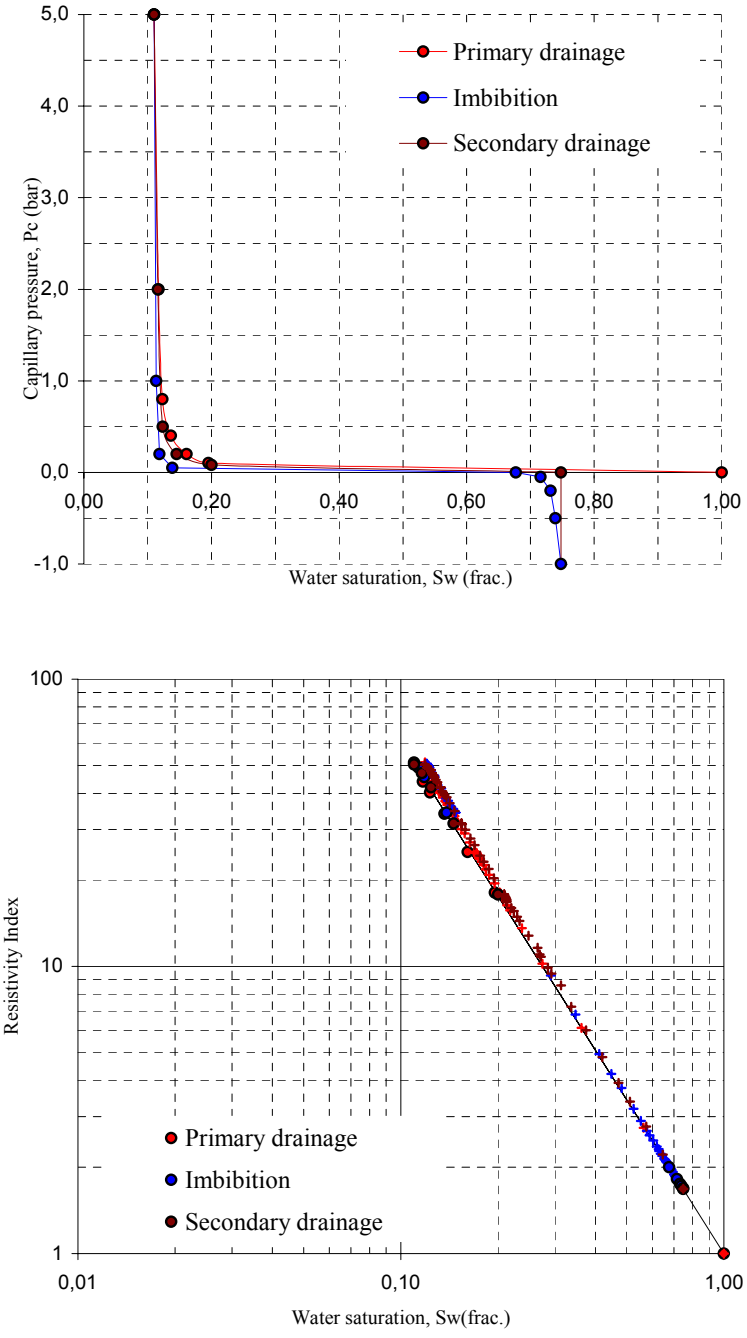

Figure 7.38 Full cycle capillary pressure and resistivity index, program C, Bentheimer no.6.

Bentheimer sample no.	: 7
Porous plate type	: Layered
Water permeability at 200 bar NCP (mD)	: 1411
Porosity at 200 bar NCP (frac.)	: 0.229
Irreducible water saturation, Pc=5 bar	: 0.108
Residual oil saturation, Pc=-1 bar	: 0.286
n exponent	: 1.81

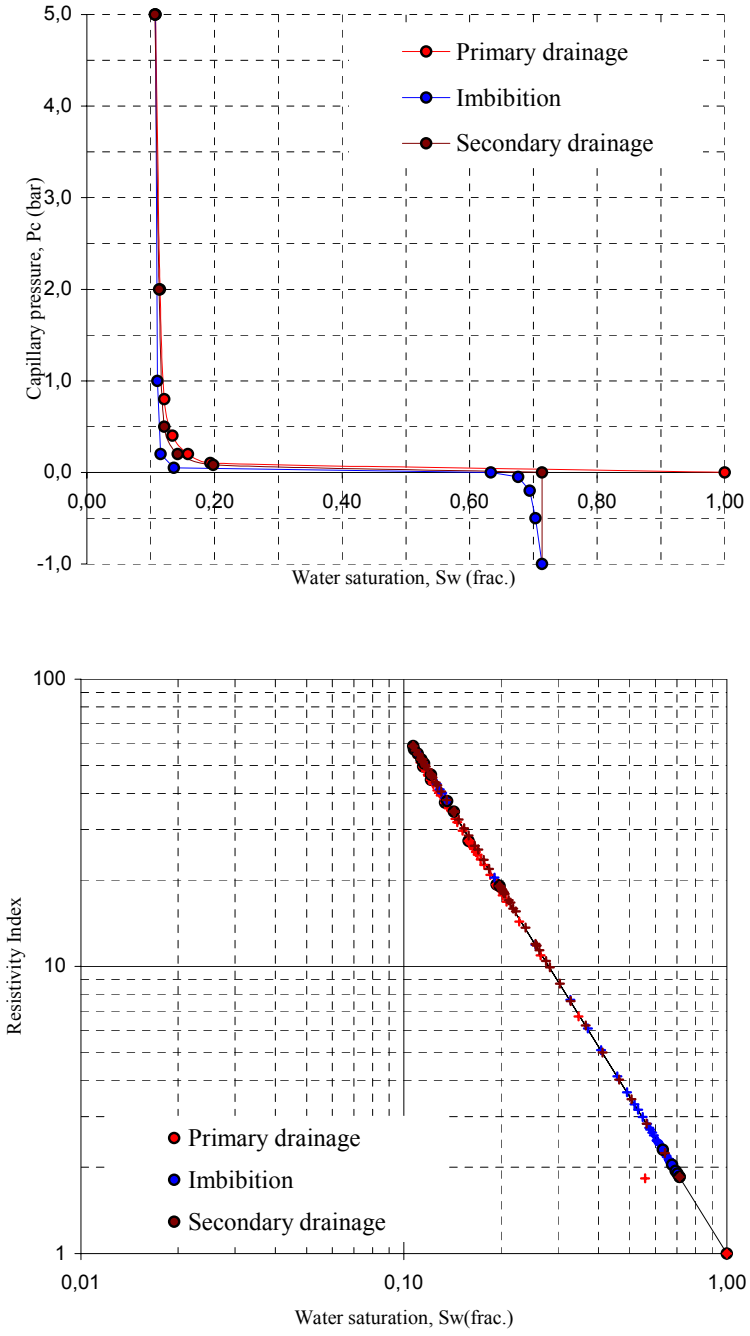

Figure 7.39 Full cycle capillary pressure and resistivity index, program C, Bentheimer no.7.

Bentheimer sample no.	: 8
Porous plate type	: Layered
Water permeability at 200 bar NCP (mD)	: 2413
Porosity at 200 bar NCP (frac.)	: 0.228
Irreducible water saturation, Pc=5 bar	: 0.093
Residual oil saturation, Pc=-1 bar	: 0.291
n exponent	: 1.85

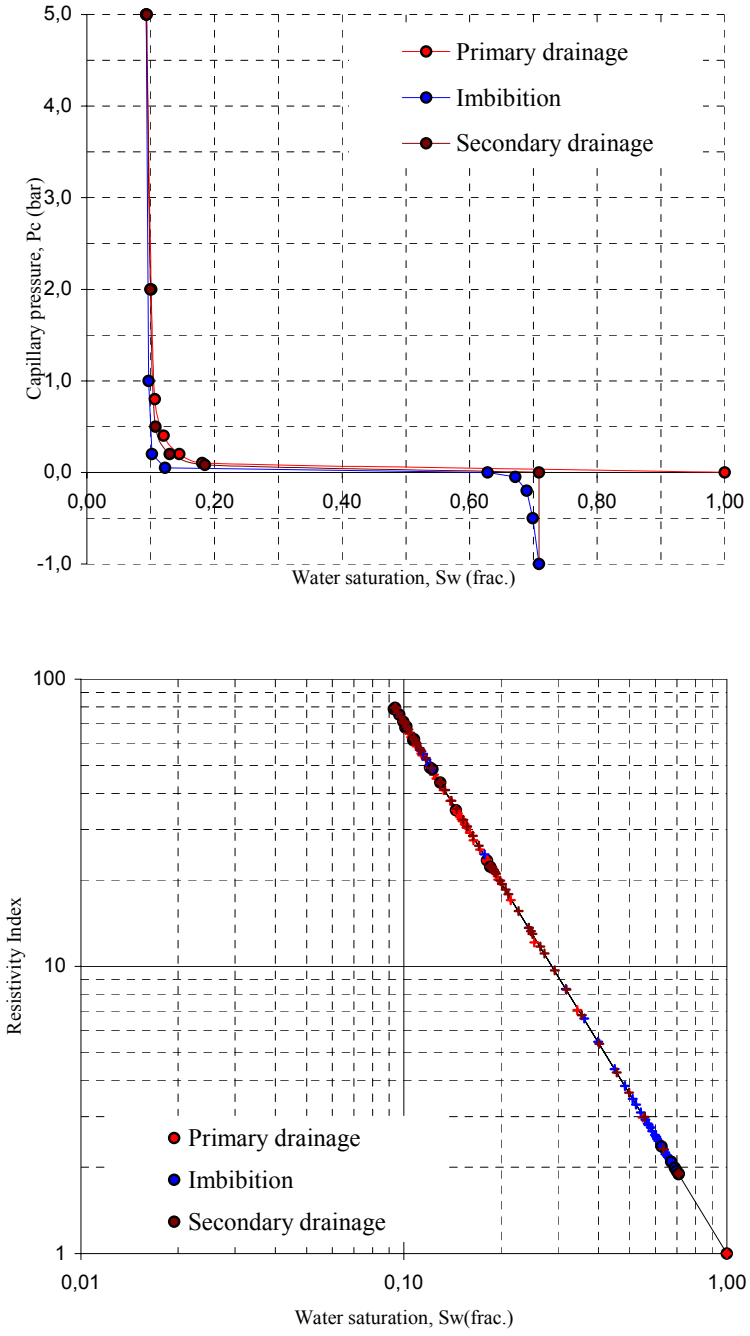

Figure 7.40 Full cycle capillary pressure and resistivity index, program C, Bentheimer no.8.

Bentheimer sample no.	: 9
Porous plate type	: Homogeneous
Water permeability at 200 bar NCP (mD)	: 2147
Porosity at 200 bar NCP (frac.)	: 0.224
Irreducible water saturation, Pc=5 bar	: 0.112
Residual oil saturation, Pc=-1 bar	: 0.284
n exponent	: 1.89

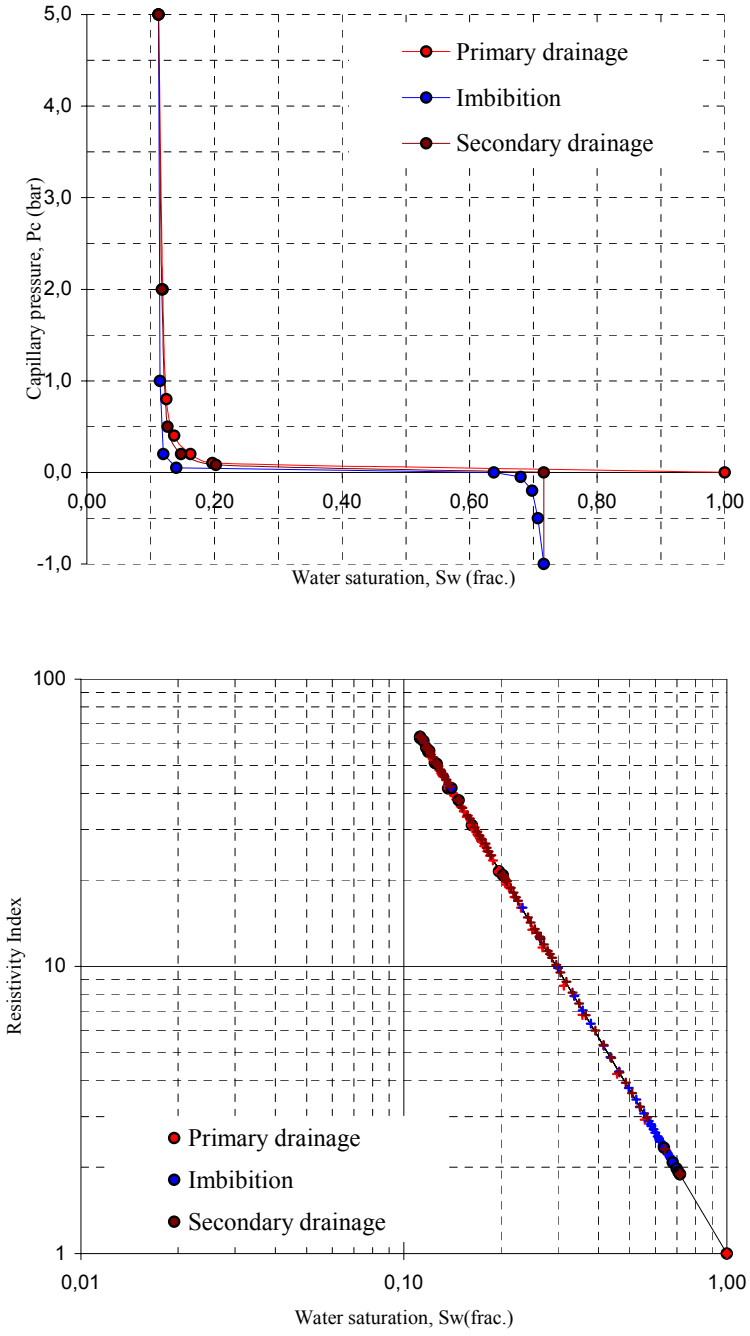

Figure 7.41 Full cycle capillary pressure and resistivity index, program C, Bentheimer no.9.

Bentheimer sample no.	: 10
Porous plate type	: Homogeneous
Water permeability at 200 bar NCP (mD)	: 2410
Porosity at 200 bar NCP (frac.)	: 0.229
Irreducible water saturation, Pc=5 bar	: 0.096
Residual oil saturation, Pc=-1 bar	: 0.291
n exponent	: 1.85

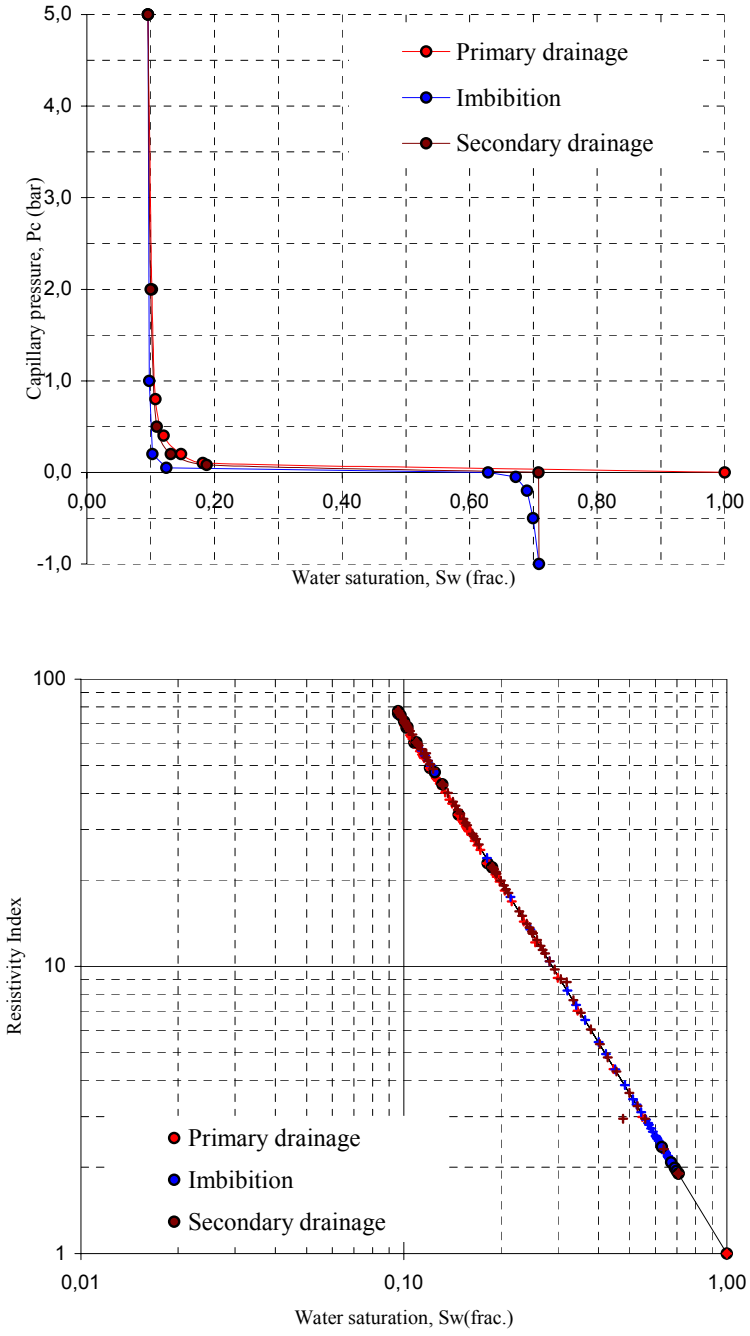

Figure 7.42 Full cycle capillary pressure and resistivity index, program C, Bentheimer no.10.

Bentheimer sample no. : 1-10

Porous plate type : Layered and Homogeneous

n exponent primary drainage : 1.83

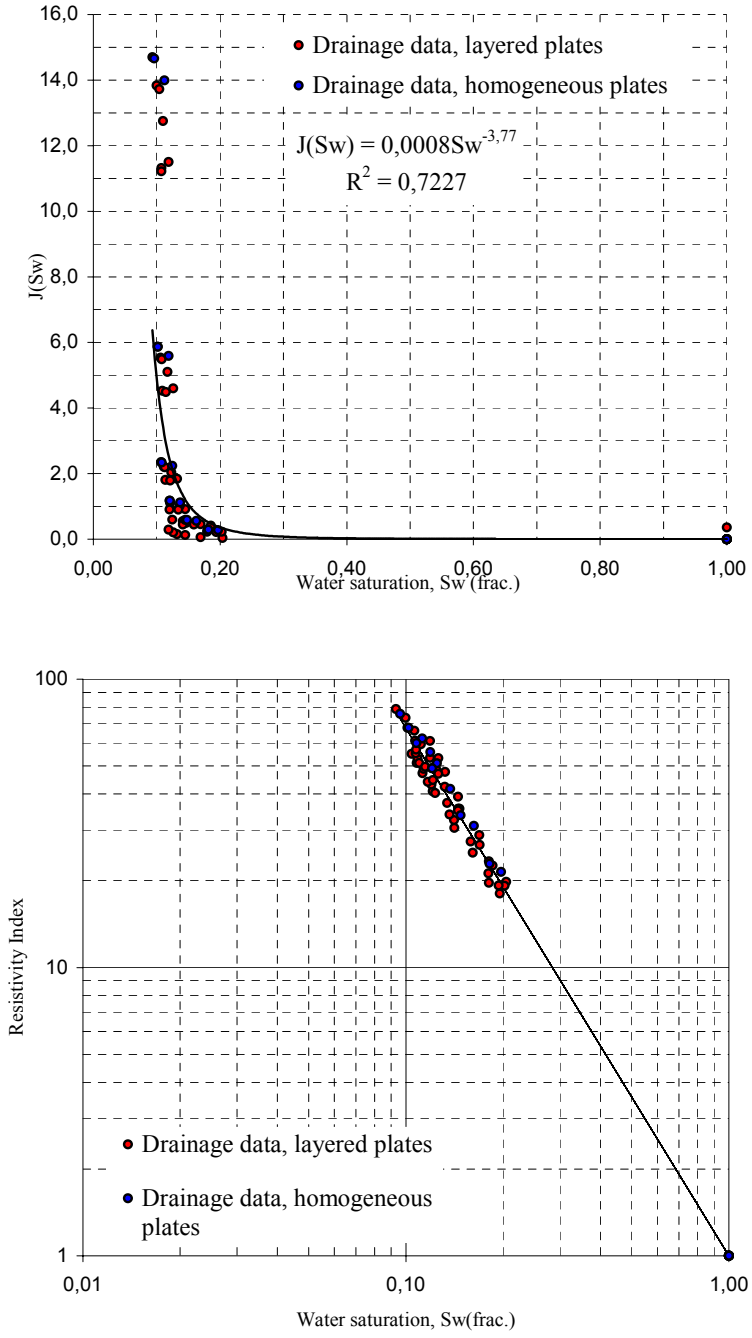

Figure 7.43 J(Sw) and resistivity index, primary drainage.

Bentheimer sample no. : 1-10

Porous plate type : Layered and Homogeneous

n exponent primary drainage : 1.83

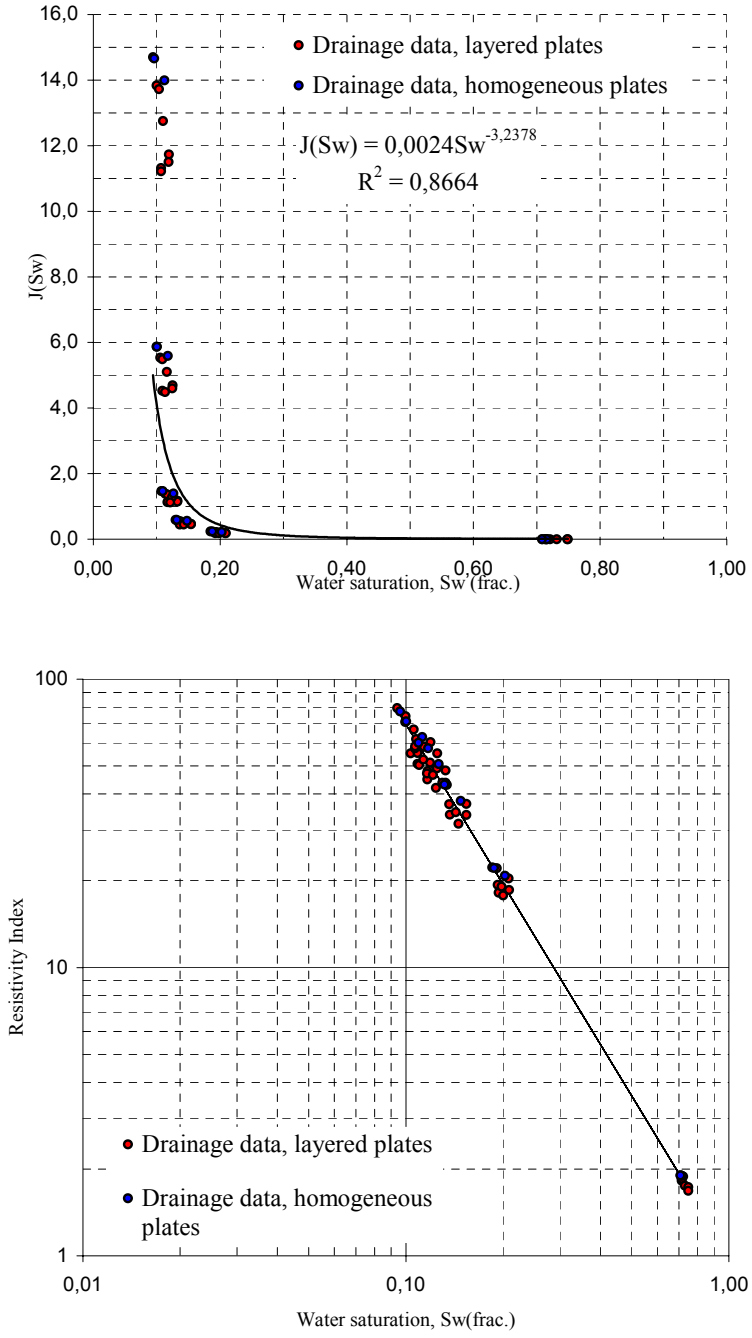

Figure 7.44 J(Sw) and resistivity index, secondary drainage.

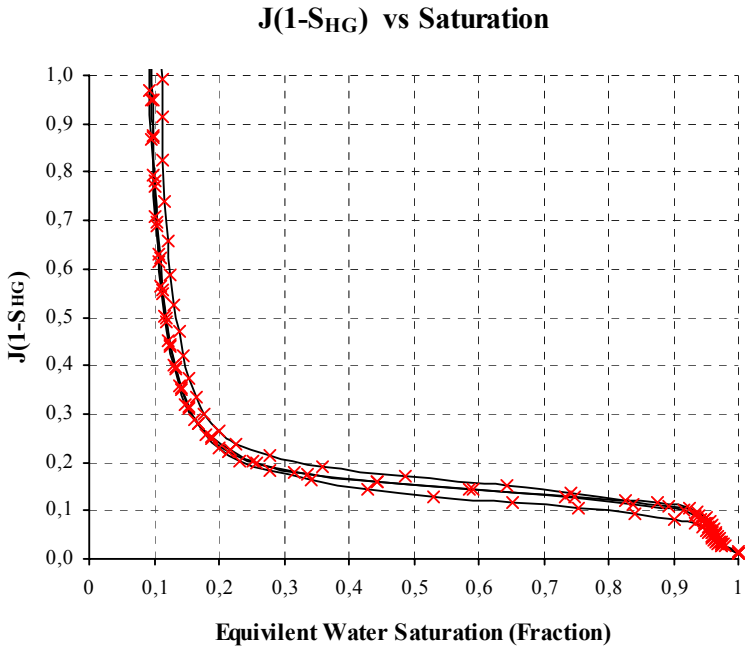

Dimensionless mercury injection data on end trimmings confirm that Bentheimer no. 1 is slightly different from the remaining samples near irreducible water saturation. Equivalent water saturation from mercury intrusion data match obtained water saturation at P_c=230 mbar and P_c=5 bar, program A and C respectively.

Figure 7.45 J(Sw) Mercury injection data.

Reproducibility, program C

The total experimental turnaround time for obtaining full cycle capillary pressure measurements using the layered porous plate technique was 209 days. Corresponding experimental turnaround time for the remaining two experiments using the homogeneous porous plate technique was 477 days.

Due to the long experimental turnaround time, it was decided to exclude investigation of reproducibility for this program. However, irreducible water saturation obtained during secondary drainage produces a fairly good match with obtained irreducible water saturation from primary drainage. In other words, mass balance in the system.

Observations and discussions, program C

Several observations can be observed by studying full cycle capillary pressure measurements. These can be summarised as follows:

Obtained irreducible water saturation is lower than water saturation obtained in program A. This is in line with expectations since irreducible water saturation is established at P_c=5 bar instead of P_c=230 mbar.

Obtained Sw-RI relationships are in good agreement with obtained Sw-RI relationships in program A.

No major hysteresis, as a function of porous plate type for the Sw-Pc or Sw-RI relationships, is seen. The only difference observed is experimental turnaround time. A total time saving factor of 2.28 is achieved from layered porous plate technique.

Description of a transient production model, program C

A primary drainage sequence is relatively easy to forecast with respect to the hierarchy involved. The hierarchy is, under normal circumstances, known as a percolation process. I.e. the next largest pore channel along the continuous non-wetting interface will be invaded next.

Capillary imbibition is a much more complex sequence. Hierarchies and mechanisms involved are a function of several parameters such as wettability and pore to throat size ratio. It is therefore difficult, if exciting, to find an analytical solution describing the influence of a ceramic plate for an imbibition process.

Lenormand et al. [11] has proven, making certain assumptions, that an analytical solution describing production for small pressure steps is a sum of exponential terms. Fleury et al.[12]

introduced a first order approximation of the analytical solution using an optimisation routine, in order to determine V_{max} and t_c. By using this, transient production after changing the capillary pressure step can be described as

$$V(t) = V_{\max} \cdot (1 - \exp(-\tfrac{t}{t_c})) \tag{39}.$$

Early observations using different ceramic plates[13] in capillary pressure measurements indicated a significant reduction in experimental turnaround time using layered porous plates. In order to detect other possible effects, we initiated this program using comparable plugs, the same capillary sequence and very strict equilibrium criteria. Hence, V_{max} can be considered as a known constant and the first order approximation can be written as

$$V_r = \frac{V(t)}{V_{\max}} = 1 - \exp(-\frac{t}{t_c}) \Rightarrow \ln(1 - V_r) = -\frac{t}{t_c} \tag{40}.$$

Characteristic time, t_c , is determined by plotting $\ln(1-V_r)$ versus t for each plug, capillary pressure and capillary sequence. After establishing characteristic time, it is possible to study the influence of porous plates by introducing the parameter characteristic time ratio ψ as

$$\psi = \frac{t_{c(\text{hom}\,ogeneous)}}{t_{c(layered)}} \tag{41}.$$

Characteristic time ratio illustrates the relative influence of porous plate type. Figure 7.46 illustrates the concept of establishing characteristic time.

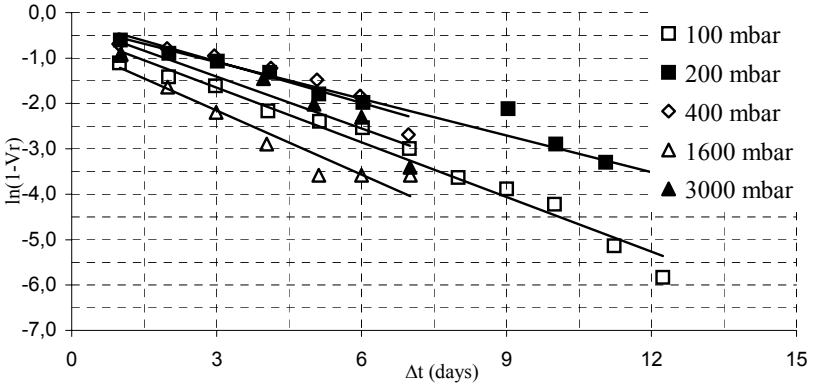

Figure 7.46 Schematic illustration of establishing characteristic time.

Determination of characteristic time at each capillary pressure step produces a set of linear functions for each plug and capillary pressure sequence.

It should be noted that equation (41) becomes unstable when V(t) goes to V_{max}. Hence transient data near equilibrium is excluded from regression analysis.

Experiment 9 and experiment 10 were initiated with homogeneous porous plates. In order to calculate characteristic time ratios, we need to compare experiment no. 9 and no. 10 with corresponding layered porous plate derived data. The petrophysical properties of Bentheimer no.9 and no. 10 match fairly well the petrophysical properties of layered experiment no. 1 and 8 respectively. It was therefore decided to study the influence of porous plates by using 1-9 and 8-10 as plug pairs. I.e. assuming perfect twins.

Table 7.7 Characteristic time ratio, Bentheimer no. 1 and no. 9.

	Layered porous plate			Homogeneous porous plate			
	Plug no. 1		n: 1.92	Plug no. 9		n: 1.89	
Pc (bar)	Sw (frac.)	Time (days)	t_c	Sw (frac.)	Time (days)	t_c	ψ
0.100	0.204	15.8	1.40	0.197	64.5	6.05	4.34
0.200	0.200	28.2	3.60	0.162	112.3	13.19	3.66
0.400	0.145	36.9	2.24	0.137	131.2	5.64	2.52
0.800	0.132	46.1	2.66	0.125	143.0	5.07	1.91
2.000	0.126	52.1	2.15	0.119	149.4	2.39	1.36
5.000	0.119	57.1	1.67	0.112	155.0	1.72	1.03
1.000	0.122	62.0	1.36	0.115	160.3	5.65	4.14
0.200	0.127	67.0	1.98	0.120	167.0	3.34	1.69
0.050	0.147	75.8	2.31	0.140	179.9	3.41	1.47
0.000	0.643	104.0	5.47	0.638	249.0	11.01	2.01
-0.050	0.685	121.0	2.47	0.680	281.3	4.07	1.65
-0.200	0.702	131.9	3.13	0.698	299.2	5.59	1.79
-0.500	0.711	140.8	2.95	0.707	309.9	3.51	1.19
-1.000	0.721	147.8	2.39	0.716	316.1	2.43	1.02
0.000	0.721	152.9		0.716	320.1		
0.080	0.208	178.8	4.42	0.203	417.9	15.77	3.57
0.200	0.154	188.9	3.90	0.148	446.3	11.04	2.83
0.500	0.133	196.9	2.21	0.126	462.0	3.51	1.56
2.000	0.125	203.8	1.97	0.117	471.4	2.80	1.42
5.000	0.119	208.9	4.42	0.112	476.5	4.56	1.03

Table 7.8 Characteristic time ratio, Bentheimer no. 8 and no. 10.

	Layered porous plate			Homogeneous porous plate			
	Plug no. 8		n: 1.85	Plug no. 10		n: 1.85	
Pc (bar)	Sw (frac.)	Time (days)	t_c	Sw (frac.)	Time (days)	t_c	ψ
0.100	0.181	15.8	1.41	0.182	64.5	6.11	4.32
0.200	0.145	28.2	3.59	0.148	112.3	13.30	3.70
0.400	0.120	36.9	2.10	0.121	131.2	5.58	2.65
0.800	0.107	46.1	3.07	0.108	143.0	5.07	1.65
2.000	0.101	52.1	1.73	0.102	149.4	2.18	1.26
5.000	0.093	57.1	1.33	0.096	155.0	1.35	1.01
1.000	0.097	62.0	1.73	0.098	160.3	5.65	3.27
0.200	0.102	67.0	2.39	0.103	167.0	3.34	1.39
0.050	0.123	75.8	2.28	0.125	179.9	3.91	1.72
0.000	0.628	104.0	5.49	0.629	249.0	11.04	2.01
-0.050	0.672	121.0	2.44	0.672	281.3	4.07	1.67
-0.200	0.690	131.9	3.15	0.690	299.2	4.98	1.56
-0.500	0.699	140.8	3.20	0.699	309.9	4.94	1.54
-1.000	0.709	147.8	2.58	0.709	316.1	2.63	1.02
0.000	0.709	152.9		0.708	320.1		
0.080	0.185	178.8	4.45	0.188	417.9	15.82	3.56
0.200	0.130	188.9	3.89	0.132	446.3	11.22	2.89
0.500	0.180	196.9	2.22	0.110	462.0	3.57	1.61
2.000	0.100	203.8	1.83	0.100	471.4	2.80	1.53
5.000	0.094	208.9	1.29	0.096	476.5	1.85	1.44

Transient behaviour for all layered and homogeneous porous plate experiments are presented in figure 7.47.

Interpretation of characteristic time ratios is presented in figure 7.48-7.50 for primary drainage, imbibition and secondary drainage respectively.

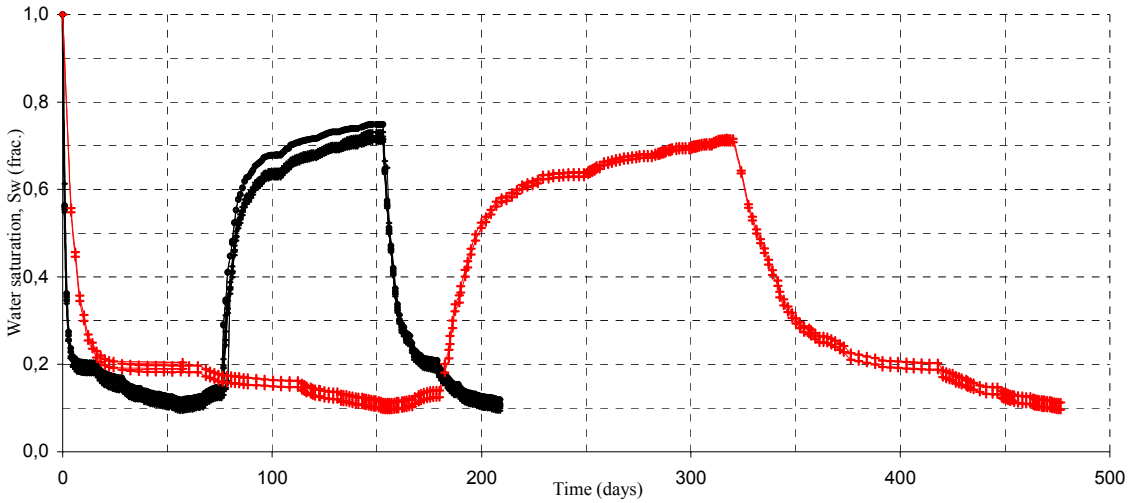

Figure 7.47 transient behaviour for layered and homogeneous porous plate technique

The figure illustrates transient production versus experimental time for experiment 1-10.

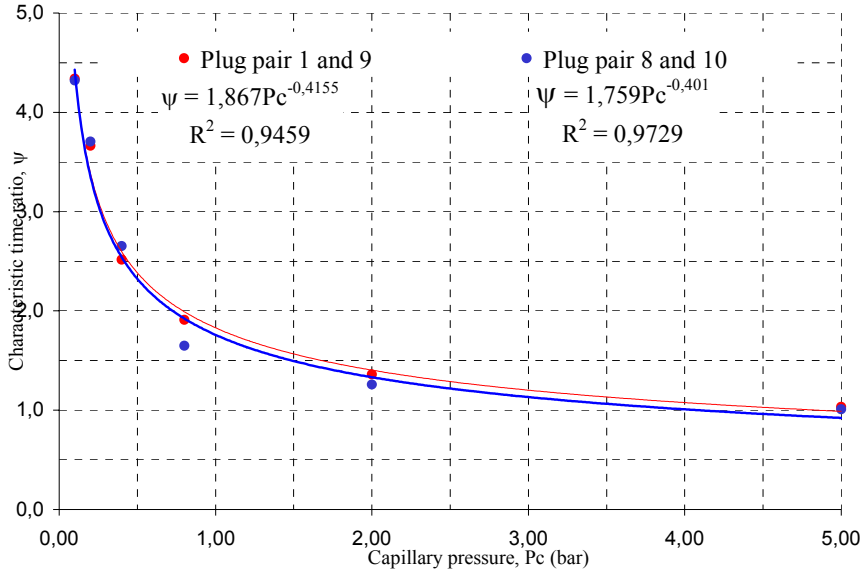

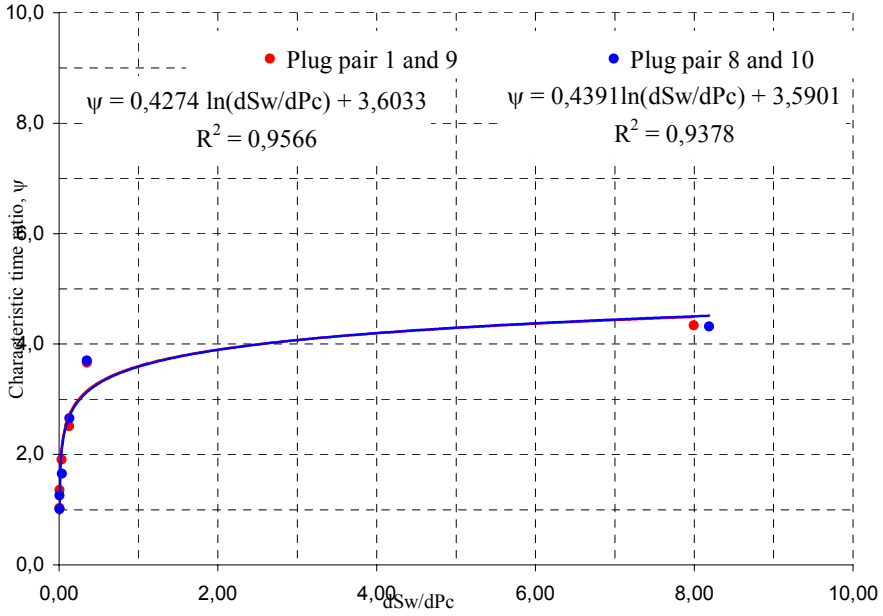

Figure 7.48 Influence of porous plates on capillary drainage, Bentheimer rocks

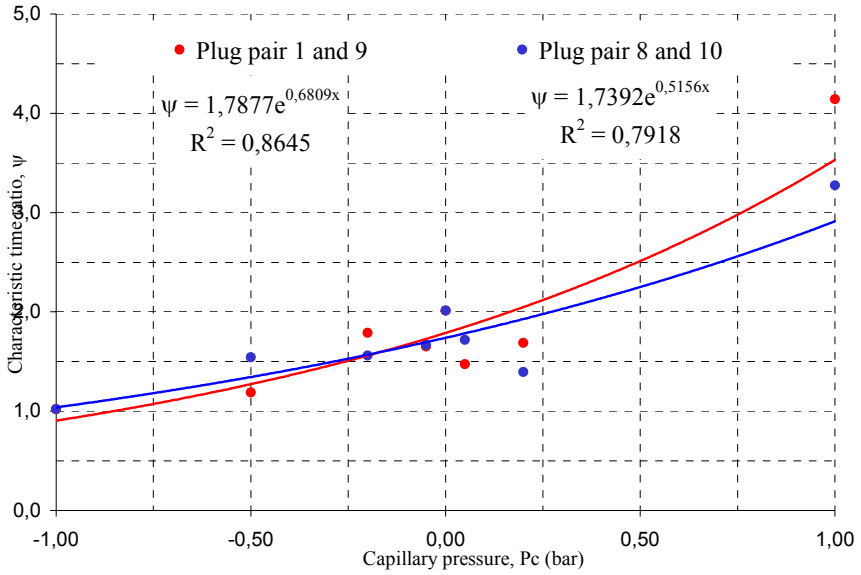

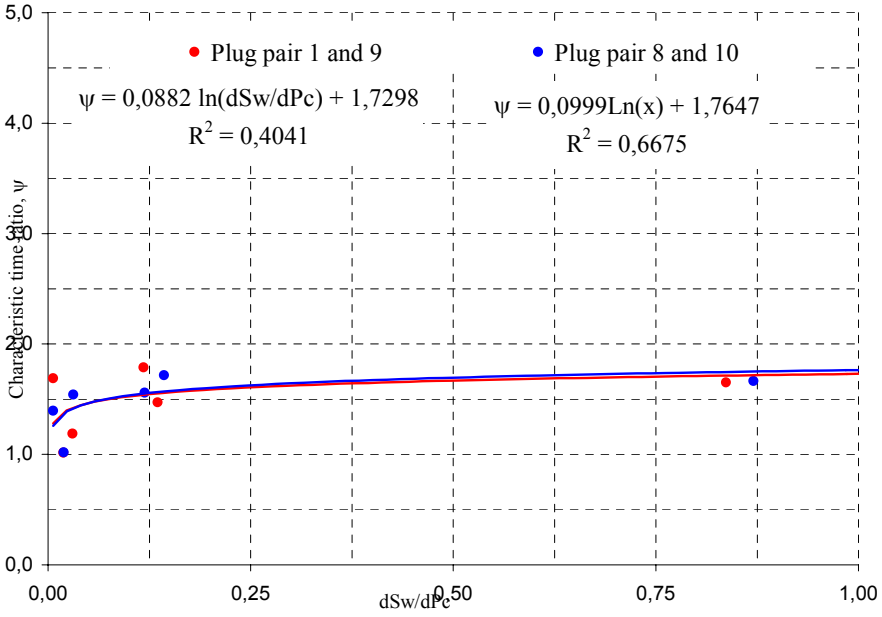

Figure 7.49 Influence of porous plates on positive and negative imbibition, Bentheimer rocks

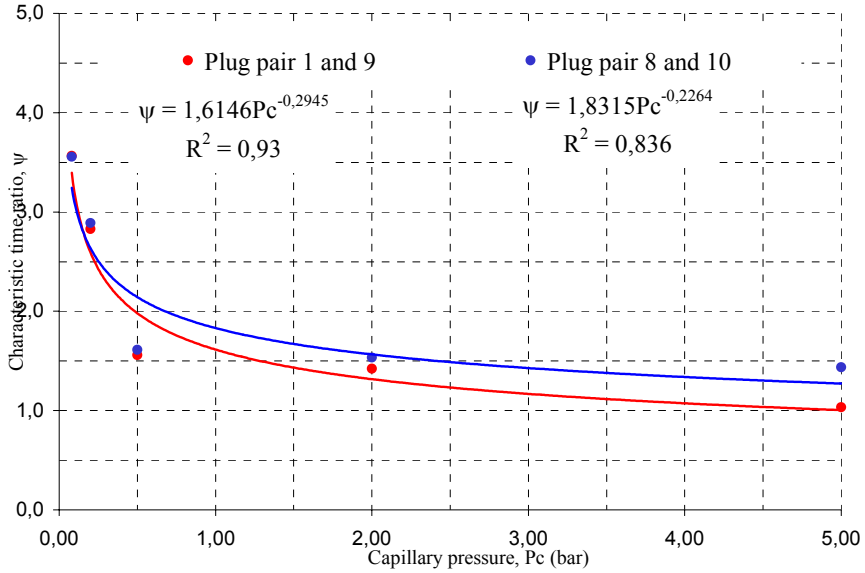

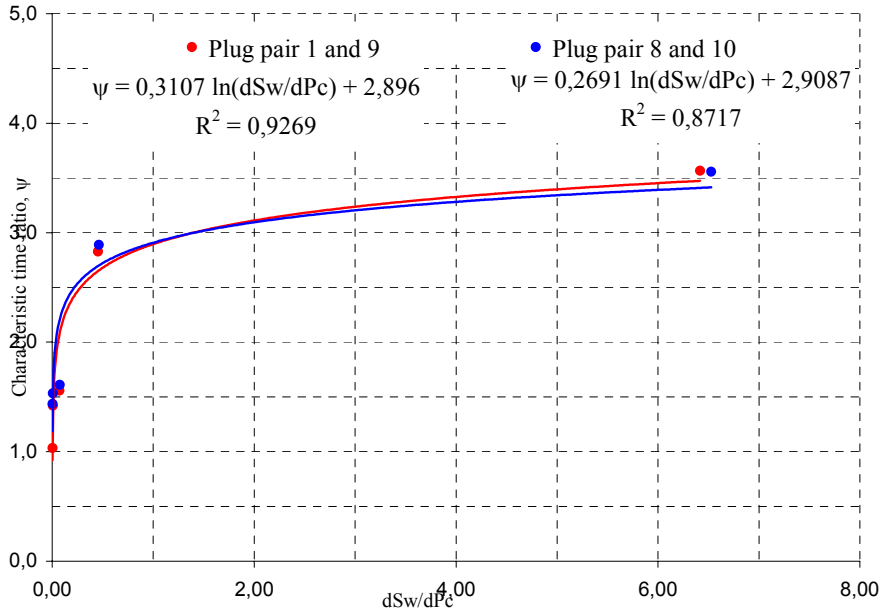

Figure 7.50 Influence of porous plates on positive and negative imbibition, Bentheimer rocks.

Conclusions, program C.

Effective drainage and imbibition rates depend on the type of porous plate used but the capillary pressure curve and electrical properties are the same.

The layered plate is faster than the homogeneous plate at all saturation levels. The difference almost disappears at low water saturation for primary drainage and at low oil saturation for forced imbibition, when the drainage and imbibition rates are controlled by the fluid mobilities in the core and not by the plate properties.

The influence of porous plates on effective rates is largest at the beginning of primary drainage and secondary drainage. I.e. when the contrast between the mobility of the core and the porous plate is large. This indicates that the porous plate influences increase with increasing permeability.

Characteristic time, established from a first order exponential approximation, is a useful parameter for evaluating the influence of porous plates at different capillary pressure steps. The method seems to be robust for most of the investigated pressure steps but becomes uncertain if the amount of transient production data is reduced.

It seems that characteristic time from transient imbibition data, at a very slow velocity, is not properly described with a first order exponential approximation. Further investigation should therefore be carried out.

The characteristic time ratio, or the relative influence of porous plate types, correlates with capillary pressure and dS_w / dP_c.

8. LIMITATIONS OF LAYERED POROUS PLATES TECHNIQUE

Objectives

The experimental programs performed on Bentheimer core plugs have proven that it is possible to obtain much faster data by using the layered porous plate technique instead of the traditional porous plate technique. In addition, it seems that the increased speed of the capillary pressure measurements will not influence the S_w-Pc or S_w-RI relationships. However, Isopar is synthetic oil, which seldom alters the wettability at any stage.

In order to find more about possible restrictions to the layered porous plate method, it needs to be tested for all types of conditions. The most used system in water or gas zones are Isopar-water or gas-brine systems at ambient temperature. In transition and oil zones the porous plate method is usually performed at pseudo reservoir condition. I.e. stock tank oil-water systems at reservoir temperature. In addition, it is possible to apply the porous plate method at full reservoir conditions. I.e. live oil water systems.

Layered porous plate method at pseudo reservoir condition

Parallel with program C, and in close cooperation with an oil company, the layered porous plate was tested on a poorly consolidated sandstone reservoir.

All experiments were performed at pseudo reservoir conditions (157 bar net confining pressure @ 85° C) using stock tank oil as the invading non-wetting fluid. Porosity varied from 0.268 to 0.272 and permeability varied from 1717 mD to 2421 mD.

Four sections of the reservoir oil zone were investigated using two comparable plugs from each section. Capillary behaviour on plug set A, plug no.1a-4a, was investigated using layered hydrophilic and hydrophobic ceramic plates. Corresponding plug set B, plug no. 1b-4b, was investigated using homogeneous plates.

In order to study how porous plate types influence time to achieve equilibrium, we decided to use the same strict equilibrium criteria as before. Equilibrium criteria required (1) no changes in water saturation and (2) no changes in resistivity index over a period of at least 48 hours. Long experimental turnaround time for the homogeneous porous plate experiments was therefore observed.

The core plugs from plug set A, using layered plates, were drained by stock tank oil to irreducible water saturation using eight capillary pressure steps. Final equilibrium, at irreducible water saturation, was reached after 76 days. Then, spontaneous imbibition was initiated using

three capillary pressure steps. Final equilibrium was reached 86 days after drainage was completed. The layered hydrophilic plates were then dismounted from the core holders and replaced by hydrophobic versions in the opposite end. Final equilibrium at residual oil saturation was reached 108 days after drainage was completed.

The core plugs from plug set B, using homogeneous plates, were investigated using the same capillary pressure steps. Corresponding comparable equilibrium data was recorded after 247, 238 and 279 days respectively.

It should be noted that the applied capillary pressure is increased or decreased after obtaining equilibrium on all core plugs from the same plug set.

Capillary pressure curves using layered porous plates are presented in Figure 8.1. The corresponding curves using homogeneous porous plates are presented in Figure 8.2. Figure 8.3 illustrating transient water saturation versus time for all the eight core plugs. A total experimental time saving factor of 2.86 is observed.

Table 8.1 Characteristic time ratio, plug no. 1a and 1b at pseudo reservoir conditions.

	Layered porous plate			Homogeneous porous plate			
	Plug no. 1a:		n: 2.04	Plug no. 1b:		n: 2.03	
Pc (bar)	Sw (frac.)	Time (days)	t_c	Sw (frac.)	Time (days)	t_c	ψ
0.000	1.000	0.0		1.000	0.0		
0.050	0.615	11.9	1.380	0.613	71.9	8.591	6.228
0.100	0.344	25.9	2.484	0.340	140.4	11.962	4.815
0.200	0.258	40.0	3.705	0.253	188.6	14.493	3.912
0.400	0.222	49.9	3.286	0.218	210.8	6.418	1.953
0.800	0.199	53.9	0.834	0.194	217.0	1.358	1.628
1.600	0.170	62.9	1.790	0.165	229.7	2.523	1.409
3.000	0.146	72.0	3.591	0.141	241.7	4.766	1.327
5.000	0.128	76.0	1.157	0.124	246.9	1.481	1.280
1.000	0.152	86.0	3.923	0.148	261.4	4.840	1.234
0.200	0.181	96.0	2.554	0.177	279.1	5.222	2.045
0.000	0.246	162.1	84.75	0.242	485.2	166.667	1.967
-0.100	0.569	169.9	1.477	0.567	503.4	3.427	2.320
-0.500	0.681	178.9	3.132	0.679	520.3	5.889	1.880
-1.000	0.692	183.9	1.009	0.691	526.2	1.180	1.169

Table 8.2 Characteristic time ratio, plug no. 2a and 2b at pseudo reservoir conditions.

	Layered porous plate Plug no. 2a:		n: 2.08	Homogeneous porous plate Plug no. 2b:		n: 2.09	
Pc (bar)	Sw (frac.)	Time (days)	t_c	Sw (frac.)	Time (days)	t_c	ψ
0.000	1.000	0.0		1.000	0.0		
0.050	0.612	11.9	1,410	0.613	71.9	11.099	7.872
0.100	0.339	25.9	2,455	0.340	140.4	16.103	6.559
0.200	0.252	40.0	3,828	0.253	188.6	14.793	3.864
0.400	0.217	49.9	3,564	0.217	210.8	7.463	2.094
0.800	0.192	53.9	0,769	0.194	217.0	1.316	1.711
1.600	0.163	62.9	1,824	0.165	229.7	2.691	1.475
3.000	0.140	72.0	3,814	0.141	241.7	5.155	1.352
5.000	0.122	76.0	1,157	0.123	246.9	1.481	1.280
1.000	0.146	86.0	3,923	0.148	261.4	5.627	1.434
0.200	0.175	96.0	2,469	0.177	279.1	5.456	2.210
0.000	0.240	162.1	74,627	0.242	485.2	172.414	2.310
-0.100	0.566	169.9	1,640	0.567	503.4	3.298	2.011
-0.500	0.679	178.9	3,139	0.679	520.3	5.838	1.860
-1.000	0.690	183.9	1,074	0.690	526.2	1.263	1.176

Table 8.3 Characteristic time ratio, plug no. 3a and 3b at pseudo reservoir conditions.

	Layered porous plate Plug no. 3a: n: 1.97			Homogeneous porous plate Plug no. 3b: n: 1.93			
Pc (bar)	Sw (frac.)	Time (days)	t_c	Sw (frac.)	Time (days)	t_c	ψ
0.000	1.000	0.0		1.000	0.0		
0.050	0.603	11.9	1.424	0.602	71.9	11.223	7.881
0.100	0.323	25.9	2,608	0.322	140.4	12.516	4.799
0.200	0.234	40.0	4.030	0.233	188.6	14.535	3.607
0.400	0.199	49.9	3.029	0.197	210.8	6.831	2.255
0.800	0.174	53.9	0.594	0.173	217.0	1.104	1.859
1.600	0.145	62.9	1.823	0.143	229.7	2.518	1.381
3.000	0.120	72.0	4.621	0.117	241.7	5.102	1.104
5.000	0.101	76.0	1.157	0.100	246.9	1.481	1.280
1.000	0.126	86.0	3.639	0.125	261.4	5.165	1.419
0.200	0.156	96.0	3.937	0.154	279.1	4.344	1.103
0.000	0.223	162.1	85.470	0.221	485.2	166.667	1.950
-0.100	0.556	169.9	1.452	0.555	503.4	3.334	2.296
-0.500	0.672	178.9	3.264	0.671	520.3	5.744	1.760
-1.000	0.683	183.9	1.078	0.681	526.2	1.117	1.036

Table 8.4 Characteristic time ratio, plug no. 4a and 4b at pseudo reservoir conditions.

	Layered porous plate Plug no. 4a:		n: 2.00	Homogeneous porous plate Plug no. 4b:		n: 2.06	
Pc (bar)	Sw (frac.)	Time (days)	t_c	Sw (frac.)	Time (days)	t_c	ψ
0.000	1.000	0.0		1.000	0.0		
0.050	0.610	11.9	1.386	0.610	71.9	8.696	6.274
0.100	0.336	25.9	2.505	0.336	140.4	13.072	5.218
0.200	0.249	40.0	3.357	0.249	188.6	14.771	4.400
0.400	0.213	49.9	2.893	0.214	210.8	6.024	2.082
0.800	0.189	53.9	0.834	0.189	217.0	1.520	1.823
1.600	0.159	62.9	1.786	0.160	229.7	2.303	1.289
3.000	0.135	72.0	4.177	0.136	241.7	5.294	1.267
5.000	0.117	76.0	1.157	0.118	246.9	1.268	1.096
1.000	0.141	86.0	4.284	0.144	261.4	5.181	1.209
0.200	0.171	96.0	2.696	0.172	279.1	3.975	1.474
0.000	0.236	162.1	82.645	0.236	485.2	163.934	1.984
-0.100	0.564	169.9	1.455	0.565	503.4	3.465	2.381
-0.500	0.677	178.9	3.010	0.678	520.3	6.046	2.009
-1.000	0.688	183.9	1.078	0.689	526.2	1.119	1.038

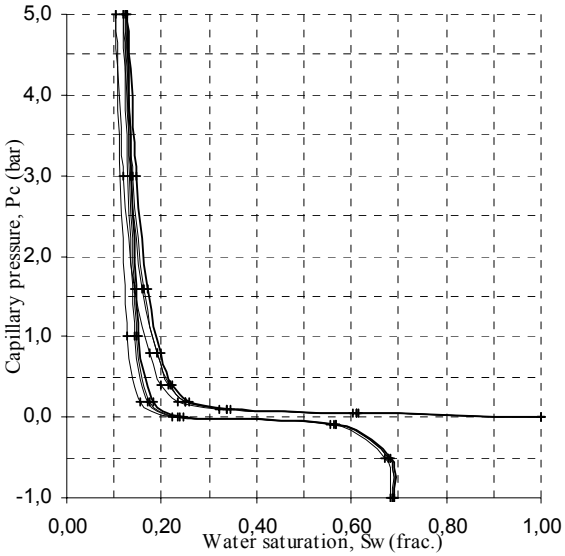

Figure 8.1 Capillary pressure, plug set A.

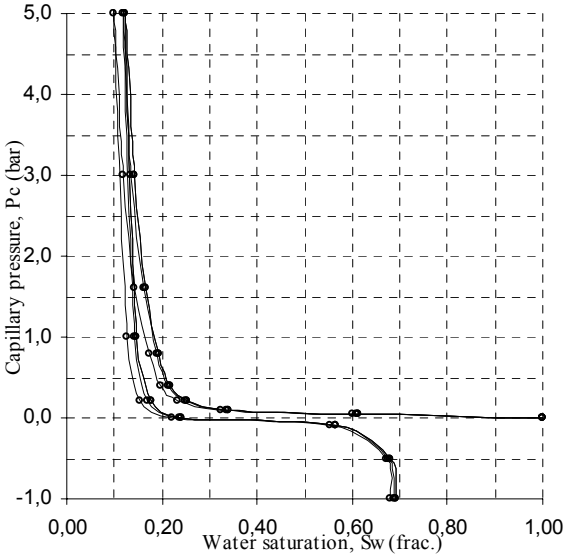

Figure 8.2 Capillary pressure, plug set B.

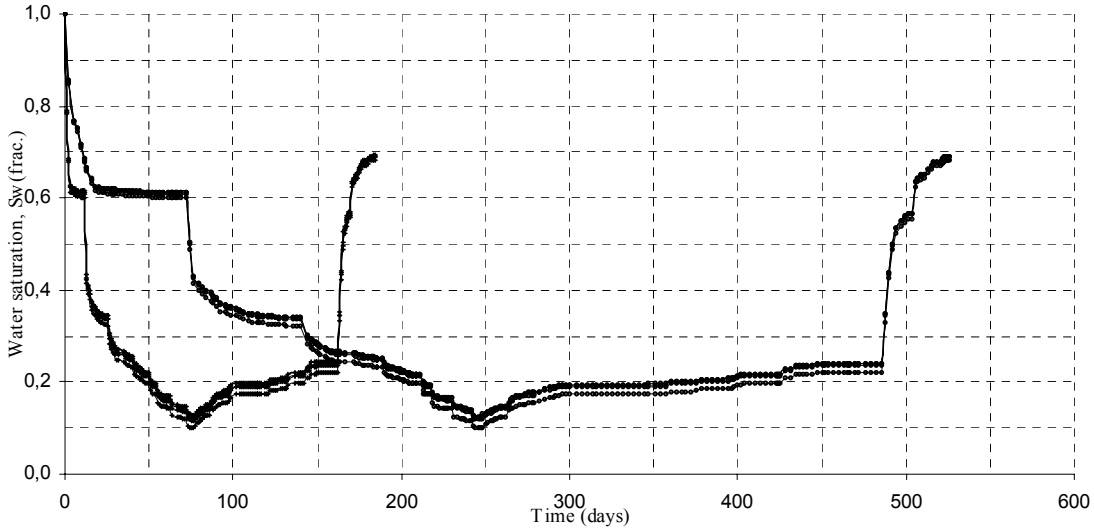

Figure 8.3 Transient capillary behaviour for layered and homogeneous porous plate experiments.

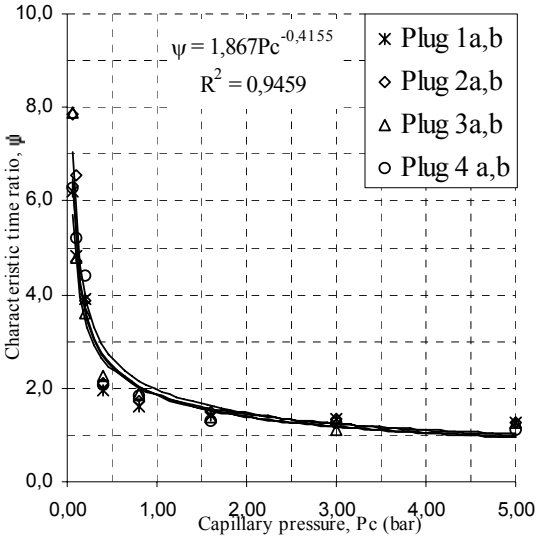

Figure 8.4 Primary drainage interpretation.

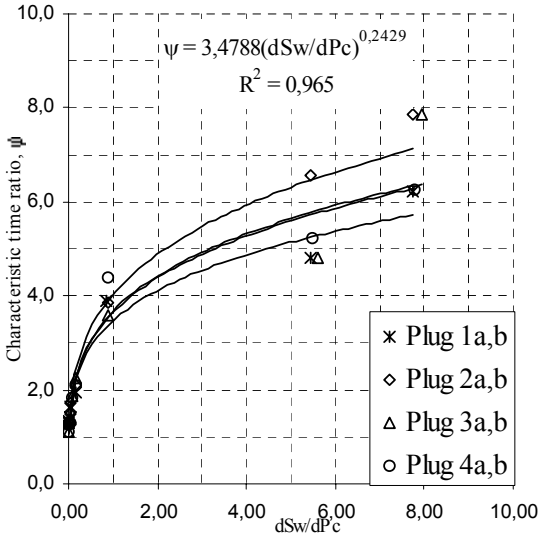

Figure 8.5 Primary drainage interpretation.

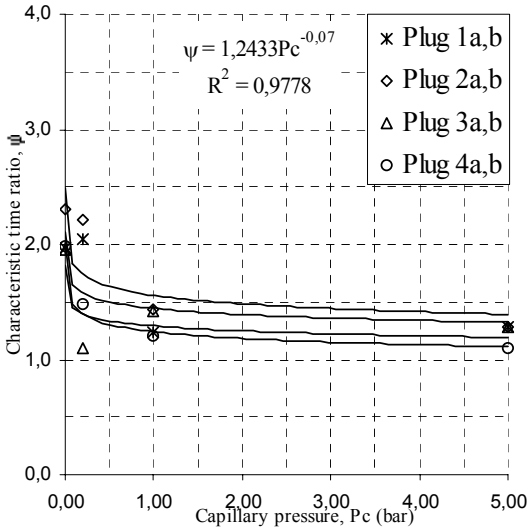

Figure 8.6 Sp. imbibition interpretation.

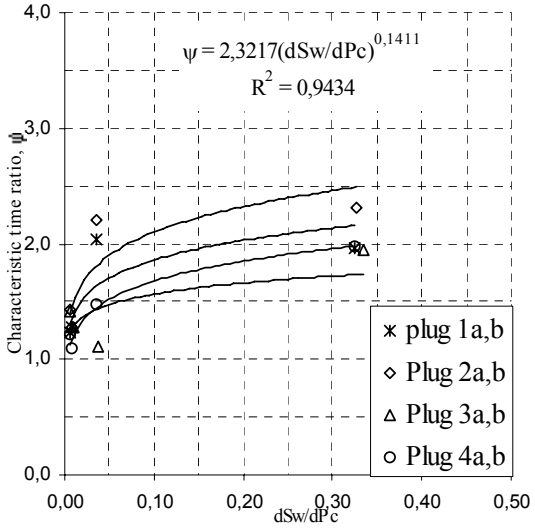

Figure 8.7 Sp. imbibition interpretation.

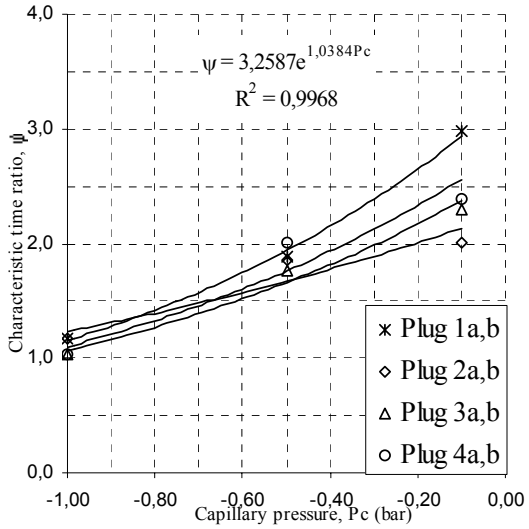

Figure 8.8 Forced imbibition interpretation.

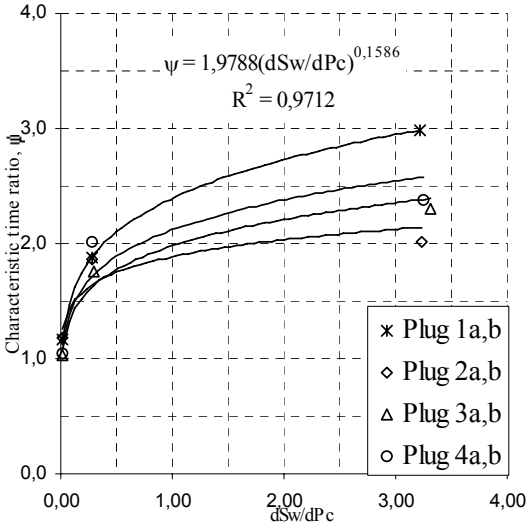

Figure 8.9 Forced imbibition interpretation.

Conclusions

In principle, the same conclusions as for program C with Bentheimer rocks can be drawn when comparing layered and homogeneous porous plate technique.

No hysteresis between layered and homogeneous porous plate techniques is observed. Negligible differences for the S_w-P_c or S_w-RI relationships are observed.

No sign of alternating wetting behaviour in the layered porous plates was seen. I.e. breakthrough.

Layered porous plate experiments for different permeability classes

In order to gain experience with the layered porous plate technique, the technique was tested for different reservoirs in the North Sea.

The curves for reservoir A, from a poorly consolidated sandstone reservoir with homogenous properties ($\varphi \approx 0.160$ and $k \approx 300mD$), are shown in figures 8.10a-c. The rocks were drained by oil to irreducible water saturation, using seven capillary pressure steps at 125 bar hydrostatic confining pressure. Final equilibrium, using layered porous plates, was reached 27 days after initiating drainage.

The curves presented for reservoir B (figures 8.11a-c), show results for a poorly consolidated sandstone reservoir in the North Sea with heterogeneous properties ($\varphi \approx 0.270 - 0.330$ and $k \approx 400 - 4000mD$). The rocks were drained by gas to irreducible water saturation, using seven capillary pressure steps at 250 bar hydrostatic confining pressure. Final equilibrium, using layered porous plates, was reached 22 days after initiating drainage.

Reservoir C (figures 8.12a-c), is a consolidated laminated sandstone reservoir in the North Sea with heterogeneous properties ($\varphi \approx 0.190 - 0.240$ and $k \approx 0.4 - 3000mD$). The rocks were drained by gas to irreducible water saturation using seven and ten capillary pressure steps at 200 bar hydrostatic confining pressure. Final equilibrium, using both layered and homogenous porous plates, was reached 71 and 207 days respectively after initiating drainage.

All reservoir data is plotted together (figures 8.13a-b) in order to illustrate the differences among them. There is a tendency towards decreasing time required as a function of increasing permeability.

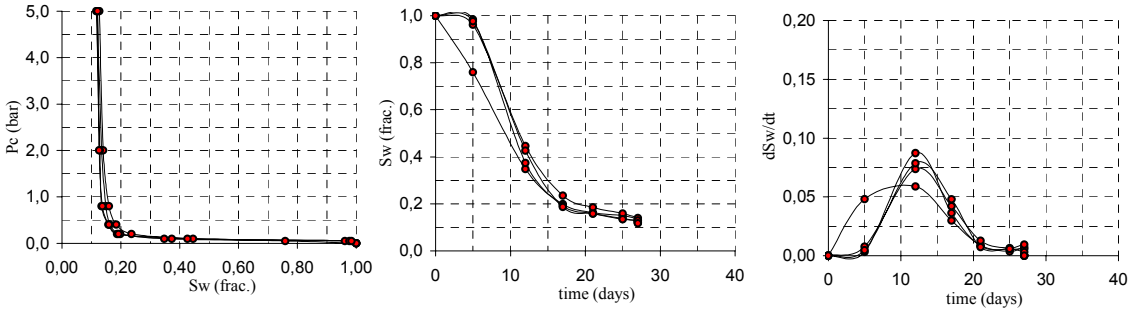

Figure 8.10 (a-c) Isopar-water primary drainage, Layered porous plate technique, reservoir A.

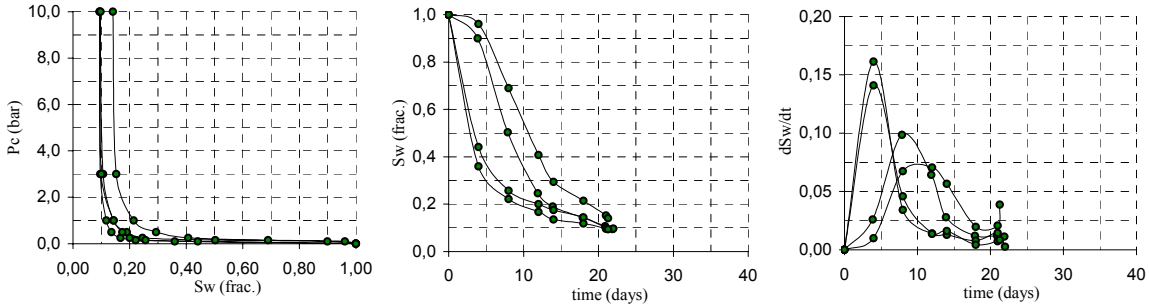

Figure 8.11(a-c) Gas-water primary drainage, Layered porous plate technique, reservoir B.

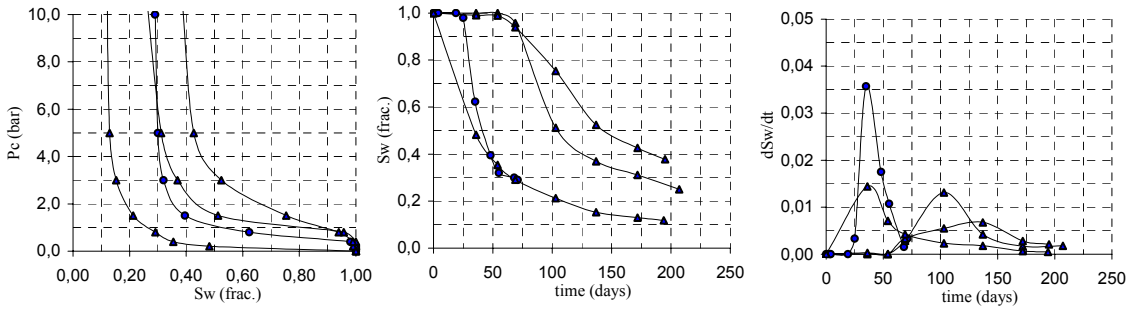

Figure 8.12(a-c) Gas-water primary drainage, Layered and homogeneous porous plate technique, reservoir C.

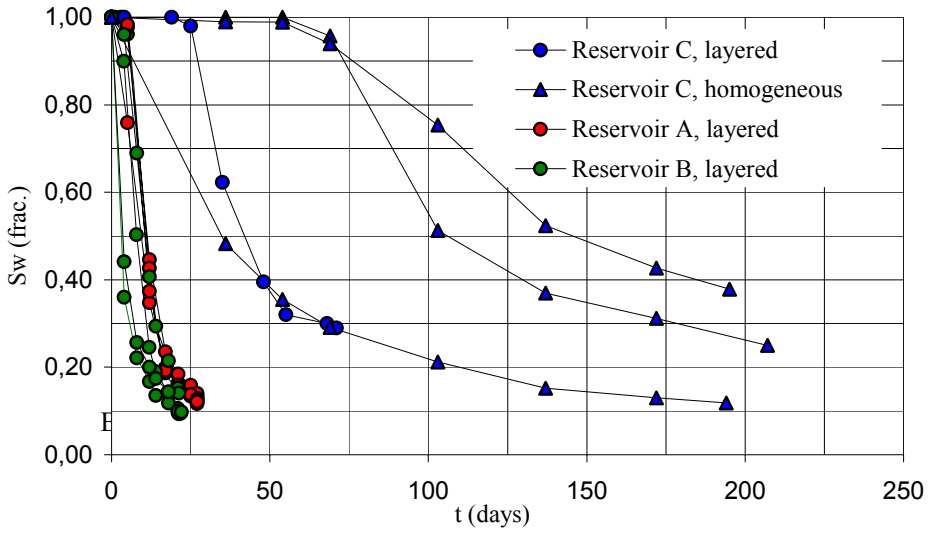

Figure 8.13a-b Experimental turnaround time, reservoir A, B and C.

Observations

Increasing gas diffusion was observed for several of the experiments initiated with layered porous plates. It seems that gas diffuses with a higher rate for the layered porous plate technique than the standard porous plate technique. Gas diffusion is also a common problem for the traditional porous plate technique.

Conclusions

Comparing primary drainage curves from different reservoirs with different permeability is like comparing apples and oranges. By restricting the discussion to primary drainage rates and taking into consideration that rates are controlled by the mobility in the wetting phase throughout capillary drainage, we can observe the following tendencies:

There is a clear tendency towards decreasing time requirements as a function of increasing permeability. Drainage from cores with layered porous plates is 3-10 times faster than homogenous porous plates in the permeability interval 2-4000 mD.

Drainage rates from the layered porous plate technique on low permeable rocks becomes more identical to homogeneous porous plate derived rates. This is in line with conclusions from program C reported in Chapter 7.

Layered porous plate technique at full reservoir condition

In order to investigate possible restrictions of the layered porous plate technique, it was decided to test a carbonate reservoir rock using a live oil-water system. Parallel with this experiment, three carbonates were tested for primary drainage and imbibition down to residual oil saturation, by the standard porous plate technique.

Taken into consideration, that the layered porous plate technique might not be suitable for gas-brine systems, it was decided to perform only primary drainage and resistivity index on this rock.

The core plug in figure 8.14 was drained to irreducible water saturation with live oil at 450 bar net overburden pressure. Pore pressure and temperature was 155 bar and 110° C respectively. The blue line is mercury injection data on corresponding end trims.

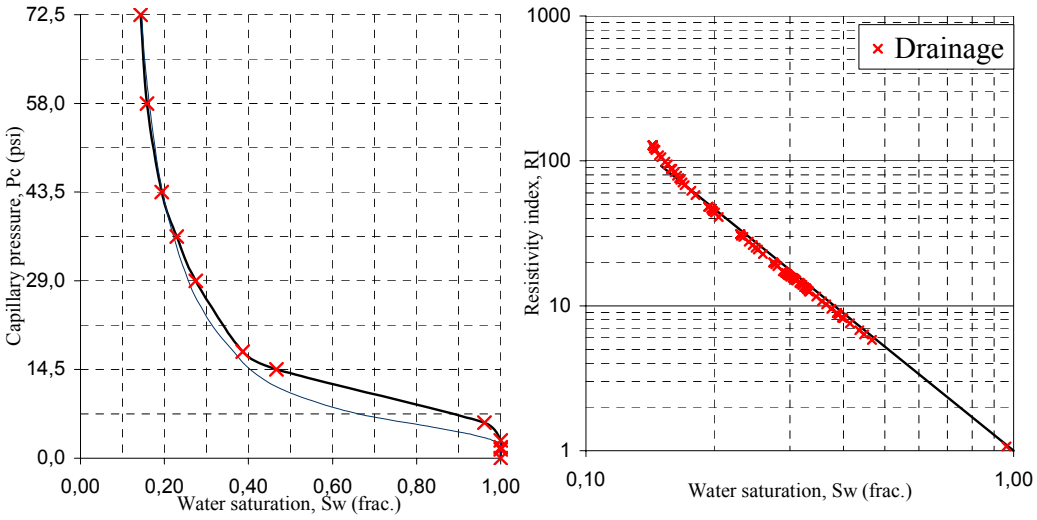

Figure 8.14 Live oil- water capillary drainage and resistivity index

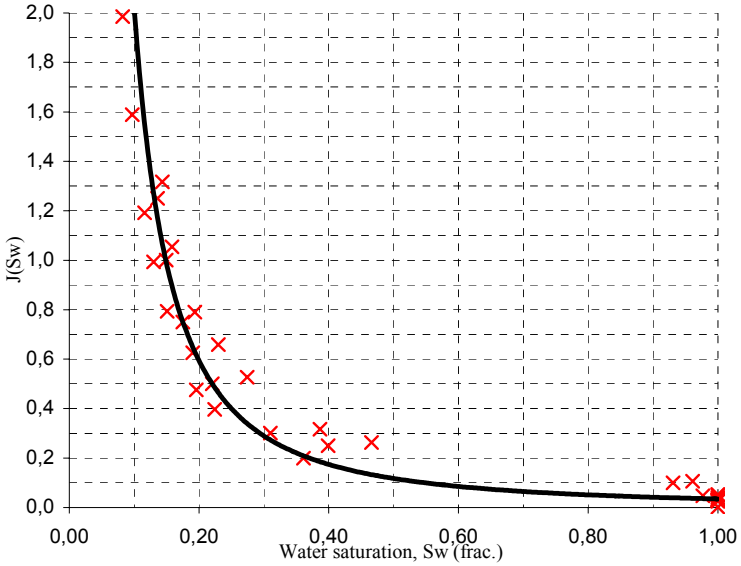

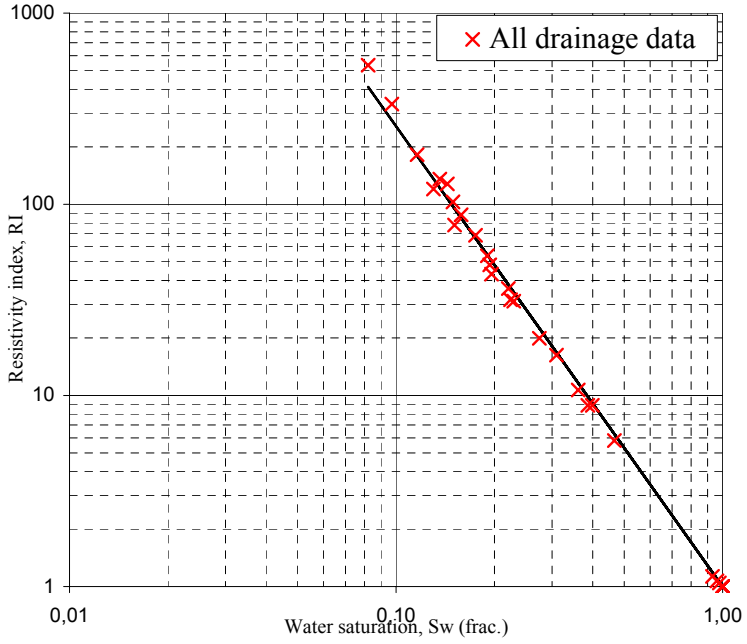

Figure 8.15 J(Sw) at full reservoir conditions

Observations

No hysteresis between the homogeneous porous plate technique and layered porous plate technique was observed. Figure 8.15 presents dimensionless primary drainage data for both homogeneous and layered porous plate experiments. In situ saturation monitoring of the porous plate, reported in figure 8.16, showed no sign of oil invasion. I.e. increasing gamma counts towards irreducible water saturation.

The Sw-RI relationship, reported in figure 8.15 for all experiments, is in line with corresponding relationships derived from standard porous plate technique. Throughout drainage an aging effect on the Sw-RI relationship is observed causing a curved relationship. This effect is seen for both techniques and might be thought of a wettability alteration. The effect is quite common for carbonate reservoirs.

A total time saving factor of 3.02 was observed relative to the corresponding porous plate technique at full reservoir condition.

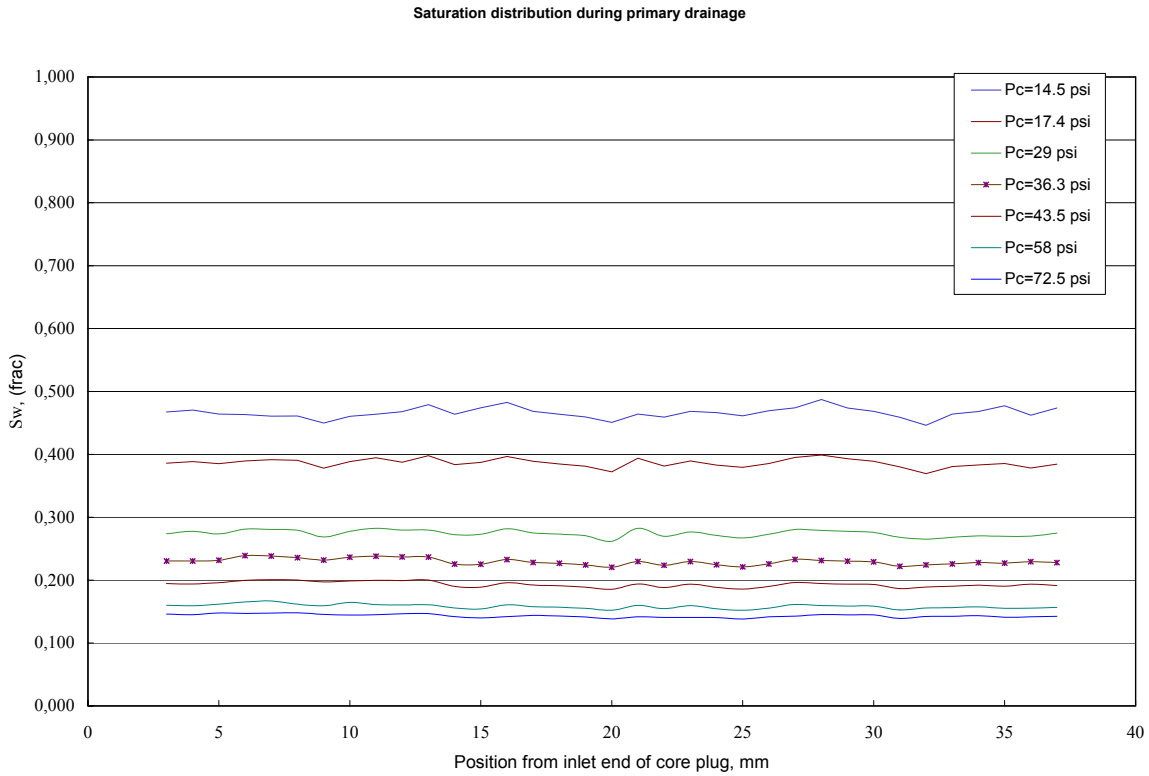

Figure 8.16 In situ saturation monitoring of live oil water experiment

9. CONCLUSIONS AND FUTURE WORK

Porous plate influence on effective drainage and imbibition rates have been studied by comparing the traditional porous plate technique with the investigated layered porous plate technique. The results from this study can be summarised as follows:

Effective drainage and imbibition rates depend on the type of porous plate used but the capillary pressure curve and electrical properties are the same as long as a strict equilibrium criteria is used.

A method of quantifying the influence of drainage and imbibition rates have been introduced. The result of this shows:

- Differences in effective rates are largest at the beginning of primary drainage and secondary drainage. I.e. when the contrast between the mobility of the core and the porous plate is large.

- The rate influence of porous plate type increases with increasing permeability of the investigated porous media.

The layered porous plate technique has been tested, in parallel with traditional porous plate technique, at ambient, pseudo reservoir and full reservoir condition without detecting possible hysteresis between the two methods. However, it seems that the layered porous plate technique is not suitable in the following cases:

- Gas-water systems due to increased gas diffusion rate.
- Coarse or sharp grains in conjunction with poorly or unconsolidated core plugs.

The layered porous plate technique improves continuous injection data with respect to obtaining lower water saturations. However, such data is strongly dependent of injection rate and the method is rather uncertain with respect to obtaining representative Sw-RI relationships.

Future work

The layered porous plate technique has been commercialised throughout this project and is now offered as a conventional service as an alternative to the porous plate technique. All research results illustrate that the only difference is experimental turnaround time.

The weakness of the method is that it is easy to puncture the capillary layer. Further work should therefore be initiated in order to improve the next generation of layered porous plates to become faster and less fragile without decreasing the threshold pressure.

The results from this study support reported[6] research for the membrane technique. This technique, or possible future techniques using other types of porous material as diaphragms, has a large potential in the core industry. Further research with respect to possible prototypes, in order to handle large stress and resist wettability change, should be carried out in order to commercialise the membrane or future techniques for use in special core analysis.

NOMENCLATURE

a	Empirical Archie constant
A	Cross sectional area
$C_O(P_O)$	Compressibility as a function of pressure
d	Diameter of core plug
FF	Formation resistivity factor
FRF	Formation resistivity factor
GD	Grain density
h_n	Water level
h_O	Reference water level
I	Gamma counts on core plug at reservoir conditions at any saturation level
Iair	Dry gamma counts
ID	Diameter of attenuation chamber
I_i	Gamma counts when the chamber is filled with a fluid over a period of one hour
I_{water}	Gamma counts on water saturated core plug at reservoir condition
$J(S_w)$	Dimensionless capillary pressure
K_L	Klinkenberg corrected gas permeability
K_w	Water permeability
L	Length
m	Cementation exponent
n	Saturation exponent
P_C	Pseudo capillary pressure/Capillary pressure
P_{entry}	Entry pressure
P_o	Pressure on the oil phase
P_w	Pressure on the water phase
Q	Rate
q_{inj}	Continuous injection rate
r	Pore entry radius
R_O	Resistivity of 100% water saturated core plug
R_t	Resistivity of core plug at all saturation levels
R_W	Resistivity of simulated formation water
S_{or}	Residual oil saturation
S_W	Wter saturation.
S_{wi}	Irreducible water saturation
t	Temperature
t_C	Characteristic time
t_{ref}	Reference temperature
u	Fluid velocity

V_{bulk}	Bulk volume
V_L	Dead volume in the inlet end piece of the core holder
V_O	Calculated volume of invaded fluid
V_{pore}	Pore volume
V_W	Calculated volume of defending fluid
Z_s	Zero set point impedance
Z_n	Measured impedance
Z_p	Resistivity of water saturated porous plate

Δ	Differential
Φ	Helium porosity
γ	Interfacial tension
λ	Position
μ	Viscosity
θ	Contact angle
ρ	Density
$\rho(t)$	Dimmensionless density correction
σ	Interfacial tension of Mercury/Air
Ψ	Characteristic time ratio
∇	Gradient

SUBSCRIPT

o	Oil
w	Water
n	Step number
nw	Non wetting

ABBREVIATIONS

CP	Confining pressure
F.O.O	Fraction of original
FWL	Free water level
ID	lug identity
LPOP	Lowest location for oil production
NCP	Net confining pressure
NOP	Net overburden pressure
PP	Pore pressure
TTZ	Top transition zone
OWC	Oil water Contact

REFERENCES

1: R. Lenormand, C. Zarcone, and A. Sarr.: "Mechanism of the displacement of one fluid by another in a network of capillary ducts" J. Fluid. Mech., 135:337-353, 1983.

2: R. Lenormand, E. Touboul, and C. Zarcone.: "Numerical models and experiments on immiscible displacements in porous media" J. Fluid Mech., 189:165-187, 1988.

3: M.C. Leverett.: "Capillary behavior in porous solids" Trans AIME, 1941, 142, 152-169.

4: W.D. Rose and W.A. Bruce.: "Evaluation of capillary character in petroleum reservoir rock" Trans AIME, 1949, 186, 127-142.

5: N.R. Morrow.: "Physics and thermodynamics of capillary action in porous media" Ind & Eng. Chem. 1970, 62, No. 6, 32-56.

6: W.L. Hammervold and S.M. Skjæveland.: "Improvement of diaphragm method for drainage capillary pressure measurement with micro pore membrane" Advances in core evaluation III, Worthington, P.F and Chardaire-Riviere, C.(eds), Gordon and Breach Science Publishers, (1992) 91-111.

7: H.P.W. Zeelenberg and .B.A.Schipper.: "Developments in I-Sw measurements" Advances in core evaluation 2, Gordon and Breach Science Publishers 1991.

8: R.Lenormand, A. Eisenzimmer and P. Delaplace.:"Improvements of the semi dynamic method for capillary pressure measurements". SCA 9531, San Francisco 1995.

9: M. Fleury.: "FRIM a new method for measureing continuous resistivity index curves"
SCA 2000, Den Hague.

10: J. Maas and N. Van der Post.:"Resistivity index measurements under week capillary forces"
SCA 2000, Abu Dhabi.

11: R. Lenormand, P. Delaplace and P. Schmitz.:" Can we really measure relative permeabilities using the micropore membrane method?" SCA 9637, Montpellier 1996.

12: M. Flurey and D. Longeron.:" Full imbibition capillary pressure measurements on preserved samples using the membrane technique" SCA9716, Calgary 1997.

13: O.B. Wilson, B.G. Tjetland and A. Skauge.:"Porous plate influence on effective drainage rates in capillary pressure experiments" SCA 2001, Edinburgh.

14: O.B.Wilson and S.M. Skjæveland.: "Porous plate influence on effective imbibition rates in capillary pressure experiments" SCA 2002, Monterey California.

15: J. Kokkede and J. Maas.:"Capillry pressure, relative permeability and resistivity index by continuous injection". 3rd international symposium on evaluation of wettability and its affect on oil recovery, Laramie, Wyoming 1994.

16: L. Sabatier.: "Comparative Study of Drainage Capillary Pressure Measurements Using Different Techniques for Different Fluid Systems," SCA-Paper 9424, presented at the SCA Symposium in Stavanger, September 12-14, 1994.

17: G.E. Archie.: "The electrical resistivity as an aid in determining some reservoir characteristics". J.Pet. Tech. January 1942. No.1.

18: Schlumberger Educational Services.: "Log interpretation-principles/applications" 2nd addition 1989.

19: W.A.Bruce and H. Welge.: "The restored state method for determination of oil in place and connate water". OGJ, July 1947.

20: N.R. Morrow.: “Interfacial phenomena in petroleum recovery”. Surfactant Science Series Vol 36. Chpater 7, 1991

21: P.D. Torray.: Producers Monthly 30(5), 1966.

22: R.J. Schilthuis.: Trans AIME 127, 1938.

23: A.D. Garison.: A.P.I. Drilling and production practice, 1935.

24: J.J. McCullough, F.W. Albaugh and P.H.Jones.: A.P.I. Drilling and Production practice, 1944.

25: D.G. Longeron, M.J. Arquad, and J.P. Feraud.: “Effect of overburden pressure, nature and microscopic distribution of fluids on electrical properties of rock samples”. SPE 15383, New Orleans 1986.

26: D.G. Longeron, M.J. Arquad, and L. Bouvier.: “Resistivity index and capillary pressure measurements under reservoir conditions”. SPE 19589, San Antonio 1989.

27: E.Søndenå, F. Bratteli and K.Kolltveit.: ” A comparison between capillary pressure data and saturation exponent obtained at ambient and reservoir conditions”. SPE 19592, San Antonio 1989.

28: W. Hammervold and S.M. Skjæveland.: ”Improvement of Diaphragm method for drainage capillary pressure measurement with micropore membrane”. SCAN news 1993.

29: Y. Guo and W. Hammervold.: ”Equilibrium time and accuracy of capillary pressure measurements using diaphragm method”. SPWLA, Calgary, June 1993.

30: D. Longeron, W. Hammervold and S.M. Skjæveland.:”Water-oil capillary pressure and wettability measurements using micropore membrane technique”. SCA, Stavanger 1994.

31: D. Longeron, W. Hammervold and S.M. Skjæveland.:”Water-oil capillary pressure and wettability measurements using micropore membrane technique”. International symposium on evaluation of reservoir wettability and its effect on oil recovery, Laramie USA 1994.

32: Z.S. Omoregie.: ” Factors affecting the equivalency of different capillary pressure measurement techniques”. SPE 15384, New Orleans 1994.

33: Dullien.: “Porous media, fluid transport and pore structure”, Academic Press INC,1992 2nd edition.

34: K.K. Mohanty and S.J.Salter.: “ Multiphase flow in porous media, pore-level modeling”. SPE11018, New Orleans September 1982.

35: K.R.Christoffersen and C.H.Whitson.:” Measuring capillary pressure on chalk samples at elevated temperature and varying interfacial tension”. North Sea Chalk Symposium, DeauvilleFrance, September 1992.

36: R.Lenormand, P. Schmitz and P. Delaplace.:”Can we really measure relative permeabilities using the micropore membrane method?”. SCA 9615, Montpellier 1996.

APPENDIX A

Capillary pressure data on Bentheimer core plugs, program A

Equilibrium data on Bentheimer no.1 and 2.

	1 bar homogeneous porous plate Plug no. 1		n: 1.91	1 bar homogeneous porous plate Plug no. 2		n: 1.86
Pc (bar)	Sw (frac.)	RI	n	Sw (frac.)	RI	n
0.000	1.000	1.00		1.000	1.00	
0.015	1.000	1.01				
0.025	0.974	1.13	4.79	0.956	1.12	2.57
0.035				0.808	1.54	2.03
0.050	0.771	1.70	2.04	0.567	2.86	1.85
0.060	0.633	2.41	1.92			
0.080	0.403	5.67	1.91	0.252	12.63	1.84
0.115	0.243	15.13	1.92	0.167	27.36	1.85
0.140	0.206	20.71	1.91	0.145	36.20	1.86
0.160	0.190	23.97	1.91	0.134	41.01	1.85
0.190	0.179	26.65	1.91	0.123	49.07	1.86
0.230	0.163	31.91	1.91	0.112	58.35	1.86

Equilibrium data on Bentheimer no.3 and 4.

	1 bar homogeneous porous plate Plug no. 3		n: 1.76	1 bar homogeneous porous plate Plug no. 4		n: 1.78
Pc (bar)	Sw (frac.)	RI	n	Sw (frac.)	RI	n
0.000	1.000	1.00		1.000	1.00	
0.050	0.699	1.88	1.77			
0.060	0.556	2.83	1.77			
0.080	0.305	8.07	1.76	0.306	8.22	1.78
0.115	0.180	20.05	1.75	0.184	20.63	1.79
0.140	0.155	26.03	1.75	0.159	26.45	1.78
0.160	0.136	32.62	1.75	0.139	33.36	1.78
0.190	0.124	39.45	1.76	0.127	39.63	1.78
0.210				0.120	43.47	1.78
0.230	0.111	47.58	1.76	0.107	53.17	1.78

Equilibrium data on Bentheimer no.5 and 6.

	1 bar homogeneous porous plate Plug no. 5		n: 1.84	1 bar homogeneous porous plate Plug no. 6		n: 1.75
Pc (bar)	Sw (frac.)	RI	n	Sw (frac.)	RI	n
0.000	1.000	1.00		1.000	1.00	
0.115	0.203	18.79	1.84			
0.140	0.164	27.71	1.84	0.160	24.72	1.75
0.160	0.150	33.01	1.85	0.147	28.80	1.75
0.190	0.136	39.14	1.84	0.120	41.80	1.76
0.210	0.122	47.84	1.84			
0.230	0.155	53.32	1.84	0.106	50.41	1.75

Equilibrium data on Bentheimer no.7 and 8.

	1 bar homogeneous porous plate Plug no. 7		n: 1.79	1 bar homogeneous porous plate Plug no. 8		n: 1.81
Pc (bar)	Sw (frac.)	RI	n	Sw (frac.)	RI	n
0.000	1.000	1.00		1.000	1.00	
0.160	0.166	24.86	1.79			
0.190	0.149	29.60	1.78	0.139	35.45	1.81
0.210	0.134	36.69	1.79	0.132	40.00	1.82
0.230	0.121	43.45	1.79	0.119	47.37	1.81

Equilibrium data on Bentheimer no.9 and 10.

	1 bar homogeneous porous plate Plug no. 9		n: 1.87	1 bar homogeneous porous plate Plug no. 10		n: 1.83
Pc (bar)	Sw (frac.)	RI	n	Sw (frac.)	RI	n
0.000	1.000	1.00		1.000	1.00	
0.210	0.152	34.05	1.87			
0.230	0.144	37.61	1.87	0.123	45.99	1.83

APPENDIX B

Continuous injection data on Bentheimer core plugs, program B

FORMATION RESISTIVITY INDEX
BY CONTINUOUS INJECTION
At 20 bar Overburden Pressure

Sample Number	: 1	Porosity (%)	: 23,4
Injection rate (ml/h)	: 0,2000	Formation Resistivity Factor	: 13,05
KL (mD) @ 20 bar	: 3280	Cementation Exponent (m)	: 1,77
Porous plate type	: Layered	Saturation Exponent (n)	: 1,68

Brine Saturation (fraction)	Formation Resistivity Index	Saturation Exponent (n)	Pseudo Capillary Pressure (bar)
1,000	1,00		0,07
0,974	1,14	5,18	0,15
0,949	1,20	3,43	0,18
0,923	1,23	2,54	0,19
0,897	1,26	2,14	0,20
0,872	1,32	2,03	0,20
0,846	1,38	1,93	0,21
0,820	1,44	1,85	0,22
0,795	1,52	1,82	0,23
0,769	1,59	1,77	0,23
0,743	1,68	1,75	0,23
0,718	1,77	1,72	0,24
0,692	1,85	1,67	0,24
0,666	1,95	1,65	0,24
0,641	2,08	1,64	0,24
0,615	2,20	1,62	0,24
0,589	2,33	1,60	0,24
0,564	2,56	1,64	0,25
0,538	2,78	1,65	0,25
0,512	3,02	1,65	0,25
0,487	3,31	1,66	0,26
0,461	3,62	1,66	0,34
0,435	4,01	1,67	0,40
0,410	4,44	1,67	0,59
0,384	4,94	1,67	0,79
0,358	5,60	1,68	1,00
0,333	6,35	1,68	1,40
0,308	7,34	1,69	2,21
0,282	8,47	1,69	3,61
0,258	10,02	1,70	5,93
0,231	11,92	1,69	9,93

FORMATION RESISTIVITY INDEX
BY CONTINUOUS INJECTION
At 20 bar Overburden Pressure

Sample Number	: 2	Porosity (%)	: 22,4
Injection rate (ml/h)	: 0,0339	Formation Resistivity Factor	: 11,81
KL (mD) @ 20 bar	: 5210	Cementation Exponent (m)	: 1,77
Porous plate type	: Layered	Saturation Exponent (n)	: 1,82

Brine Saturation (fraction)	Formation Resistivity Index	Saturation Exponent (n)	Pseudo Capillary Pressure (bar)
1,000	1,00		0,09
0,974	1,04	1,48	0,13
0,948	1,09	1,68	0,13
0,922	1,15	1,69	0,13
0,896	1,21	1,71	0,13
0,868	1,28	1,73	0,14
0,844	1,34	1,74	0,14
0,818	1,42	1,74	0,14
0,792	1,51	1,76	0,15
0,766	1,60	1,76	0,15
0,740	1,70	1,77	0,15
0,714	1,82	1,78	0,15
0,688	1,95	1,79	0,16
0,670	2,05	1,79	0,16
0,636	2,25	1,79	0,16
0,610	2,43	1,80	0,17
0,584	2,63	1,80	0,17
0,558	2,86	1,80	0,17
0,532	3,13	1,81	0,18
0,506	3,48	1,83	0,18
0,480	3,86	1,84	0,18
0,459	4,20	1,84	0,18
0,428	4,77	1,84	0,19
0,402	5,40	1,85	0,19
0,376	6,06	1,84	0,19
0,350	6,91	1,84	0,20
0,324	7,96	1,84	0,20
0,298	9,29	1,84	0,20
0,272	10,85	1,83	0,20
0,246	13,04	1,83	0,21
0,220	15,76	1,82	0,28
0,194	19,78	1,82	0,79
0,169	25,03	1,81	2,67
0,145	33,78	1,82	6,79
0,123	45,40	1,82	14,23

FORMATION RESISTIVITY INDEX
BY CONTINUOUS INJECTION
At 20 bar Overburden Pressure

Sample Number	: 3	Porosity (%)	: 23,5
Injection rate (ml/h)	: 0,0339	Formation Resistivity Factor	: 12,61
KL (mD) @ 20 bar	: 4100	Cementation Exponent (m)	: 1,76
Porous plate type	: Homogeneous	Saturation Exponent (n)	: 1,74

Brine Saturation (fraction)	Formation Resistivity Index	Saturation Exponent (n)	Pseudo Capillary Pressure (bar)
1,000	1,00		0,09
0,971	1,04	1,25	0,15
0,941	1,08	1,33	0,16
0,911	1,14	1,39	0,17
0,881	1,20	1,44	0,17
0,850	1,32	1,69	0,18
0,822	1,41	1,74	0,19
0,792	1,51	1,78	0,19
0,762	1,64	1,83	0,20
0,733	1,76	1,82	0,21
0,703	1,90	1,82	0,21
0,673	2,05	1,81	0,22
0,644	2,22	1,81	0,23
0,623	2,35	1,80	0,24
0,584	2,63	1,80	0,24
0,555	2,87	1,79	0,25
0,525	3,17	1,79	0,26
0,495	3,49	1,78	0,26
0,465	3,87	1,77	0,27
0,436	4,35	1,77	0,28
0,406	4,88	1,76	0,29
0,382	5,40	1,75	0,30
0,346	6,32	1,74	0,32
0,317	7,38	1,74	0,36
0,287	8,65	1,73	0,56
0,258	10,29	1,72	0,93
0,228	12,68	1,72	1,51
0,200	15,72	1,71	3,61
0,173	20,53	1,72	8,72
0,146	27,98	1,73	14,50

FORMATION RESISTIVITY INDEX
BY CONTINUOUS INJECTION
At 20 bar Overburden Pressure

Sample Number	: 4	Porosity (%)	: 23,5
Injection rate (ml/h)	: 0,2000	Formation Resistivity Factor	: 12,86
KL (mD) @ 20 bar	: 3360	Cementation Exponent (m)	: 1,76
Porous plate type	: Homogeneous	Saturation Exponent (n)	: 1,63

Brine Saturation (fraction)	Formation Resistivity Index	Saturation Exponent (n)	Pseudo Capillary Pressure (bar)
1,000	1,00		0,08
0,974	1,14	4,84	0,27
0,948	1,26	4,22	0,42
0,921	1,37	3,87	0,33
0,895	1,46	3,43	0,34
0,868	1,52	2,98	0,36
0,842	1,58	2,65	0,37
0,816	1,60	2,32	0,39
0,789	1,64	2,09	0,41
0,763	1,67	1,89	0,42
0,737	1,73	1,80	0,43
0,710	1,82	1,75	0,45
0,684	1,91	1,70	0,46
0,658	2,00	1,66	0,47
0,631	2,11	1,62	0,49
0,605	2,21	1,58	0,50
0,579	2,33	1,55	0,51
0,552	2,48	1,53	0,54
0,526	2,69	1,54	0,56
0,500	2,95	1,56	0,58
0,473	3,26	1,58	0,60
0,447	3,60	1,59	0,80
0,420	4,04	1,61	0,95
0,394	4,51	1,62	1,39
0,368	5,09	1,63	1,80
0,342	5,68	1,62	2,48
0,316	6,45	1,62	3,61
0,291	7,48	1,63	5,92
0,266	8,74	1,64	10,13

FORMATION RESISTIVITY INDEX
BY CONTINUOUS INJECTION
At 20 bar Overburden Pressure

Sample Number	: 5	Porosity (%)	: 22,3
Injection rate (ml/h)	: 0,0605	Formation Resistivity Factor	: 14,11
KL (mD) @ 20 bar	: 2650	Cementation Exponent (m)	: 1,76
Porous plate type	: Layered	Saturation Exponent (n)	: 1,79

Brine Saturation (fraction)	Formation Resistivity Index	Saturation Exponent (n)	Pseudo Capillary Pressure (bar)
1,000	1,00		0,08
0,975	1,04	1,67	0,14
0,950	1,09	1,69	0,15
0,925	1,14	1,72	0,15
0,900	1,20	1,74	0,16
0,876	1,26	1,76	0,17
0,851	1,33	1,76	0,17
0,826	1,40	1,76	0,18
0,801	1,48	1,76	0,18
0,776	1,57	1,77	0,19
0,751	1,66	1,78	0,20
0,726	1,77	1,78	0,20
0,701	1,89	1,79	0,21
0,676	2,02	1,80	0,22
0,651	2,16	1,80	0,22
0,627	2,33	1,81	0,23
0,602	2,52	1,82	0,23
0,577	2,74	1,83	0,24
0,552	2,99	1,84	0,25
0,527	3,25	1,84	0,25
0,502	3,58	1,85	0,26
0,477	3,91	1,84	0,27
0,452	4,28	1,83	0,27
0,427	4,70	1,82	0,28
0,402	5,20	1,81	0,28
0,377	5,78	1,80	0,29
0,352	6,47	1,79	0,30
0,327	7,29	1,78	0,30
0,303	8,30	1,77	0,32
0,278	9,53	1,76	0,51
0,253	11,25	1,76	0,71
0,228	13,66	1,77	1,04
0,204	16,95	1,78	2,05
0,180	21,10	1,78	4,32
0,144	31,95	1,79	11,95

FORMATION RESISTIVITY INDEX
BY CONTINUOUS INJECTION
At 20 bar Overburden Pressure

Sample Number	: 6	Porosity (%)	: 23,8
Injection rate (ml/h)	: 0,0605	Formation Resistivity Factor	: 12,43
KL (mD) @ 20 bar	: 4580	Cementation Exponent (m)	: 1,76
Porous plate type	: Homogeneous	Saturation Exponent (n)	: 1,76

Brine Saturation (fraction)	Formation Resistivity Index	Saturation Exponent (n)	Pseudo Capillary Pressure (bar)
1,000	1,00		0,09
0,976	1,04	1,56	0,20
0,953	1,08	1,59	0,21
0,929	1,13	1,64	0,22
0,905	1,18	1,66	0,22
0,881	1,24	1,69	0,23
0,858	1,30	1,73	0,24
0,834	1,37	1,73	0,25
0,810	1,44	1,74	0,26
0,786	1,53	1,76	0,27
0,763	1,62	1,77	0,28
0,739	1,71	1,78	0,28
0,715	1,82	1,79	0,29
0,692	1,94	1,80	0,30
0,668	2,09	1,82	0,31
0,644	2,24	1,83	0,32
0,620	2,41	1,84	0,33
0,597	2,60	1,85	0,33
0,573	2,77	1,83	0,34
0,549	3,00	1,83	0,35
0,525	3,21	1,81	0,36
0,501	3,44	1,79	0,37
0,478	3,70	1,77	0,38
0,454	4,02	1,76	0,39
0,430	4,34	1,74	0,39
0,407	4,75	1,73	0,40
0,383	5,32	1,74	0,42
0,359	6,01	1,75	0,45
0,335	6,62	1,73	0,61
0,312	7,60	1,74	0,88
0,288	8,81	1,75	1,33
0,265	10,35	1,76	2,06
0,242	12,18	1,76	3,08
0,219	14,68	1,77	5,26
0,184	20,42	1,78	10,96

FORMATION RESISTIVITY INDEX
BY CONTINUOUS INJECTION
At 20 bar Overburden Pressure

Sample Number	: 7	Porosity (%)	: 23,7
Injection rate (ml/h)	: 0,1027	Formation Resistivity Factor	: 12,52
KL (mD) @ 20 bar	: 3690	Cementation Exponent (m)	: 1,76
Porous plate type	: Layered	Saturation Exponent (n)	: 1,65

Brine Saturation (fraction)	Formation Resistivity Index	Saturation Exponent (n)	Pseudo Capillary Pressure (bar)
1,000	1,00		0,07
0,976	1,04	1,47	0,14
0,951	1,08	1,55	0,15
0,927	1,13	1,57	0,16
0,903	1,20	1,80	0,17
0,879	1,26	1,79	0,18
0,854	1,33	1,79	0,19
0,830	1,39	1,78	0,20
0,806	1,47	1,77	0,21
0,781	1,55	1,77	0,22
0,757	1,63	1,76	0,23
0,733	1,72	1,75	0,24
0,708	1,82	1,74	0,25
0,684	1,94	1,74	0,26
0,660	2,05	1,73	0,27
0,636	2,18	1,72	0,28
0,611	2,32	1,71	0,29
0,587	2,49	1,71	0,30
0,563	2,64	1,69	0,31
0,538	2,85	1,69	0,32
0,514	3,06	1,68	0,33
0,489	3,30	1,67	0,34
0,465	3,56	1,66	0,35
0,441	3,86	1,65	0,36
0,417	4,20	1,64	0,37
0,392	4,64	1,64	0,38
0,368	5,15	1,64	0,41
0,344	5,76	1,64	0,45
0,320	6,49	1,64	0,71
0,295	7,30	1,63	1,01
0,271	8,38	1,63	1,54
0,248	9,87	1,64	2,22
0,224	11,81	1,65	3,71
0,202	14,05	1,65	7,11
0,180	17,29	1,66	11,67

FORMATION RESISTIVITY INDEX
BY CONTINUOUS INJECTION
At 20 bar Overburden Pressure

Sample Number	: 8	Porosity (%)	: 23,6
Injection rate (ml/h)	: 0,1027	Formation Resistivity Factor	: 12,78
KL (mD) @ 20 bar	: 4160	Cementation Exponent (m)	: 1,76
Porous plate type	: Homogeneous	Saturation Exponent (n)	: 1,66

Brine Saturation (fraction)	Formation Resistivity Index	Saturation Exponent (n)	Pseudo Capillary Pressure (bar)
1,000	1,00		0,10
0,976	1,03	1,19	0,23
0,952	1,08	1,47	0,25
0,927	1,12	1,55	0,26
0,903	1,19	1,73	0,28
0,879	1,25	1,74	0,29
0,854	1,32	1,75	0,31
0,830	1,39	1,77	0,33
0,806	1,46	1,75	0,34
0,782	1,54	1,74	0,36
0,757	1,62	1,74	0,37
0,733	1,71	1,73	0,39
0,709	1,81	1,72	0,41
0,684	1,92	1,72	0,42
0,660	2,04	1,71	0,44
0,636	2,17	1,71	0,45
0,612	2,30	1,70	0,47
0,587	2,47	1,70	0,48
0,563	2,63	1,68	0,50
0,539	2,83	1,68	0,52
0,514	3,04	1,67	0,52
0,490	3,27	1,66	0,53
0,466	3,54	1,65	0,54
0,441	3,83	1,64	0,56
0,417	4,17	1,63	0,56
0,393	4,61	1,64	0,58
0,369	5,14	1,64	0,80
0,345	5,81	1,65	1,11
0,321	6,62	1,66	1,56
0,297	7,45	1,65	2,37
0,273	8,32	1,63	3,60
0,250	9,80	1,65	5,61
0,228	11,72	1,67	10,16

FORMATION RESISTIVITY INDEX
BY CONTINUOUS INJECTION
At 20 bar Overburden Pressure

Sample Number	: 9	Porosity (%)	: 23,2
Injection rate (ml/h)	: 0,1838	Formation Resistivity Factor	: 12,92
KL (mD) @ 20 bar	: 3760	Cementation Exponent (m)	: 1,75
Porous plate type	: Layered	Saturation Exponent (n)	: 1,57

Brine Saturation (fraction)	Formation Resistivity Index	Saturation Exponent (n)	Pseudo Capillary Pressure (bar)
1,000	1,00		0,25
0,980	1,13	6,15	0,30
0,960	1,16	3,69	0,32
0,940	1,17	2,60	0,33
0,921	1,23	2,47	0,34
0,901	1,27	2,25	0,34
0,881	1,30	2,04	0,36
0,861	1,35	2,00	0,38
0,841	1,40	1,93	0,38
0,821	1,42	1,78	0,39
0,801	1,46	1,70	0,39
0,781	1,50	1,64	0,40
0,761	1,54	1,57	0,40
0,741	1,61	1,59	0,40
0,721	1,70	1,62	0,40
0,702	1,76	1,60	0,40
0,682	1,84	1,59	0,41
0,662	1,92	1,58	0,42
0,642	2,03	1,59	0,42
0,622	2,13	1,59	0,50
0,602	2,23	1,58	0,57
0,582	2,33	1,56	0,78
0,562	2,44	1,55	0,98
0,543	2,57	1,54	1,31
0,523	2,70	1,53	1,80
0,503	2,87	1,54	2,21
0,484	3,03	1,53	2,88
0,464	3,26	1,54	3,70
0,445	3,48	1,54	4,55
0,426	3,76	1,55	6,03
0,408	4,08	1,57	8,16

FORMATION RESISTIVITY INDEX
BY CONTINUOUS INJECTION
At 20 bar Overburden Pressure

Sample Number	: 10	Porosity (%)	: 23,7
Injection rate (ml/h)	: 0,1838	Formation Resistivity Factor	: 12,56
KL (mD) @ 20 bar	: 4220	Cementation Exponent (m)	: 1,76
Porous plate type	: Homogeneous	Saturation Exponent (n)	: 1,47

Brine Saturation (fraction)	Formation Resistivity Index	Saturation Exponent (n)	Pseudo Capillary Pressure (bar)
1,000	1,00		0,09
0,980	1,12	5,34	0,36
0,959	1,17	3,67	0,39
0,939	1,14	2,05	0,43
0,918	1,14	1,55	0,46
0,897	1,17	1,45	0,49
0,877	1,20	1,39	0,53
0,856	1,23	1,35	0,56
0,836	1,28	1,38	0,59
0,815	1,33	1,41	0,63
0,795	1,39	1,43	0,66
0,774	1,45	1,46	0,73
0,753	1,52	1,47	0,73
0,733	1,59	1,49	0,83
0,713	1,68	1,52	1,00
0,692	1,74	1,51	1,30
0,672	1,82	1,50	1,60
0,651	1,90	1,49	2,00
0,631	2,00	1,51	2,51
0,611	2,10	1,51	3,01
0,591	2,20	1,50	3,41
0,570	2,30	1,48	4,02
0,550	2,41	1,47	5,04
0,531	2,54	1,47	6,11
0,511	2,67	1,46	7,22
0,491	2,83	1,46	8,42
0,471	2,99	1,46	9,76
0,451	3,21	1,47	11,88
0,432	3,44	1,47	14,10

APPENDIX C

Capillary pressure data on Bentheimer core plugs, program C

Bentheimer sample no.:	: 1
Porous plate type:	: Layered
Porosity at 200 bar NCP/20° C (frac.)	: 0,226
Water permeability at 200 bar NCP/20° C (mD)	: 1523
Irreducible water saturation at 200 bar NCP/20° C (frac.)	: 0,119
Residual oil saturation at 200 bar NCP/20° C (frac.)	: 0,279
Primary drainage saturation exponent at 200 bar NCP/20° C	: 1,91
Imbibition saturation exponent at 200 bar NCP/20° C	: 1,93
Secondary drainage saturation exponent at 200 bar NCP/20° C	: 1,93
Saturation exponent at 200 bar NCP/20° C	: 1,92

Date, time	P_c (bar)	S_w (frac.)	RI	$J(S_w)$	Δ_t (days)
3.5.02 13:02	0,000	1,000	1,00	0,000	0,0
3.21.02 7:50	0,100	0,204	19,81	0,23	15,8
4.2.02 16:54	0,200	0,169	28,78	0,47	28,2
4.11.02 11:26	0,400	0,145	39,18	0,94	36,9
4.20.02 14:54	0,800	0,132	47,70	1,88	46,1
4.26.02 14:33	2,000	0,126	53,28	4,69	52,1
5.1.02 16:14	5,000	0,119	61,03	11,73	57,1
5.6.02 13:38	1,000	0,122	57,85	2,35	62,0
5.11.02 12:42	0,200	0,127	53,52	0,47	67,0
5.20.02 8:53	0,050	0,147	40,34	0,12	75,8
6.17.02 12:42	0,000	0,643	2,34	0,00	104,0
7.4.02 12:04	-0,050	0,685	2,07	-0,12	121,0
7.15.02 11:06	-0,200	0,702	1,98	-0,47	131,9
7.24.02 7:39	-0,500	0,711	1,93	-1,17	140,8
7.31.02 9:14	-1,000	0,721	1,88	-2,35	147,8
8.5.02 11:41	0,000	0,721	1,88	0,00	152,9
8.31.02 8:33	0,080	0,208	20,36	0,19	178,8
9.10.02 11:26	0,200	0,154	36,99	0,47	188,9
9.18.02 10:05	0,500	0,133	48,29	1,17	196,9
9.25.02 8:47	2,000	0,125	55,38	4,69	203,8
9.30.02 9:47	5,000	0,119	60,47	11,73	208,9

Bentheimer sample no.:	: 2
Porous plate type:	: Layered
Porosity at 200 bar NCP/20° C (frac.)	: 0,235
Water permeability at 200 bar NCP/20° C (mD)	: 2203
Irreducible water saturation at 200 bar NCP/20° C (frac.)	: 0,100
Residual oil saturation at 200 bar NCP/20° C (frac.)	: 0,284
Primary drainage saturation exponent at 200 bar NCP/20° C	: 1,86
Imbibition saturation exponent at 200 bar NCP/20° C	: 1,87
Secondary drainage saturation exponent at 200 bar NCP/20° C	: 1,87
Saturation exponent at 200 bar NCP/20° C	: 1,87

Date, time	P_c (bar)	S_w (frac.)	RI	$J(S_w)$	Δ_t (days)
3.5.02 13:02	0,000	1,000	1,00	0,000	0,0
3.21.02 7:50	0,100	0,185	22,56	0,28	15,8
4.2.02 16:54	0,200	0,146	35,57	0,55	28,2
4.11.02 11:26	0,400	0,125	48,34	1,11	36,9
4.20.02 14:54	0,800	0,111	59,44	2,21	46,1
4.26.02 14:33	2,000	0,106	66,34	5,53	52,1
5.1.02 16:14	5,000	0,100	73,44	13,83	57,1
5.6.02 13:38	1,000	0,102	71,20	2,77	62,0
5.11.02 12:42	0,200	0,107	65,56	0,55	67,0
5.20.02 8:53	0,050	0,127	47,11	0,14	75,8
6.17.02 12:42	0,000	0,633	2,34	0,00	104,0
7.4.02 12:04	-0,050	0,677	2,07	-0,14	121,0
7.15.02 11:06	-0,200	0,695	1,97	-0,55	131,9
7.24.02 7:39	-0,500	0,704	1,92	-1,38	140,8
7.31.02 9:14	-1,000	0,716	1,88	-2,77	147,8
8.5.02 11:41	0,000	0,716	1,88	0,00	152,9
8.31.02 8:33	0,080	0,191	22,07	0,22	178,8
9.10.02 11:26	0,200	0,134	43,04	0,55	188,9
9.18.02 10:05	0,500	0,114	58,34	1,38	196,9
9.25.02 8:47	2,000	0,106	66,93	5,53	203,8
9.30.02 9:47	5,000	0,100	74,34	13,83	208,9

Bentheimer sample no.:	: 3
Porous plate type:	: Layered
Porosity at 200 bar NCP/20° C (frac.)	: 0,227
Water permeability at 200 bar NCP/20° C (mD)	: 2094
Irreducible water saturation at 200 bar NCP/20° C (frac.)	: 0,104
Residual oil saturation at 200 bar NCP/20° C (frac.)	: 0,286
Primary drainage saturation exponent at 200 bar NCP/20° C	: 1,76
Imbibition saturation exponent at 200 bar NCP/20° C	: 1,77
Secondary drainage saturation exponent at 200 bar NCP/20° C	: 1,77
Saturation exponent at 200 bar NCP/20° C	: 1,77

Date, time	P_c (bar)	S_w (frac.)	RI	$J(S_w)$	Δ_t (days)
3.5.02 13:02	0,000	1,000	1,00	0,000	0,0
3.21.02 7:50	0,100	0,181	19,66	0,27	15,8
4.2.02 16:54	0,200	0,141	30,46	0,55	28,2
4.11.02 11:26	0,400	0,121	40,83	1,10	36,9
4.20.02 14:54	0,800	0,113	47,19	2,20	46,1
4.26.02 14:33	2,000	0,108	51,22	5,49	52,1
5.1.02 16:14	5,000	0,104	55,03	13,72	57,1
5.6.02 13:38	1,000	0,106	53,10	2,74	62,0
5.11.02 12:42	0,200	0,111	49,27	0,55	67,0
5.20.02 8:53	0,050	0,130	37,22	0,14	75,8
6.17.02 12:42	0,000	0,634	2,24	0,00	104,0
7.4.02 12:04	-0,050	0,677	2,00	-0,14	121,0
7.15.02 11:06	-0,200	0,696	1,90	-0,55	131,9
7.24.02 7:39	-0,500	0,703	1,86	-1,37	140,8
7.31.02 9:14	-1,000	0,714	1,82	-2,74	147,8
8.5.02 11:41	0,000	0,714	1,82	0,00	152,9
8.31.02 8:33	0,080	0,194	18,19	0,22	178,8
9.10.02 11:26	0,200	0,137	33,85	0,55	188,9
9.18.02 10:05	0,500	0,116	44,95	1,37	196,9
9.25.02 8:47	2,000	0,109	50,85	5,49	203,8
9.30.02 9:47	5,000	0,103	55,31	13,72	208,9

Bentheimer sample no.:	: 4
Porous plate type:	: Layered
Porosity at 200 bar NCP/20° C (frac.)	: 0,227
Water permeability at 200 bar NCP/20° C (mD)	: 1424
Irreducible water saturation at 200 bar NCP/20° C (frac.)	: 0,107
Residual oil saturation at 200 bar NCP/20° C (frac.)	: 0,268
Primary drainage saturation exponent at 200 bar NCP/20° C	: 1,79
Imbibition saturation exponent at 200 bar NCP/20° C	: 1,81
Secondary drainage saturation exponent at 200 bar NCP/20° C	: 1,81
Saturation exponent at 200 bar NCP/20° C	: 1,80

Date, time	P_c (bar)	S_w (frac.)	RI	$J(S_w)$	Δ_t (days)
3.5.02 13:02	0,000	1,000	1,00	0,000	0,0
3.21.02 7:50	0,100	0,180	21,21	0,23	15,8
4.2.02 16:54	0,200	0,141	32,46	0,45	28,2
4.11.02 11:26	0,400	0,120	43,10	0,91	36,9
4.20.02 14:54	0,800	0,113	48,85	1,81	46,1
4.26.02 14:33	2,000	0,109	52,97	4,53	52,1
5.1.02 16:14	5,000	0,107	55,30	11,31	57,1
5.6.02 13:38	1,000	0,114	50,86	2,26	62,0
5.11.02 12:42	0,200	0,117	48,76	0,45	67,0
5.20.02 8:53	0,050	0,131	39,78	0,11	75,8
6.17.02 12:42	0,000	0,634	2,27	0,00	104,0
7.4.02 12:04	-0,050	0,677	2,04	-0,11	121,0
7.15.02 11:06	-0,200	0,696	1,94	-0,45	131,9
7.24.02 7:39	-0,500	0,719	1,81	-1,13	140,8
7.31.02 9:14	-1,000	0,732	1,75	-2,26	147,8
8.5.02 11:41	0,000	0,732	1,75	0,00	152,9
8.31.02 8:33	0,080	0,193	19,36	0,18	178,8
9.10.02 11:26	0,200	0,136	36,89	0,45	188,9
9.18.02 10:05	0,500	0,117	48,03	1,13	196,9
9.25.02 8:47	2,000	0,109	55,47	4,53	203,8
9.30.02 9:47	5,000	0,107	57,46	11,31	208,9

Bentheimer sample no.:	: 5
Porous plate type:	: Layered
Porosity at 200 bar NCP/20° C (frac.)	: 0,216
Water permeability at 200 bar NCP/20° C (mD)	: 1401
Irreducible water saturation at 200 bar NCP/20° C (frac.)	: 0,119
Residual oil saturation at 200 bar NCP/20° C (frac.)	: 0,251
Primary drainage saturation exponent at 200 bar NCP/20° C	: 1,86
Imbibition saturation exponent at 200 bar NCP/20° C	: 1,87
Secondary drainage saturation exponent at 200 bar NCP/20° C	: 1,87
Saturation exponent at 200 bar NCP/20° C	: 1,86

Date, time	P_c (bar)	S_w (frac.)	RI	$J(S_w)$	Δ_t (days)
3.5.02 13:02	0,000	1,000	1,00	0,000	0,0
3.21.02 7:50	0,100	0,202	19,21	0,23	15,8
4.2.02 16:54	0,200	0,169	26,65	0,46	28,2
4.11.02 11:26	0,400	0,145	35,56	0,92	36,9
4.20.02 14:54	0,800	0,132	42,38	1,84	46,1
4.26.02 14:33	2,000	0,126	47,00	4,60	52,1
5.1.02 16:14	5,000	0,119	53,44	11,51	57,1
5.6.02 13:38	1,000	0,122	50,77	2,30	62,0
5.11.02 12:42	0,200	0,127	47,53	0,46	67,0
5.20.02 8:53	0,050	0,147	35,90	0,12	75,8
6.17.02 12:42	0,000	0,680	2,05	0,00	104,0
7.4.02 12:04	-0,050	0,716	1,87	-0,12	121,0
7.15.02 11:06	-0,200	0,732	1,78	-0,46	131,9
7.24.02 7:39	-0,500	0,740	1,76	-1,15	140,8
7.31.02 9:14	-1,000	0,749	1,72	-2,30	147,8
8.5.02 11:41	0,000	0,749	1,73	0,00	152,9
8.31.02 8:33	0,080	0,209	18,58	0,18	178,8
9.10.02 11:26	0,200	0,154	33,80	0,46	188,9
9.18.02 10:05	0,500	0,133	43,68	1,15	196,9
9.25.02 8:47	2,000	0,125	49,11	4,60	203,8
9.30.02 9:47	5,000	0,119	51,33	11,51	208,9

Bentheimer sample no.:	: 6
Porous plate type:	: Layered
Porosity at 200 bar NCP/20° C (frac.)	: 0,230
Water permeability at 200 bar NCP/20° C (mD)	: 1833
Irreducible water saturation at 200 bar NCP/20° C (frac.)	: 0,110
Residual oil saturation at 200 bar NCP/20° C (frac.)	: 0,252
Primary drainage saturation exponent at 200 bar NCP/20° C	: 1,77
Imbibition saturation exponent at 200 bar NCP/20° C	: 1,79
Secondary drainage saturation exponent at 200 bar NCP/20° C	: 1,79
Saturation exponent at 200 bar NCP/20° C	: 1,78

Date, time	P_c (bar)	S_w (frac.)	RI	$J(S_w)$	Δ_t (days)
3.5.02 13:02	0,000	1,000	1,00	0,000	0,0
3.21.02 7:50	0,100	0,195	18,05	0,26	15,8
4.2.02 16:54	0,200	0,161	25,01	0,51	28,2
4.11.02 11:26	0,400	0,136	33,98	1,02	36,9
4.20.02 14:54	0,800	0,123	40,34	2,04	46,1
4.26.02 14:33	2,000	0,117	44,02	5,10	52,1
5.1.02 16:14	5,000	0,110	51,27	12,75	57,1
5.6.02 13:38	1,000	0,113	49,26	2,55	62,0
5.11.02 12:42	0,200	0,118	45,66	0,51	67,0
5.20.02 8:53	0,050	0,139	34,30	0,13	75,8
6.17.02 12:42	0,000	0,677	2,00	0,00	104,0
7.4.02 12:04	-0,050	0,716	1,82	-0,13	121,0
7.15.02 11:06	-0,200	0,731	1,75	-0,51	131,9
7.24.02 7:39	-0,500	0,739	1,72	-1,28	140,8
7.31.02 9:14	-1,000	0,748	1,69	-2,55	147,8
8.5.02 11:41	0,000	0,748	1,68	0,00	152,9
8.31.02 8:33	0,080	0,200	17,80	0,20	178,8
9.10.02 11:26	0,200	0,146	31,49	0,51	188,9
9.18.02 10:05	0,500	0,124	42,00	1,28	196,9
9.25.02 8:47	2,000	0,116	47,10	5,10	203,8
9.30.02 9:47	5,000	0,110	50,45	12,75	208,9

Bentheimer sample no.:	: 7
Porous plate type:	: Layered
Porosity at 200 bar NCP/20° C (frac.)	: 0,229
Water permeability at 200 bar NCP/20° C (mD)	: 1411
Irreducible water saturation at 200 bar NCP/20° C (frac.)	: 0,108
Residual oil saturation at 200 bar NCP/20° C (frac.)	: 0,286
Primary drainage saturation exponent at 200 bar NCP/20° C	: 1,80
Imbibition saturation exponent at 200 bar NCP/20° C	: 1,82
Secondary drainage saturation exponent at 200 bar NCP/20° C	: 1,82
Saturation exponent at 200 bar NCP/20° C	: 1,81

Date, time	P_c (bar)	S_w (frac.)	RI	$J(S_w)$	Δ_t (days)
3.5.02 13:02	0,000	1,000	1,00	0,000	0,0
3.21.02 7:50	0,100	0,194	19,27	0,22	15,8
4.2.02 16:54	0,200	0,159	27,35	0,45	28,2
4.11.02 11:26	0,400	0,134	37,20	0,90	36,9
4.20.02 14:54	0,800	0,121	44,67	1,79	46,1
4.26.02 14:33	2,000	0,115	49,65	4,49	52,1
5.1.02 16:14	5,000	0,108	56,98	11,21	57,1
5.6.02 13:38	1,000	0,110	55,10	2,24	62,0
5.11.02 12:42	0,200	0,115	50,83	0,45	67,0
5.20.02 8:53	0,050	0,136	37,60	0,11	75,8
6.17.02 12:42	0,000	0,633	2,30	0,00	104,0
7.4.02 12:04	-0,050	0,676	2,04	-0,11	121,0
7.15.02 11:06	-0,200	0,694	1,94	-0,45	131,9
7.24.02 7:39	-0,500	0,703	1,90	-1,12	140,8
7.31.02 9:14	-1,000	0,714	1,85	-2,24	147,8
8.5.02 11:41	0,000	0,714	1,85	0,00	152,9
8.31.02 8:33	0,080	0,198	19,07	0,18	178,8
9.10.02 11:26	0,200	0,143	34,57	0,45	188,9
9.18.02 10:05	0,500	0,121	46,54	1,12	196,9
9.25.02 8:47	2,000	0,113	52,60	4,49	203,8
9.30.02 9:47	5,000	0,107	58,53	11,21	208,9

Bentheimer sample no.:	: 8
Porous plate type:	: Layered
Porosity at 200 bar NCP/20° C (frac.)	: 0,228
Water permeability at 200 bar NCP/20° C (mD)	: 2413
Irreducible water saturation at 200 bar NCP/20° C (frac.)	: 0,093
Residual oil saturation at 200 bar NCP/20° C (frac.)	: 0,291
Primary drainage saturation exponent at 200 bar NCP/20° C	: 1,84
Imbibition saturation exponent at 200 bar NCP/20° C	: 1,85
Secondary drainage saturation exponent at 200 bar NCP/20° C	: 1,85
Saturation exponent at 200 bar NCP/20° C	: 1,85

Date, time	P_c (bar)	S_w (frac.)	RI	$J(S_w)$	Δ_t (days)
3.5.02 13:02	0,000	1,000	1,00	0,000	0,0
3.21.02 7:50	0,100	0,181	23,36	0,29	15,8
4.2.02 16:54	0,200	0,145	35,02	0,59	28,2
4.11.02 11:26	0,400	0,120	49,15	1,18	36,9
4.20.02 14:54	0,800	0,107	61,24	2,35	46,1
4.26.02 14:33	2,000	0,101	67,83	5,88	52,1
5.1.02 16:14	5,000	0,093	78,77	14,70	57,1
5.6.02 13:38	1,000	0,097	75,22	2,94	62,0
5.11.02 12:42	0,200	0,102	68,51	0,59	67,0
5.20.02 8:53	0,050	0,123	48,58	0,15	75,8
6.17.02 12:42	0,000	0,628	2,36	0,00	104,0
7.4.02 12:04	-0,050	0,672	2,09	-0,15	121,0
7.15.02 11:06	-0,200	0,690	1,99	-0,59	131,9
7.24.02 7:39	-0,500	0,699	1,94	-1,47	140,8
7.31.02 9:14	-1,000	0,709	1,89	-2,94	147,8
8.5.02 11:41	0,000	0,709	1,90	0,00	152,9
8.31.02 8:33	0,080	0,185	22,23	0,24	178,8
9.10.02 11:26	0,200	0,130	43,75	0,59	188,9
9.18.02 10:05	0,500	0,108	61,90	1,47	196,9
9.25.02 8:47	2,000	0,100	71,13	5,88	203,8
9.30.02 9:47	5,000	0,094	79,46	14,70	208,9

Bentheimer sample no.:	: 9
Porous plate type:	: Homogeneous
Porosity at 200 bar NCP/20° C (frac.)	: 0,224
Water permeability at 200 bar NCP/20° C (mD)	: 2147
Irreducible water saturation at 200 bar NCP/20° C (frac.)	: 0,112
Residual oil saturation at 200 bar NCP/20° C (frac.)	: 0,284
Primary drainage saturation exponent at 200 bar NCP/20° C	: 1,89
Imbibition saturation exponent at 200 bar NCP/20° C	: 1,90
Secondary drainage saturation exponent at 200 bar NCP/20° C	: 1,90
Saturation exponent at 200 bar NCP/20° C	: 1,89

Date, time	P_c (bar)	S_w (frac.)	RI	$J(S_w)$	Δ_t (days)
12.21.01 9:26	0,000	1,000	1,00	0,000	0,0
2.23.02 20:43	0,100	0,197	21,45	0,28	64,5
4.12.02 16:09	0,200	0,162	31,02	0,56	112,3
5.1.02 13:45	0,400	0,137	41,63	1,12	131,2
5.13.02 9:32	0,800	0,125	51,09	2,24	143,0
5.19.02 19:57	2,000	0,119	55,92	5,59	149,4
5.25.02 9:45	5,000	0,112	62,25	13,99	155,0
5.30.02 16:31	1,000	0,115	61,00	2,80	160,3
6.6.02 8:17	0,200	0,120	56,33	0,56	167,0
6.19.02 7:09	0,050	0,140	41,70	0,14	179,9
8.27.02 8:58	0,000	0,638	2,34	0,00	249,0
9.28.02 16:01	-0,050	0,680	2,08	-0,14	281,3
10.16.02 13:43	-0,200	0,698	1,98	-0,56	299,2
10.27.02 7:50	-0,500	0,707	1,93	-1,40	309,9
11.2.02 10:43	-1,000	0,716	1,89	-2,80	316,1
11.6.02 10:41	0,000	0,716	1,89	0,00	320,1
2.12.03 7:50	0,080	0,203	20,80	0,22	417,9
3.12.03 16:26	0,200	0,148	37,88	0,56	446,3
3.28.03 10:00	0,500	0,126	50,76	1,40	462,0
4.6.03 19:07	2,000	0,117	57,67	5,59	471,4
4.11.03 21:02	5,000	0,112	63,03	13,99	476,5

Bentheimer sample no.:	: 10
Porous plate type:	: Homogeneous
Porosity at 200 bar NCP/20° C (frac.)	: 0,229
Water permeability at 200 bar NCP/20° C (mD)	: 2410
Irreducible water saturation at 200 bar NCP/20° C (frac.)	: 0,096
Residual oil saturation at 200 bar NCP/20° C (frac.)	: 0,291
Primary drainage saturation exponent at 200 bar NCP/20° C	: 1,84
Imbibition saturation exponent at 200 bar NCP/20° C	: 1,85
Secondary drainage saturation exponent at 200 bar NCP/20° C	: 1,85
Saturation exponent at 200 bar NCP/20° C	: 1,85

Date, time	P_c (bar)	S_w (frac.)	RI	$J(S_w)$	Δ_t (days)
12.21.01 9:26	0,000	1,000	1,00	0,000	0,0
2.23.02 20:43	0,100	0,182	22,91	0,29	64,5
4.12.02 16:09	0,200	0,148	33,74	0,59	112,3
5.1.02 13:45	0,400	0,121	49,02	1,17	131,2
5.13.02 9:32	0,800	0,108	60,11	2,34	143,0
5.19.02 19:57	2,000	0,102	67,88	5,86	149,4
5.25.02 9:45	5,000	0,096	75,89	14,66	155,0
5.30.02 16:31	1,000	0,098	74,88	2,93	160,3
6.6.02 8:17	0,200	0,103	68,14	0,59	167,0
6.19.02 7:09	0,050	0,125	47,49	0,15	179,9
8.27.02 8:58	0,000	0,629	2,35	0,00	249,0
9.28.02 16:01	-0,050	0,672	2,08	-0,15	281,3
10.16.02 13:43	-0,200	0,690	1,99	-0,59	299,2
10.27.02 7:50	-0,500	0,699	1,94	-1,47	309,9
11.2.02 10:43	-1,000	0,709	1,90	-2,93	316,1
11.6.02 10:41	0,000	0,708	1,90	0,00	320,1
2.12.03 7:50	0,080	0,188	22,15	0,23	417,9
3.12.03 16:26	0,200	0,132	43,05	0,59	446,3
3.28.03 10:00	0,500	0,110	60,21	1,47	462,0
4.6.03 19:07	2,000	0,100	71,39	5,86	471,4
4.11.03 21:02	5,000	0,096	77,36	14,66	476,5

APPENDIX D

Pore size distribution from Mercury injection on Bentheimer core material

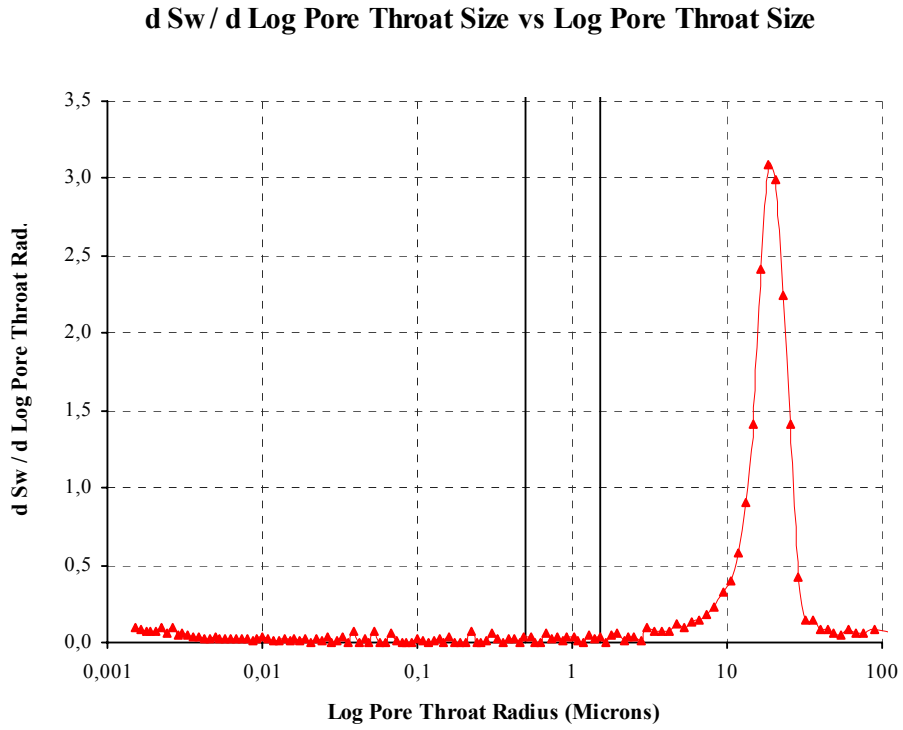

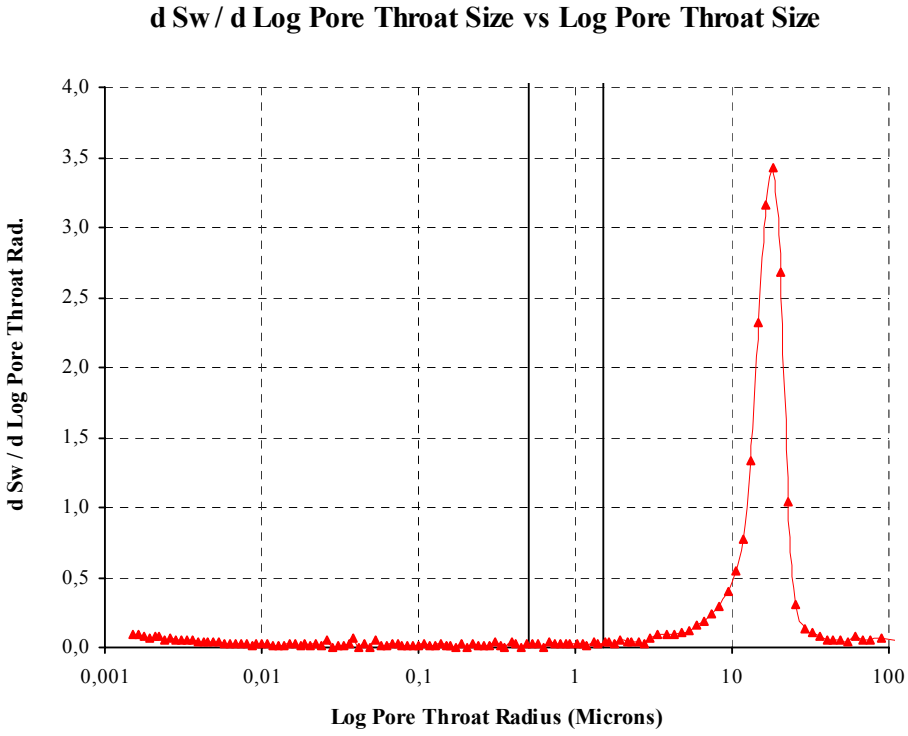

Pore size distribution Bentheiemer no.1 and no.3

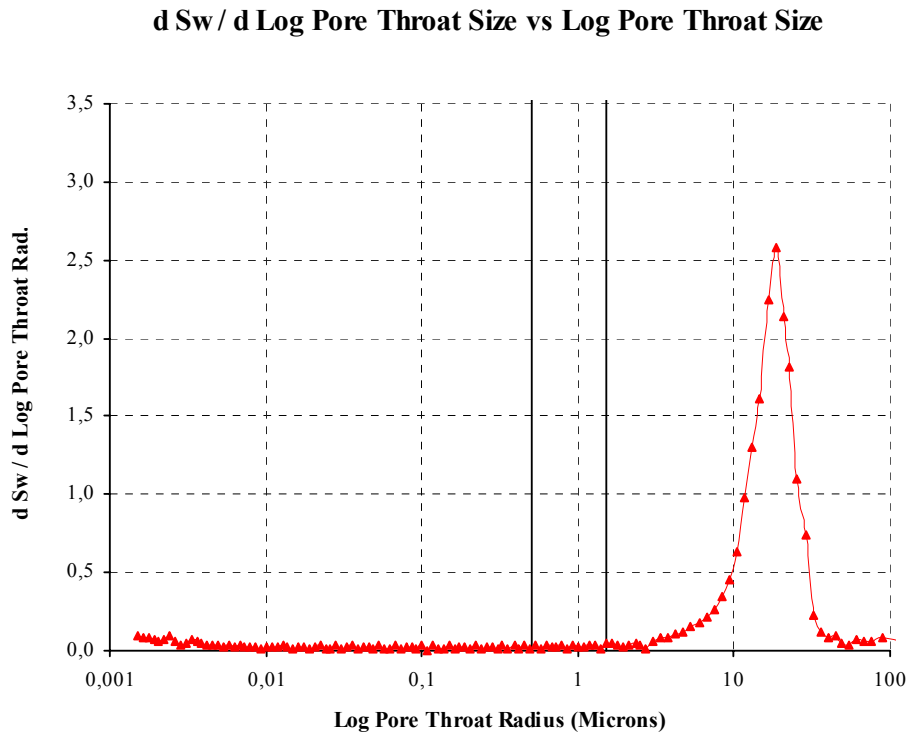

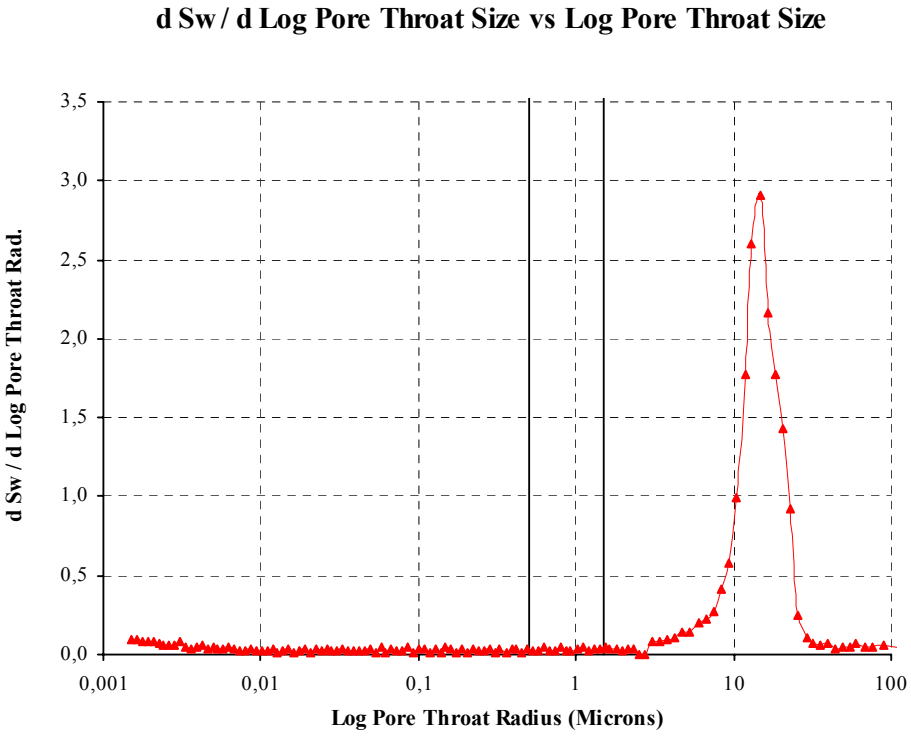

Pore size distribution Bentheiemer no.4 and no.7